A STUDY OF HYBRID POWERTRAINS AND PREDICTIVE ALGORITHMS APPLIED TO ENERGY MANAGEMENT IN REFUSE-COLLECTING VEHICLES

A Dissertation Presented by:

Francisco Soriano

In Partial Fulfillment of
the Requirements for
the Degree of
Doctor of Philosophy in
Thermal Engineering

Polytechnic University of Catalonia
Barcelona, Spain
April 24th, 2015

Supervisors:
Dr. Jesús Andrés Álvarez Florez
Dr. Juan Manuel Moreno Eguilaz

UNIVERSITAT POLITÈCNICA DE CATALUNYA
BARCELONATECH
Escola de Doctorat

Acta de calificación de tesis doctoral	Curso académico:

Nombre y apellidos

Programa de doctorado

Unidad estructural responsable del programa

Resolución del Tribunal

Reunido el Tribunal designado a tal efecto, el doctorando / la doctoranda expone el tema de la su tesis doctoral titulada _____

_____.

Acabada la lectura y después de dar respuesta a las cuestiones formuladas por los miembros titulares del tribunal, éste otorga la calificación:

☐ NO APTO ☐ APROBADO ☐ NOTABLE ☐ SOBRESALIENTE

(Nombre, apellidos y firma) Presidente/a		(Nombre, apellidos y firma) Secretario/a
(Nombre, apellidos y firma) Vocal	(Nombre, apellidos y firma) Vocal	(Nombre, apellidos y firma) Vocal

_____, _____ de _____ de _____

El resultado del escrutinio de los votos emitidos por los miembros titulares del tribunal, efectuado por la Escuela de Doctorado, a instancia de la Comisión de Doctorado de la UPC, otorga la MENCIÓN CUM LAUDE:

☐ SÍ ☐ NO

(Nombre, apellidos y firma) Presidente de la Comisión Permanente de la Escuela de Doctorado	(Nombre, apellidos y firma) Secretario de la Comisión Permanente de la Escuela de Doctorado

Barcelona a _____ de _____ de _____

Dedicado a Daniel Soriano Alonso,
valga este PhD por el PFC que él no pudo entregar.

Abstract

There is an increasing demand for vehicles with lower environmental impact and higher fuel efficiency. To meet these requirements, powertrain hybridization has been introduced in both academia and industry during recent years.

In this work we have carried out an in-depth analysis of the potential reduction in fuel consumption of refuse-collecting vehicles (RCV), based on different hybridization technologies. This study has been structured in four work packages: RCV energy model development, predictive algorithms aimed at energy management for RCV drive cycles, analysis of hybrid hydraulic powertrains for RCV and analysis of hybrid electric powertrains for RCV.

RCV energy model development: the process of simulation starts with the RCV energy model development, which is based on the improvement of the classic approach (breaking down the energy consumption into aerodynamics, rolling resistance, road profile and inertias), and adding the RCV ancillaries' (lifter, compactor and unloading devices) consumption. The adjustments and validation methodology applied to the models is based on the use of low-cost hardware and post-processing data by use of GPS and cartography. Working with this method it has been empirically demonstrated that high accuracy energy consumption estimations are possible through the use of these models.

Predictive algorithms aimed at energy management for RCV drive cycles: based on the principle that RCV drive cycles are repetitive, the typical RCV drive cycle has been modeled and its main characteristics parameterized. The model is separated into different drive cycles which are related to different power consumption modes. Based on this analysis two algorithms are presented, which can identify in which drive mode the vehicle is operating; these algorithms are based on deterministic principles and on artificial intelligence respectively. Also, an algorithm which can estimate the energy needed to finish the current trip is presented; this algorithm is based on information inferred from previous trips, statistics and infinitesimal calculus.

Once the drive cycle of an RCV is analyzed and modeled, the working modes of a standard internal combustion engine on real drive cycles are presented and contrasted with fuel consumption maps. This study concludes that, because of the typical drive cycles of RCV, an ICE is oversized most of the time and tends to work in low efficiency points. Based on this information a basic alternative powertrain architecture is proposed

Analysis of hybrid hydraulic powertrain for RCV: hybrid hydraulic powertrains are often used in heavy duty vehicles in which big power flows can be found. As RCV represent an application with big power flows, the performance of this technology applied to RCV has been analyzed. This study is based on the development of models for each of the components of the powertrain, and the simulation of the whole powertrain model on real routes. All the component models are based on information provided

by the manufacturers, and the routes have been logged in real RCV drive cycles. The conclusion is that an important fuel saving can be achieved by the hydraulic hybridization of the powertrain.

Analysis of hybrid electric powertrain for RCV: hybrid electric powertrains are often used in cars and light duty vehicles. As RCV represents a light to medium duty application the performance of this technology applied to RCV has been analyzed. As in the hybrid hydraulic case, this study is based on the development of models for each of the powertrain components, and the simulation of the whole powertrain model on real routes. All the component models are based on information found in scientific literature reviews or supplied by the manufacturers, and the routes are the same as those used in the hybrid-hydraulic powertrain, which have been logged in real RCV drive cycle.

Finally a comparison between the hybrid electric and the hybrid hydraulic is established, identifying the more efficient technology and the advantages and inconveniences of each. And establishing what would be, according to the authors, the most interesting technological powertrain evolution in the mid and long term for this kind of vehicle.

Acknowledgements – Agradecimientos - Agraïments

A Lidia por creer en lo que nadie más creía.

A David y a Eva por dormirse a su hora.

A Manolo y a Jesús por acceder a dirigir a una tesis vía teléfono y Skype. Y por no cesar de animarme durante este proyecto de tesis.

Al Jordi per introduirme al mon de les piles de combustible i per aportar millores al meu treball.

A Mónica por contestar con normalidad a las preguntas que son normales.

A Miguel y a Joan Marc por arrimar el hombro cada vez que se lo pedí.

To Ralph Staley for his help with the english technical writing.

Al Joan per fer l'esforç de comprendre la meva determinació front a aquesta tesis.

A l'Antonio Jiménez y al Xavier Mauri de Ferrovial Servicios per facilitar-me la tasca de l'adquissició de dades.

Contents

List of Figures

List of Tables

Acronyms

AC. Air Conditioning

AI. Artificial Intelligence

BSFC. Brake Specific Fuel Consumption. A measure of the fuel efficiency of any prime mover that burns fuel and produces rotational, or shaft, power. It is typically used for comparing the efficiency of internal combustion engines with a shaft output.

CAN. Control Area Network. A vehicle bus standard designed to allow microcontrollers and devices to communicate with each other within a vehicle without a host computer.

CAN Open. Control Area Network Open. A communication protocol and device profile specification for embedded systems used in automation.

CBD. The Central Business District (CBD) Cycle is a chassis dynamometer testing procedure for heavy-duty vehicles *[*SAE J1376*]*. The CBD cycle is part of the Advanced Bus Design cycle that was created by the US Department of Transportation and the Urban Mass Transit Association as part of the specifications for assessing bus performance.

ECE. Economic Commission for Europe. The ECE-15 is a drivecycle designed to represent typical driving conditions of busy European cities, and is characterized by low engine load, low exhaust gas temperature, and a maximum speed of 50 km/h.

ECS. Energy Consumption System.

EGS. Energy Generation System.

EMS. Energy Management System

ESS. Energy Storing System.

EUDC. Extra-Urban Driving Cycle. Drivecycle designed to represent more aggressive, high speed driving modes. The maximum speed of the EUDC cycle is 120 km/h; low-powered vehicles are limited to 90 km/h.

EV. Electric Vehicle.

FC. Fuel Cell.

FMVT. Family of Medium Tactical Vehicles (military vehicles).

FTP. Federal Test Procedure. series of tests defined by the US Environmental Protection Agency (EPA) to measure tailpipe emissions and fuel economy of passenger cars (excluding light trucks and heavy-duty vehicles).

FUDS. Federal Urban Driving Schedule. Test included in the FTP test procedure.

GPS. Global Positioning System.

HEV. Hybrid Electric Vehicle.

HHV. Hybrid Hydraulic Vehicle.

HWFET. Highway Fuel Economy Driving Schedule. Test included in the FTP test procedure.

ICE. Internal Combustion Engine.

J1939. CAN based vehicle bus recommended practice for communication and diagnostics among vehicle components.

NEDS. New European Driving Cycle. A driving cycle designed to assess the emission levels of car engines and fuel economy in passenger cars.

PI. Proportional Integral controller.

PLC. Programmable Logic Controller.

RCV. Refuse Collecting Vehicle.

RPM. Revolutions Per Minute.

SC. Supercapacitor / Ultracapacitor.

SUV. Sports Utility Vehicle.

UDDS. Urban Dynamometer Driving Schedule, refers to an United States Environmental Protection Agency mandated dynamometer test on fuel economy that represents city driving conditions which is used for light duty vehicle testing.

US06. Drive cycle in the representation of aggressive, high speed and/or high acceleration driving behavior, rapid speed fluctuations, and driving behavior following startup.

Symbols

α	angle of the road [radians]
a	longitudinal acceleration of the vehicle [m/s^2]
Ax	x component of acceleration value read from the inclinometer [m/s^2]
Ay	y component of acceleration value read from the inclinometer [m/s^2]
Cx	aerodynamic drag coefficient [dimensionless]
C_{rr}	rolling resistance coefficient of the tire [kg/kg]
D	hydraulic pump displacement [m3/rev]
E_{BAT}	energy of the battery [kWh]
E_{MAX_BAT}	maximum energy of the battery [kWh]
E_{MAX_SC}	maximum energy of the ultracapacitors [kWh]
Eff	efficiency [%]
E_L	energy left [kWh]
E_{sc}	energy of the ultracapacitor [kWh]
F_{mf}	force that the vehicle has to do to move forward (N)
g	gravity constant [m/s2]
i	gradient of the road [%]
i_t	transmission ratio [dimensionless]
i_f	differential ratio [dimensionless]
J_e	inertia of the engine [kg·m2]
J_w	inertia of the wheels [kg·m2]
K1	vehicle speed correction factor [dimensionless]
K_{SAV}	unitary saving related to the substitution of fossil fuel [euro/trip]
K_{OCOST}	unitary overcost related to the substitution of fossil fuel [euro/failure]
L	wheelbase [mm]
l	load of the vehicle [kg]
m	mass of the vehicle [kg]
mt	total dynamic vehicle mass [kg]
Na	number of arrows [dimensionless]
Nr	number of rows [dimensionless]
n_t	transmission efficiency [%]
n_f	differential efficiency [%]
ϕ	raw measured inclination [degrees]
P	pressure [Pa]

P0	gas pre-charge value [bar]
P1	lower working pressure [bar]
P2	higher working pressure [bar]
P_{CH}	charge power [kW]
P_{DSCH}	discharge power [kW]
P_{max}	maximum power [kW]
P_{mean}	mean power [kW]
Q	hydraulic oil flow [m3/s]
ρ	air density [kg/m3]
R_a	aerodynamic resistance [N]
R_i	inertial resistance [N]
RLFAL	relative level front axle left [mm]
RLFAR	relative level front axle right [mm]
RLRAL	relative level rear axle left [mm]
RLRAR	relative level rear axle left [mm]
R_{rp}	road profile resistance [N]
R_{rr}	rolling resistance [N]
RPM	angular speed of the engine [revs/min or rad/s]
rw	equivalent wheel radius [mm]
S	vehicle frontal surface [m2]
SOC	status of charge [%]
SOE	status of energy [%]
Sr	zone identification success rate [%]
T	torque [Nm]
v	speed of the car [m/s]
V	volume [m^3]
V0	effective gas volume [m^3]
V_{sc}	voltage ultracapacitor [volts]

1.
Introduction

This chapter outlines the main lines of inquiry on which this thesis research is engaged. It takes the reader from an introduction of the research field to the thesis's contents, through the hypothesis statements and the exposition of the specific objectives.

CONTENTS:

1.1. Background and Definitions

Ros Roca S.A. is a major refuse-collecting vehicle (RCV) manufacturer, whose headquarters are located in Tárrega (Spain). Starting its industrial activity in the 1940s, it produces around 2200 units yearly worldwide.

An RCV is a truck specially designed to collect solid waste and transport the collected waste to a treatment facility such as a landfill. Common names for this type of truck include trash truck, rubbish truck, bin wagon, dustcart, bin lorry or bin van. Technical names include refuse-collecting vehicle or waste-collecting vehicle. Depending on the technique used to load the RCV it can be classified as a front loader, side loader or rear loader.

Front loaders are generally used to collect large refuse containers. The RCV is equipped with forks on the front which the driver aligns with sleeves on the waste container. The waste container is then lifted over the truck to be emptied.

Fig 1. Front loader RCV

Rear loaders are generally used to collect medium to small waste containers. They have an opening at the rear into which the operators can throw waste bags or empty the contents of bins. In continental Europe they usually have a lifting mechanism to automatically empty bins or containers without the operator having to lift the waste by hand.

Fig 2. Rear loader RCV

Side loaders can be used to collect any volume waste container. They are usually loaded from one side (right or left), usually with the assistance of a controlled robotic arm, used to automatically lift and tip bins into the RCV hopper.

Fig 3. Side loader RCV

One specific application of side loaders is the bilateral lifting system, in which a crane placed between the truck cabin and the body can collect containers on both sides, lifting them over the hopper and unloading them from above the truck.

Fig 4. Bilateral side loader RCV

RCVs can be split into two main components, the body and the chassis.

The **body** is the component manufactured by a bodybuilder, which executes the refuse collection and compaction work. It is usually composed of a bin/container lifter, a refuse compactor and a refuse unloading mechanism. The elements which form the body are called **ancillaries** in this work. In most commercial RCVs the ancillaries are hydraulically powered by a hydraulic pump which is usually fitted to a power take off installed on the chassis engine or gearbox.

In the RCV sector the **chassis** is the name given to a truck which will be equipped with a body.

Before the start of this research project (end of 2009) Ros Roca had detected, among its clients, a keen interest in any technological developments which could reduce RCV fuel consumption.

When analyzing the operation costs of an RCV at the end of its lifecycle (typically about 10 years) it can be appreciated that fuel costs can represent about 25 to 45% of the total amount. At the end of a regular lifecycle the total amount of fuel consumed can be as high as 350,000 euros for a diesel truck. Few cost reducing alternatives are available industrially, the replacement of diesel powertrains by CNG powertrains being the most frequently used nowadays.

By the beginning of 2010 the price of a barrel of crude was over 100 $ [1] and an increase in this cost was forecast at the time. In this scenario the development of technologies which may lead to a reduction in fuel consumption is highly appreciated. High accuracy fuel consumption models are necessary in order to perform energy optimization studies with reasonable quality.

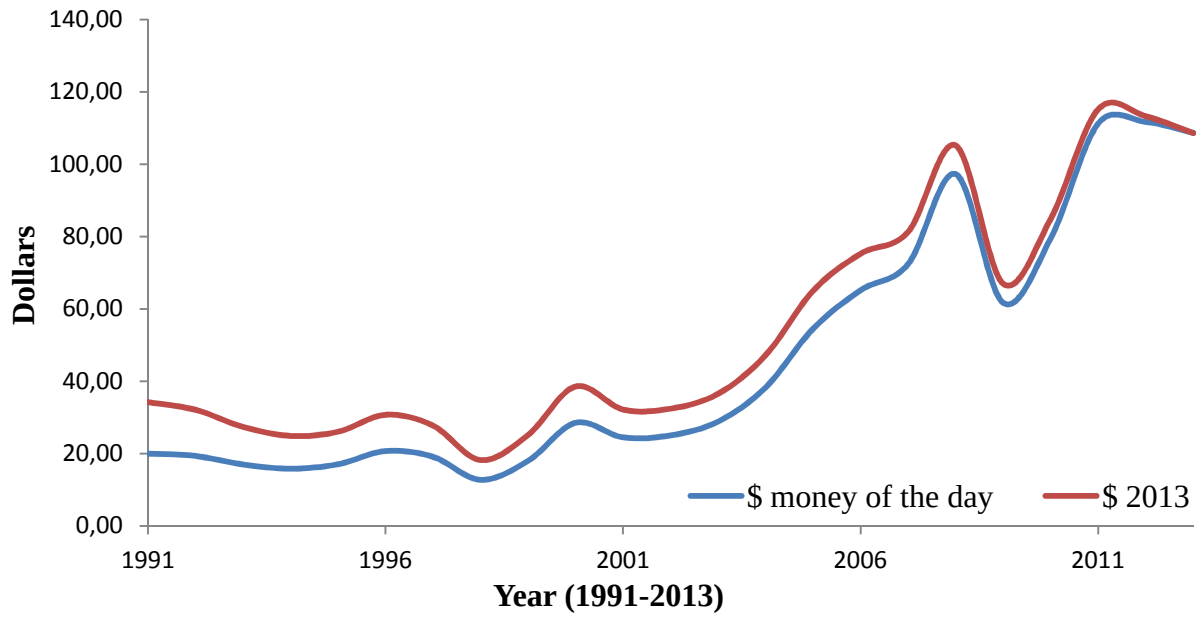

Fig 5. Historic Evolution of oil prices, 1991 to 2013

1.2. Research topic

Mathematical models describe our beliefs about how the real world functions. Translating these beliefs into mathematical language has many advantages. Probably the most important is the possibility of implementing these models in computers, which means they can be tested cheaply and quickly under different circumstances.

The use of mathematical models applied to engineering has been a revolution, and has speeded up the development of products and processes while increasing accuracy and efficiency.

In the automotive industry the use of mathematical models and simulation reaches all the facets of the technology related to the product development such as mechanics, aerodynamics, powertrain, combustion or electronics.

Refuse collecting vehicles represent an application which shares many aspects with other vehicles, but which also has specific circumstances. Among these specific circumstances we could mention the fact that the vehicle has a body which consumes power, that the vehicles are driven along the same routes daily, the possibility of predicting parameters during the drive cycles and the combination of large masses with an aggressive driving style.

The aim of this dissertation is to develop specific knowledge related to RCV drive cycles, to their alternative powertrain options and to the opportunities of predicting the drive cycle in real time.

Fig 6. Typical European RCV rear (left) and side (right) loader

Our proposal is to develop a new working concept which will serve to develop and validate fuel consumption models of Refuse Collecting Vehicles (RCVs). The model development is based on the improvement of the classic approach to vehicle dynamics. The validation methodology is based on recording vehicle drive cycles by the use of a low cost data acquisition system and post processing them by the use of GPS and map data. The corrected data are then used to feed the mathematical energy models and the fuel consumption is estimated.

Based on the fact that RCV are driven along the same route daily, specific algorithms which serve to estimate the driving mode of the vehicle and the energy that is needed to finish the route (energy left 'EL') can be estimated.

The driving mode identification is of major importance when developing hybrid-vehicle management strategies because the power demand varies, and so the powertrain can be prepared to deliver the energy demand before it arises.

Energy demand estimation (energy necessary to finish the route and arrive at the base) can be essential when working with fleets which have plug-in electric energy available at the base, which is the case of RCV. If this information is available, the vehicle management system can arrive at the base with the batteries depleted. In this way, the fossil energy consumption can be partially replaced by electric energy.

Finally, different power train configurations, based on different physical principles (hydraulic and electric) will be tested, in order to analyze and understand the advantages and disadvantages of each.

1.3. Research problem

Given the serious environmental problems and the anticipated fuel shortage of the next decades there is increasing demand for a lower environmental impact of RCVs. There is a lack of knowledge and research with regard to RCV energetic models, the analysis of their drive cycles and the impact of the main alternative powertrain architectures on its powering.

In order to reduce the RCVs emissions of contaminants, three main targets have been defined for this study:

The first target is the development of accurate RCV energetic models; these models have to be based on the coast down tests of the vehicle's energetic consumption, including aerodynamics, rolling resistance, inertias and road profile. It should also focus on the coast down of the body ancillaries, differentiating the elements of the body according the pump which feeds them. All the elements of the coast down have to be reduced to analytic expressions which will be directly implemented in the simulation software. As the final goal is to run the models on real routes, a data acquisition system capable of feeding the analytic expressions of the model will have to be developed.

The second target is to study the possibility of developing algorithms which can predict parameters of the RCV **in real time**. These parameters should include the possibility of estimating the amount of energy we will need to finish the current route, and the power demand mode of the power train. The power demand mode identification (transport or collection) is of major importance when developing hybrid-vehicle management strategies because the power demand varies in level and in terms of its transient characteristics for transport and collection. The energy generation system on board (fuel cells, engines, batteries) can be prepared before the energy demand arises. Energy demand estimation (energy necessary to finish the route and arrive at the base) can be essential when working with fleets which have plug-in electric energy available at the base. If this information is available, the vehicle management system can arrive at the base with the batteries depleted. In this way, the fossil energy consumption can be partially replaced by electric energy.

The third target is to study the performance of different possible architectures for an RCV, considering the hybrid-hydraulic and hybrid-electric as the main possibilities. Compared to electric hybridization, the hydraulic hybridization offers higher power density but lower energy density [2]. Hydraulic hybridization seems to be the technical option which is best suited to vehicles with high power flows, such as heavy machinery. On the other hand, electric hybridization seems to be the best technical option for cars. Refuse collecting vehicles (RCV) and urban buses remain in an intermediate situation. In this part of the work different architectures based on these technologies should be modeled and simulated and their fuel consumption results compared.

1.4. State of the Art – Literature Review

Due to the increasing public interest in environmental issues in general and fuel consumption reduction in particular, a variety of transport related strategies and technologies are currently under development to reduce the energy consumption of road traffic.

This thesis is focused on the analysis of energy flows and intelligent energy management systems for refuse collecting vehicles (RCV), as well as the application of this knowledge to RCV powertrains. The research work has been organized into four work packages which correspond to four different publications: the RCV energy models, the RCV drive cycle identification and energy demand estimation, the hybrid-hydraulic powertrains for RCV and the hybrid-electric powertrains for RCV.

The literature review, carried out prior to the thesis development, has also been organized around these four work packages, adding a final section which comments on the commercial proposals for hybrid RCV.

State of the Art of RCV energy models:

High accuracy fuel consumption models are necessary for performing energy optimization or pollution emissions studies with reasonable quality. Working with these models, fuel consumption optimization can be carried out by analyzing different vehicle architectures as well as alternative powertrain performances or power split control strategies, in the event of different power sources on board. The use of these methods can also predict the local emissions of vehicles during a drive cycle.

RCVs energy models are in fact an evolution of vehicle energy models which consider the consumption of the body ancillaries. There is a classic approach for deterministic vehicle energy models [3]-[6] which is based on breaking down the energy consumption of the vehicle into aerodynamics (R_a), rolling resistance (R_{rr}), road profile (R_{rp}) and vehicle inertia (R_i considering both linear and rotational) as follows:

$$R = R_a + R_{rr} + R_{rp} + R_i \tag{1}$$

$$P(kW) = \frac{1}{2}\rho(SC_x)v^3 + C_{rr}(m+l)gv + mg(sin\alpha)v + m_t av \tag{2}$$

Despite the fact that the deterministic energy models are well known, the parameters necessary to use these models are usually unknown. The most difficult parameters to identify are the road profile (α), the vehicle drag (SC_x aerodynamic coefficient) and the vehicle speed (v), which is a value that usually has errors associated with wheel deformation because of the tire wear and vehicle load. In the case of RCVs the hydraulic flow is also a difficult parameter to estimate.

To estimate the road profile of a road geolocation [7], loads per axle [3] or inclinometers [8] can be used, with some authors [3, 8] proposing the use of test rigs or test tracks as patterns to calibrate the measurements.

For the vehicle drag estimation the use of wind tunnels is the best option, despite the fact that cheaper (and less accurate) options exist, such as the vehicle coastdown test.

In all the studies found [3, 7, 8] the vehicle speed is taken straight from the vehicle J1939, geolocation or tachograph. But no follow up treatment is proposed to improve this measure.

Until now little work has been done in the model development, drive cycle studies or fuel consumption estimation of Refuse Collecting Vehicles (RCVs) [9]-[17], which have a very specific drive cycle.

Regarding the drive cycle studies, some authors [9]-[10] have proposed the use of data logging systems and statistical analysis to show how the drive cycles are composed, and use this knowledge to generate fictitious but realistic drive cycles in which the vehicle models can be run. These drive cycles can be used to estimate the fuel consumption of vehicle models [9] or size powertrains [10]. This working technique can reduce the virtual drive cycles generation cost but is less accurate than working with complete real routes.

Other authors build RCV drive cycles by logging part of a real cycle, and repeating this register over time [11], assuming that the cycle is always the same. In this work the drive cycles are used to simulate simplified powertrain models for RCVs (models based on theoretical approaches rather than on models empirically contrasted), whose components' size is optimized by the use of the Simplex method. This way the proposed components are optimally sized for a certain drive cycle, but the variability which can be found in real cycles [9, 10] is not considered.

In other published works related to RCV models [12] the drive cycles are built by data logging systems and statistical analysis, but the parameters' input is reduced by assuming the drive cycles to be unrealistic up to some point. According to the authors the road profile and the vehicle load were supposed to be constant. This simplifies the data acquisition and the vehicle model development, but introduces significant errors in some cases. E.g. the city of Vigo (North-Western Spain) has several streets with profiles of over 25%, and an RCV of 27m3 can increase its load by 15 tons during the collection work (about 100% weight increase from the starting value).

Some authors [13, 14] have also proposed works related to RCV models which focus on the control strategies of the powertrain components, analyzing the dynamic performances of the powertrain instead of their efficiency or fuel consumption; these works are based on simplified vehicle models and do not use complete drive cycles but segments of the drive cycles.

To end with the state of the art RCV models, other authors [16] have proposed the use of real drive cycles, powertrain models based on engine BSFC maps and PI based controllers, which match the model speed with the real logged speeds. This project was focused on the study of powertrain characteristics and the vehicle power consumption was reduced to rolling resistance and aerodynamics, ignoring rolling inertias and road profiles.

Finally, regarding the RCV energetic and pollution studies: one work [15] can be found which proposes the use of portable laboratories to measure the pollutant emissions of RCVs. The study compares the emissions of diesel fuel ICE with two different natural gas ICEs. This test is performed by running the vehicles on the CBD test, which is a drive cycle conceived for testing buses rather than RCVs. The use of high accuracy RCV models could be used for these estimations.

The use of expensive or inaccurate measurement techniques remains a difficulty for testing. Any option which could lead to a cost reduction in estimating these parameters accurately would be appreciated. The development of these models and data logging techniques is the goal of chapter 3 of this thesis.

State of the Art of Drive Cycle Identification and Energy Demand Estimation:

Drive cycle identification and future energy-demand prediction are advantageous when developing hybrid propulsion systems. They are applicable to vehicles that are driven along the same route everyday, such as buses, refuse-collecting vehicles (RCVs) or delivery vehicles.

Drive cycle identification can be used to identify what power transients can be expected to prepare the power train to operate under these conditions.

Knowing the future power demands of a drive cycle is advantageous for these algorithms [18]. Therefore, the development of this knowledge is the main goal of chapter 4 of this thesis.

Several authors have proposed the use of on-board GPS systems that record the parameters of repetitive drive cycles. As the vehicle is run daily on the same route, the previously generated information is used to predict these parameters in real time for the current drive cycle [19]. The use of this technique in a real test reduced the fuel consumption of a vehicle by 5%.

The use of geolocation has also been used to infer the relative position of a vehicle on a well-defined route, associating this relative position with the statistical knowledge of the power demand has proved useful in significantly reducing fuel consumption [20], achieving fuel savings of 6 to 9%.

Based also on the use of geolocation, a study has been found which focuses on the analysis of the regularity of a driver's travelling behavior, concluding that a large portion of a typical driver's trip is repeated [21]. This is of major importance for the development of artificial intelligence systems which

can predict drive cycles, because the repetition opens the possibility of developing learning algorithms which can make predictions in the future.

Other authors have developed artificial intelligence (AI) systems which can acquire the essential knowledge about fuel efficiency on well defined drive cycles (pattern cycles) with their associated road types and traffic congestion levels. These AI algorithms, once trained, can also predict the road types and traffic congestion levels in real time, adapting the powertrain control strategy to reduce fuel consumption [22].

The application of artificial intelligence has also been proposed for the identification of driving environments, the driving style of the driver and the driver's operating mode [23]-[24]. In these works the information inferred is used to define the power split strategy of hybrid vehicles, optimizing fuel economy and reducing emissions.

If the energy management algorithm of a hybrid vehicle can account for future energy demand, then it can be arranged in such a way that the non-fossil-fuel energy sources (such as electricity stored in a battery) are fully depleted at the end of the drive cycle.

Related to this subject two patents have been found. The first one [25] proposes a charge depletion method and hardware concept for operating the electric motor and range extender, in a hybrid electric vehicle (HEV). In this patent the operation of the electric motor and range extender are coordinated as a function of a control strategy for the range extender, based on the desired minimum fuel consumption or minimum vehicle pollutant emissions.

The second patent [26] integrates an on-board geolocation system to provide parameters for energy management for an electric vehicle (EV) or a hybrid-electric vehicle (HEV). In the associated strategy, a vehicle system controller integrates the geolocation system information with energy management while en route to a known destination. Current vehicle location is continuously monitored, expectations of driver demand are determined, and vehicle accommodations are made.

State of the Art of Hybrid Hydraulic Powertrains Applied to RCVs:

There is a strong impetus for development of fuel efficient vehicle propulsion systems, with hybridization being the only approach offering significant energy breakthroughs in the short and midterm.

This technological option is particularly interesting, although complex, when combining vehicles with significant weight, power, and drive cycles with a large number of starts and stops. This is the case of urban buses or refuse collecting vehicles [10, 16, 27, 28]. Compared to electric hybridization, hydraulic hybridization offers high power density but lower energy density [2].

Several works have been found which focus on the study of hybrid hydraulic powertrains [19], [2], [29]-[34].

In [19] a clutchable hybrid-hydraulic architecture is proposed. This architecture is implemented both on a theoretical model and on a real vehicle. Working on simulations of the theoretical models a rule-based software is developed, which can make predictions on the route, and this software is implemented in the real vehicle. The kind of vehicles in which the system is implemented and the route predicted are inspired by RCVs, but are not real RCVs.

A similar proposal can be found in [31] and [34], replacing the fixed rule-based software by a strategy optimized by the use of dynamic programming. Also the paper [32] works according to this concept, being different because the work considers the ensemble ICE-hydraulic system for the study, developing a powertrain specifically conceived for working in urban cycles (NEDC and FPT75).

In [2] a parallel hybrid hydraulic architecture is proposed and simulated. The most interesting aspect of this work is that the models are based on real components, which are mass produced and commercially available. The simulation is performed on a short route which maintains the similarities with RCVs or urban buses, but yet again are not real RCVs.

Regarding the theoretical models which are focused on approximations to real components, the best technique is the hardware in the loop. This is a technique that is used in the development and testing of complex real-time embedded systems, and it allows the interaction of real components, with models implemented in computers which can be either real or theoretical. Several papers based on this technique can be found which study the impact of the hydraulic hybridization.

In [29] the authors implement a real powertrain composed of an engine, a hydraulic motor and hydraulic accumulators on a test bench. Based on the hardware in the loop technique the real powertrain powers a virtual vehicle and runs it on a digitalized real route, and the real emissions of the engine are measured. The kind of vehicle and the kind of drivecycle are not related to RCVs.

The use of hybrid hydraulic powertrains has also been studied in FMVT [29] (tactical vehicles for military applications), simulating this kind of vehicle in a FUDS cycle and achieving fuel savings of about 20%.

Before closing this section it has to be commented that the only work found which studies HHV applications on RCV is [16]. In this work the route logging system is based on [27], which takes information straight from the J1939 and J1708 buses of the vehicle, including information from an internal GPS which is installed on the vehicle. Despite the fact that the datalogging kit [27] generates data to estimate the road profile (known as *vehicle head* in this work), in [16] the road profile is always assumed to be zero, which would introduce significant errors in certain cities, as commented in the “State of the Art of RCV energy models” section.

State of the Art of Hybrid Electric Powertrains Applied to RCVs:

Different factors, such as the decrease of fossil fuel reserves, high oil prices, energy security concerns and climatic change, indicate that a progressive reduction in the use of ICEs for the transport sector is desired.

One of the most interesting alternatives is the introduction of devices that could use the energy in a more rational way, storing energy during regenerative breaks or when the ICE is working at high efficiency points; and assisting it when high power demands are required or when the ICE is working at low efficiency points.

Considering these kinds of devices, several studies can be found in literature. Different alternatives are described, the electric hybridization [35]-[42] and hydraulic hybridization [2],[19], [29]-[33] being the most typical ones.

The studies related to electric hybridization focus on topologies/architectures [36, 40, 41, 43, 44] control strategies [14, 35, 38, 39, 42] or analysis of the state of the art of the technology [37].

Most of the reviewed work is based on simulation of a real vehicle on standard cycles not related to RCV. In [36] a virtual vehicle is simulated on a FUDS drive cycle to analyze an improved topology (FC-Battery-SC) which allows the suppression of one inverter wihout losing power control performance. In [44] a study comparing different electric architectures (FC-Battery, FC-SC and FC-Battery-SC) is presented, the vehicle model is inspired by a real SUV (GM Equinox) and the drivecycles are also standard (FUDS), and in [42] a tourism car model is run on different drive cycles (UDDS, HWFET, US06 and ECE/EUDC) in order to test an energy management strategy based on fuzzy logic.

In [35] and [43] detailed studies of the application of fuel cells to electric automotive applications have been proposed. The first one is focused on the hybridization degree analysis and the electrical topology while the second one focuses on the energy management strategies. Both papers perform their simulations on standard cycles (NEDC, UDDS, FTP, HWFET).

Some works can be found which perform the simulations in a piece of a real drivecycle [14, 38]. The potential implementation of hybrid powertrains is also being studied in non-road vehicles; in [38] the potential implementation of an FC/Battery/SC hybrid system for a railway is studied.

The use of electric powertrains in applications for vehicles with big power flows remains residual, and none of the previously commented articles are related to RCV vehicles or drivecycles.

The only research work found which focuses on electric powertrains for RCVs is [14]. In this work a real electric-hybrid vehicle developed by an RCV manufacturer (Mc Nellius, Oshkosh corporation) is modelled for simulation. The drivecycles used in simulations are pieces of real drivecycles instead of complete RCV routes, and the road profiles are supposed to be null during all the simulation work. This paper implements optimization algorithms to minimize the fuel consumption, based on Pontryagin's

minimum principle. The power demand is assumed to be a known parameter of the algorithm. Working with this technique the authors obtained fuel consumption reductions of 5 to 11% in simulations; no empirical contrasting of the models has been found.

Commercial Proposals for Hybrid RCV:

A list of the vehicles commercially available or subject to demo tests is presented below; in each of them the technically available information is summarized.

1. MAN Metropolis:

Hybrid electric series vehicle based on a MAN TGS 6x2-4. Modular lithium-ion battery with a maximum capacity of 105 kWh. An electrical motor (203 kW) drives the truck's rear wheels via a two-speed automatic gearbox. The range extender is a compact diesel engine V6 TDI from the Volkswagen Group: in conjunction with a generator it delivers 150 kW (204 hp)

Fig 7. MAN Metropolis hybrid electric RCV

2. PVI Full Electric.

Full electric vehicle. Motor: 103 kW / 400 V LQ 160P asynchronous electric. Gearbox: ZF 6S800 TSO manual, automated by air activators. Batteries: 2 Lithium-ion battery packs with a total charge of 170 kWh (battery weight: 2 tons). Battery recharge: Mains 380 V/64A outlet and braking energy recovery Full charging time: approx. 7h. Operating range: 120 km (without partial recharge).

Fig 8. PVI full electric RCV

3. FCC Full Electric with range extender:

Full electric vehicle equipped with a range extender. Range extender CNG Engine 200 kW and Genset 150 kW [45]. Electric traction motor 300 kW. Electric batteries from 70kWh to 150 kWh (no additional information available).

Fig 9. FCC full electric with range extender

4. Renault Trucks Hybris:

Hybrid-electric parallel vehicle based on a 26 t Renault Premium 6x2 with 340 cv engine Euro V. Electric motor 70 kW. Electric batteries 85 *kWh* lithium iron phosphate battery pack (138 Ah / 615 V).

Fig 10. Renault Trucks Hybris RCV

5. Dennis Eagle Hybrid Urban Commercial Vehicle (HiUCV):

This vehicle is currently under development (February 2015) and no technical information is available to date.

Fig 11. Dennis Eagle Hybrid Urban Commercial Vehicle (HiUCV)

6. Parker RunWise:

Hybrid-Hydraulic clutchable parallel powertrain based on Autocar RCV. As the engine is the original ICE the only performance affected is the fuel consumption (reduction over 30% according to commercial information).

Fig 12. Autocar RCV equipped with a Parker Runwise system

7. Motiv Full Electric:

Full electric vehicle based on a CCC (Crane Carrier Company). Lithium ion modular battery of 200 kWh. Maximum speed 50 mph. Electric traction motor 280 kW. Range 60 miles.

Fig 13. Motiv full electric vehicle

1.5. Hypothesis

In order to address the presented research problems, the following hypotheses have been proposed as the starting point for this research work:

- When the vehicle is being driven its energy consumption can be modeled like the consumption of any other vehicle.

- When the vehicle is stopped and the ancillaries activated, its energy consumption can be modeled like the consumption of a steady hydraulic machine which is powered from an internal combustion engine.

- The aerodynamic coefficient of the machine will remain constant and will be the same as the coefficient measured on the coastdown test, with the compactor on the top and without operatives on the footboards.

- The rolling resistance of the vehicle can be reduced to the tires' resistance, as this value is preponderant. The values considered will be the same as those the tire manufacturer measured in its tests.

- The minor errors detected in the inclinometer signals will not be considered for the simulation, which means that the models will occasionally have to assume unrealistic transients.

- Wind speeds lower than 10 km/h do not affect energy consumption substantially.

- The lower heating values of the fuels will be the same as the tabulated values found in [46].

- Quasi-static simulations are accepted as valid for analyzing both steady and transient energy flows.

- BSFC maps (g/kWh) are valid to estimate the engine fuel consumption.

These hypotheses represent the basis of the resulting thesis research. The assumptions are investigated by means of the research work reflected in this dissertation.

1.6. Aims and objectives

- Develop energetic models of RCV based on the classic energetic coast down which includes: aerodynamics, rolling resistance, road profile and vehicle inertia.

- Improve the energetic models based on the classic energetic coast down by including the models of the body ancillaries' power consumption.

- Build a data acquisition system able to log all the parameters included in the RCV improved energetic model, and develop tests conceived to post-process and adjust the logged parameters.

- Test experimentally these models and evaluate their accuracy.

- Develop an algorithm which can identify the current drive cycle of a RCV in real time.

- Develop an algorithm which can predict the energy needed to finish the current route in real time. This algorithm has to be fully implementable in an automotive processor, and has to be programmable to estimate any necessary parameter by itself.

- Develop and test a hybrid-hydraulic power train model based on the study of the ICE work and evaluate its performance.

- Develop and test a hybrid-electric power train model based on the study of the ICE work and evaluate its performance.

- Contrast the performance of the different architecture proposals and draw conclusions.

1.7. Chapter descriptions

In order to cover the disclosed objectives, the research work of this thesis has been divided into nine different stages with an additional chapter commenting on the dissemination of the results. All of them are reflected in the chapters described below

A literature review of previous works related to RCV, to drive cycle analysis and to the study of hybrid-hydraulic and hybrid-electric power train is shown in **chapter 1**.

In **chapter 2,** based on experimental data acquired from the real services of refuse collectors, the drive cycle of an RCV is analyzed. The drive cycle is separated into its main segments which are the same for any RCV route, and the power demand mode of each segment is analyzed and identified.

In **chapter 3**, the RCV energetic models have been developed. A new technique based on cartography and geolocation, which is used to adjust parameters in the RCV models, has been developed and its accuracy has been assessed by an experimental dispositive. Finally the performance of the whole model has been contrasted with experimental data.

In **chapter 4**, an algorithm is developed to estimate in which of the segments, identified in chapter 2, the vehicle is driving and its accuracy is evaluated. As a result the power demand mode associated to the driving cycle is identified.

In **chapter 5**, an algorithm capable of estimating the energy necessary to finish the current route (E_L) is developed and its accuracy is evaluated.

In **chapter 6** the principal conclusions related to the analysis of the working modes of the ICE of an RCV are presented.

In **chapter 7**, a hybrid hydraulic architecture is proposed and its fuel consumption is evaluated in a set of real drive cycles. Also this hybrid-hydraulic architecture is used to estimate the impact of the knowledge of the power demand mode on vehicle efficiency.

In **chapter 8**, three hybrid-electric power train architectures based on combinations of fuel cells, batteries and ultracapacitors have been proposed. They have been dimensioned so as to reproduce the performance of the ICE, and their fuel consumption, operating on the same set of routes used in chapter 7, is estimated.

Each chapter concludes with a partial conclusion focused on its respective subject; in **chapter 9** general conclusions considered from a global point of view are presented, and the industrial implications of each of the conclusions are emphasized.

Finally, the publications and collaborations resulting from the research work development are presented in **chapter 10**.

2.
Refuse Collectors Drive Cycle

This chapter proposes an RCV drive cycle analysis based on real data, identifies a universal speed profile of the drive cycle and proposes a method to fit any real profile into this theoretical speed profile by the use of parameterization.

CONTENTS:

2.1. Introduction

Drive cycle identification is advantageous when developing hybrid propulsion systems. It is applicable to vehicles that are driven along the same route every day, such as buses, refuse-collection vehicles (RCVs) or delivery vehicles [47].

Drive cycle identification can be used to identify which power transients can be expected, in order to prepare the powertrain to operate under these conditions.

Given that RCVs always drive in similar drive cycles, a drive cycle has been modeled and its main characteristics parameterized. The model is separated into different drive cycle segments which are related to different power-consumption modes.

This part of the work sets the basis of the knowledge of RCV drive cycles, which will be used in chapter 4 to implement algorithms that will identify in which driving mode the vehicle is working, in chapter 7 to define hydraulic powertrains and in chapter 8 to define electric powertrains.

2.2. Drive Cycle Background and Definitions

An RCV **'route'** includes pick-up of bins and containers (waste receptacles as defined in the standard EN 840 or equivalent) on designated locations, which have to be collected by the same vehicle. In some countries, the concept of bins or containers in the streets is unusual; in this case, the route is a list of streets of buildings that have to be driven through by the RCV.

RCVs which work any one area are usually operated by a services company which has a specific space to park, clean, and maintain its vehicles. In this work, this space will be called **'base'**.

When RCV routes are designed, one of the factors considered is that they have to be performed in a standard working day (7 to 8 hours). On this route, the vehicle driver must at least be able to drive from the base to an area of the city; do the refuse collection; take the refuse to the transfer station (or landfill site); and come back to the base (in this work, this drive cycle will be called a **'trip'**). The most common case is to do two trips on a standard working day. Then the route can be divided into eight route segments which define the drive cycle, referred from now on as **'RCV route segments'**.

These route segments are:

1. Vehicle heating up and testing.
2. Trip from the base to the collecting area 1.
3. Collecting work in area 1.
4. Trip from the collecting area 1 to the landfill.
5. Trip from the landfill to the collecting area 2.
6. Collecting work in area 2.
7. Trip from the collecting area 2 to the landfill.
8. Trip from the landfill to the base.

The 'unloads' at the landfill site of the refuse collected at areas 1 and 2 are performed after the route segments 4 and 7, respectively.

RCVs drive through the same route (or routes) daily but the drive cycle is not the same each time. The working crew can drive through different streets because of maintenance operations in the streets, emergency vehicles working (such as those of the police or firefighters), traffic flows (traffic lights or jams), or just use different ways because the crew driver is substituted. This situation generates an ideal environment to develop tools which can predict information for energy management algorithms applied to vehicles which run on repetitive routes.

In this work, the RCV's daily route is considered a parameterized route. The daily drive cycle always has the same morphological speed profile but a list of parameters will add modifications generating similar but different drive cycles. These are distance travelled, vehicle instantaneous speed, number of bins lifted, compaction cycles, and number of RCV unloads.

In the parameterized route, the vehicle is considered to work in eight different route segments (introduced in the previous page), which belong to two different working modes of the power train.

Fig. 14. Theoretical speed profile of an RCV route (speed vs. time) and associated eight route segments

The first mode is the vehicle transport part of the drive cycle, in which the drive cycle is characterized by higher speeds and slower power transitions. This usually happens on major roads, where the vehicle maintains high speed for a longer time. RCV route segments 2, 4, 5, 7, and 8 are characteristic of this mode.

The second mode is the refuse-collecting drive cycle. In this mode, the vehicle is accelerated and stopped aggressively from one bin collection to the next one, when the vehicle is stopped, the bin lifting machinery and the compacting machinery are actuated. This working mode is characterized by lower speeds but faster and bigger power transitions. This happens almost always in urban areas. RCV route segments 3 and 6 are characteristic of this mode.

The RCV road segments 2, 4, 5, 7 and 8 on the one hand and 3 and 6 on the other hand could be considered as the two main categories (transport and collection respectively).

Nevertheless, we have decided to keep the eight-route segment identification because this information could be of interest for future works related to RCV power management strategies. The differences in the segments included in these two main categories of the route segments can be observed. For example, route segment 3 finishes when the vehicle body is filled with refuse, but route segment 6 finishes when the last bin/container of the route is reached. The weight transported on routes 4 and 7 will not be the same, what then would affect the vehicle dynamics. In a big RCV, such as a 27-m^3 body, the vehicle can transport up to 15 tons of refuse. Route segments 2, 4, 5, 7, and 8 would show the differences. Route segments 2, 5, and 8 are performed with an empty RCV body; route segment 4 is performed at full body load; and route segment 7 is performed at partial load.

In Fig. 15 and Fig. 16, two real speed profiles are plotted. The first one corresponds to a route with long trips on the RCV route segments 2, 4, 5, 7, and 8. The second one corresponds to a route with short trips on the same route segments. The difference can be easily observed on the higher and wider

profiles of the first plot. In both cases, the theoretical profile is the same but the parameters' speed and distance travelled mean that this is a different drive cycle.

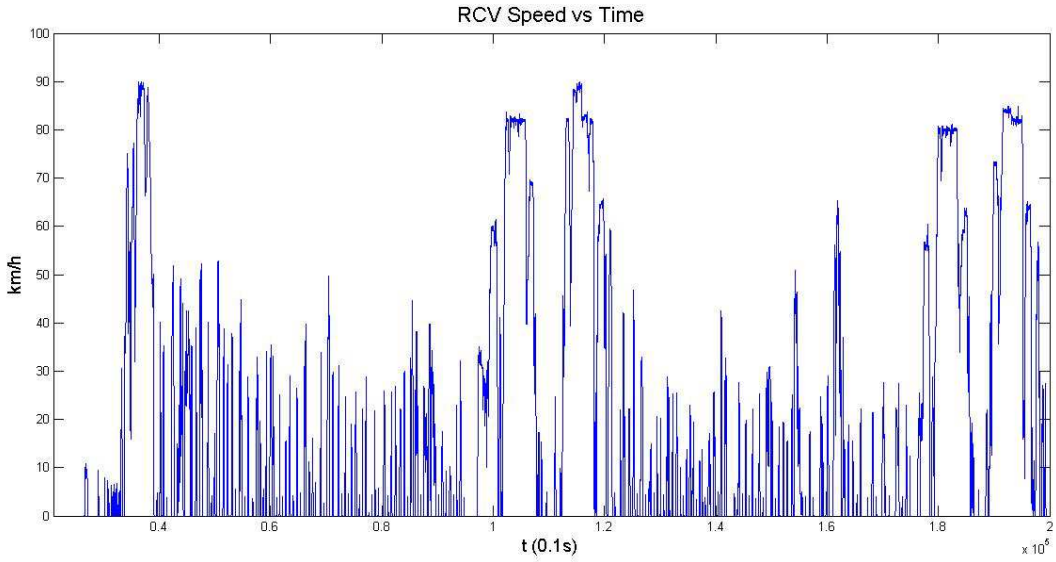

Fig. 15. Real speed profile of an RCV route, with long trips on route segments 2, 4, 5, 7, and 8

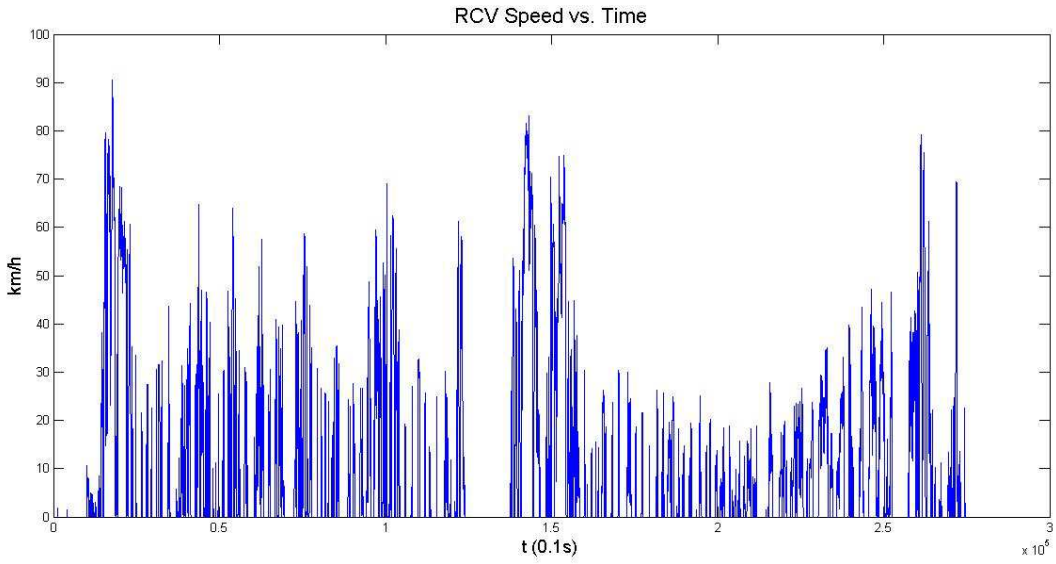

Fig. 16. Real speed profile of an RCV route, with short trips on route segments 2, 4, 5, 7, and 8

RCV route segment 1 is to the vehicle heating up and testing on the base before starting the collection cycle, as its time and energy consumption are very small it is not considered as a relevant working mode and is neglected in this study.

2.3. Power Consumption in Transport Mode and in Collecting Mode

Due to the fact that the different RCV route segments have different power demand characteristics, the capacity to know in which RCV route segment the vehicle is working is an advantage for the management algorithms in case of use of hybrid powertrains. So there is an interest in **Drive Cycle Identification** (chapter 4 of this thesis) and **Energy Demand Estimation** (chapter 5 of this thesis).

The power demand-mode identification (transport or collection) is of main importance when developing hybrid-vehicle management strategies because the power demand varies in level and in terms of its transient characteristics for transport and collection.

The transport mode is characterized by power demands with high mean values, few transients and no regenerative breaking. In this mode, the energy storage systems (batteries, ultracapacitors) should be charged at its maximum levels to be able to assist energy generation systems (engine, fuel cells) when high power demands happen. This power-demand mode identification is meaningful under some circumstances such as engine downsizing, or the use of energy-generation systems with slow dynamics.

As an application example, devices such as fuel cell range extenders have slow power dynamics compared with the power train needs which means that they need to be prepared to deliver a certain power amount before the power demand exists. The RCV route segment identification can provide this information.

Experimental measurements show that the average power consumption of RCV in this mode is about 90 to 120 kW.

The collection mode is characterized by low power demand, with strong transients and regenerative breaking. In this mode, the energy storage systems should have the capacity available to absorb energy when breaking. This power demand mode identification is relevant when defining SOC set points in energy storage systems, and also when defining the working points of the energy generation systems, which can work at steady conditions while the transients are assumed by the energy storage systems.

Experimental measurements show that the average power consumption of RCV in this mode is about 17 to 25 kW.

2.4. Discussions and conclusions

Based on the analysis of real RCV drive cycles has been found that in all the analyzed cases the RCV vehicles are operated in the same way. They are parked in a base where maintenance and cleaning works are performed, they are driven to an area of the city where the refuse collecting work is performed, and are driven to a place where the refuse is dumped (landfill or transference station).

It has been found that all the RCV drive cycles follow an arrangement which can be divided in eight segments. And each one of these segments has a well defined power consumption pattern.

As a result there is the possibility to define a parameterized pattern which can match any RCV real drive cycle just tuning parameters, and associate power consumption with the instant of the drive cycle.

3.
Refuse Collectors Energetic Models

This chapter defines how the models which will serve to simulate the RCV are built, how the parameters to tune these models can be measured, and how the real data necessary to run simulations can be acquired from real RCV services. To end with, an experimental device is operated specifically to measure the accuracy of the whole working concept.

CONTENTS:

3.1. Introduction

The main goal of chapter 3 of this thesis is to define the vehicle energetic models which will be used later in the vehicle simulations; this is done by identifying the forces acting on the vehicle and the equations which will serve to estimate these forces.

In this project the primary forces of interest in the simulation of vehicle dynamics are those acting on the longitudinal axis of the vehicle (longitudinal dynamics), those acting on the vehicle via the tire-road interface, aerodynamics, the road profile resistance and the vehicle inertia. These forces act to both accelerate and brake the car.

All the equations associated with the longitudinal dynamics of a vehicle are very well known and the main difficulty lies not in the identification of these equations but in estimating some of the parameters necessary for use in these equations.

Some parameters, such as the aerodynamic coefficient or the rolling resistance, need expensive facilities in order to be measured accurately. Some others, such as the vehicle speed or road profile, can have important inexactitudes in the standard measurement system.

In the current chapter of this thesis the RCV energetic models are built, specific tests have been carried out to measure all necessary parameters and a specific data logging system to acquire real vehicle data has been developed. To avoid the use of expensive facilities or hardware, low cost hardware and information freely available on Internet has been used.

To finish with, a specific test has been carried out to test the model's accuracy, by contrasting the vehicle fuel consumption as measured in the fuel pump with the fuel estimated via the developed models.

3.2. Vehicle Dynamics Theoretical Approach

Using the classical approach found in literature [4, 5, 6], the vehicle power and energy breakdown has been done as follows:

3.2.1. Aerodynamic Drag

In automotive aerodynamics, the drag (sometimes called air resistance or aerodynamic resistance) refers to forces acting opposite to the relative motion of the vehicle moving with respect to the surrounding air. It can be estimated as:

$$R_a = \frac{1}{2}\rho(SC_x)v^2 \quad (3)$$

where:

1. ρ ≡ air density [kg/ m3].
2. S ≡ vehicle frontal surface [m2].
3. C_x ≡ aerodynamic drag coefficient [dimensionless].
4. v ≡ speed of the car [m/s].

3.2.2. Rolling Resistance

In automotive engineering the Rolling resistance is the force resisting the motion when the tires rolls on the road. It is mainly caused by non-elastic effects; that is, not all the energy needed for tire deformation is recovered when the pressure is removed. In a broader sense the rolling resistance incudes also the friction of the powertrain from the gearbox secondary shaft to the wheel axis. It can be estimated as:

$$R_{rr} = C_{rr}(m + l)g \quad (4)$$

where:

1. m ≡ mass of the vehicle [kg].
2. l ≡ load of the vehicle [kg].
3. C_{rr} ≡ rolling resistance coefficient of the tire [kg/kg].
4. g≡ gravity constant [m/s^2]

3.2.3. Road Profile Resistance

When the road in which a vehicle is driving through is not flat, the gravity force vector is not perpendicular to the road surface. As a consequence the gravity force vector is decomposed in two vectors being one perpendicular to the road surface and the other parallel. This parallel vector will develop a force whose sense depends on the angle of the road (road profile). Depending on the sense

this resulting vector will be in favor or against the movement of the vehicle, adding or subtracting power to the vehicle dynamics.

In automotive engineering this parallel force vector is the Road Profile Resistance (Rrp).

The gravity force, as shown in Fig.17, is decomposed as:

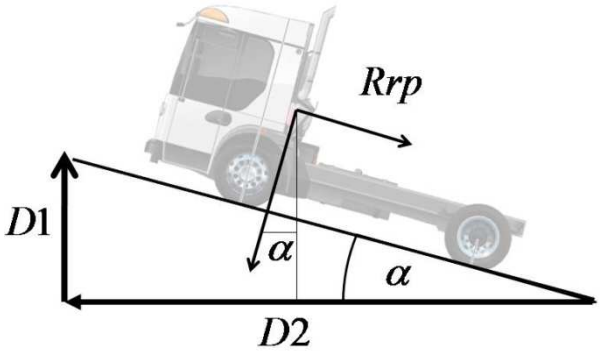

Fig. 17. Gravity vector decomposition

$$i\% = \frac{D_1}{D_2}100 = 100tan\alpha \quad (5)$$

$$R_{rp} = g(m + l)sin\alpha \quad (6)$$

where:

1. g ≡ gravity acceleration [m/s^2].
2. α ≡ angle of the road [radians].
3. i ≡ gradient of the road [%].

3.2.4. Inertial Resistance

Inertia is the resistance of any physical object to any change in its state of motion, including changes to its speed and direction.

In automotive engineering this resistance to change this state of motion is known as inertial resistance. When the vehicle changes its speed, two types of inertia will resist the acceleration. These inertias are related to the rotating components (engine components, gearbox, wheels, etc.) and to the linear movement of the vehicle mass.

$$R_i = (m_t)a \quad (7)$$

$$m_t = m + \frac{J_w}{r_w^2} + \frac{i_t^2 i_f^2 n_t n_f J_e}{r_w^2} \quad (8)$$

where:

1. m_t ≡ total dynamic vehicle mass [kg].
2. Jw, Je ≡ inertia of the wheels and engine [kg·m^2].
3. i_t, i_f ≡ gear and differential ratios [dimensionless]
4. n_t, n_f ≡ efficiencies [dimensionless]
5. r_w ≡ equivalent wheel radius [m]

3.2.5. Body Ancillaries

Some special application vehicles also consume energy to operate the body, and this is true of most RCVs. A typical RCV has a compactor and a lifter, which are powered from the engine through a hydraulic pump.

The method to calculate the Body Ancillaries instantaneous power consumption is:

$$P(kW) = Q \cdot P \tag{9}$$

where:

1. Q ≡ hydraulic oil flow [m^3/s].
2. P ≡ pressure [Pa].

3.2.6. Total Power Consumption

The total power consumption can be expressed as the force that the vehicle has to do to move forward (F_{mf}) multiplied by its speed plus the body power consumption:

$$Power = vF_{mf} + Body_{PC} \tag{10}$$

The resistance to the forward motion can be expressed as the sum of all the resistances (aerodynamic, rolling, road profile and inertia):

$$R = R_a + R_{rr} + R_{rp} + R_i \tag{11}$$

Finally, the power consumed by the vehicle will be expressed as follows (a hydraulic body is assumed, as it is the most common):

$$P(kW) = v\begin{bmatrix}\frac{1}{2}\rho(SC_x)v^2 + C_{rr}(m+l)g + \\ mg(sin\alpha) + m_t a\end{bmatrix} + QP \tag{12}$$

$$P(kW) = \left[\frac{1}{2}\rho(SC_x)\right]v^3 + [C_{rr}(m+l)g + mg(sin\alpha)]v + m_t av + QP \tag{13}$$

$$P(kW) = \left[\frac{1}{2}\rho(SC_x)\right]v^3 + [C_{rr}(m+l)g + mg(sin\alpha)]v + m_t\frac{\delta v}{\delta t}v + QP \tag{14}$$

Considering in the discrete domain, the power consumption at a certain instant is:

$$P(kW) = \left[\frac{1}{2}\rho(SC_x)\right]v(t)^3 + g[C_{rr}(m+l) + m(sin\alpha)]v(t) + m_t\frac{v(t)-v(t-\Delta t)}{\Delta t}v + Q(t)P(t) \tag{15}$$

A summary of the parameters needed to calculate power and energy is shown in Table I.

TABLE I
PARAMETERS NEEDED TO CHARACTERIZE A ROUTE

SYMBOL	QUANTITY	UNITS
v	Vehicle speed	m/s
α	Route gradient	radian
l	Vehicle load	kg
Q	Hydraulic oil flow	m3/s
P	Hydraulic oil pressure	Pa
S	Vehicle frontal surface	m2
C_x	Aerodynamic drag coefficient	Dimensionless
m	Vehicle mass	kg
m_t	Dynamic Vehicle mass	kg
C_{rr}	Rolling resistance Coefficient	kg/kg
ρ	Air density	kg/m3

3.3. Data Logging System

Once the necessary data has been identified, a methodology to acquire measurements has to be defined. An on board kit for real time data acquisition is required, one of the goals is to have a kit which can be easily and cheaply replicated. This kit is composed by:

1. CAN Datalogger: CANalyzer CANCase XL with two CAN ports (SN 007130-011289)
2. PLC: IFM CR0505 (SN 024137). Analog channel resolution 12 bits, resolution ±1.0% FS.
3. GPS: RM Michaelides CAN link 2105 (part no. 253004018), fullscale 0.00001º L/l, 0.1m height, CEP 3.5m,
4. Inclinometer: STW YNGS1ST2 with CAN Open port (part no. 080537682003). Range ±6g resolution 0.2 mg.
5. Pressure sensor IFM 9021 (SN 12911 A) Range 0..250 bar, ±0.25 BFSL, ±0.5LS

Fig. 18. Detail of the datalogging system

The first port of the CAN datalogger is connected on to one of the CAN J1939 buses of the vehicle.

The second port is connected to a small CANOpen network, consisting of a GPS device, a PLC with CAN ports for mobile applications and an inclinometer. According to the technical specifications of the device manufacturer, the GPS position error is less than 3.5 meters.

The inclinometer is a gravity sensor, which means that its output will be contaminated by any other source of acceleration in the vehicle [8]

The cost of the whole kit remains under 2200 euros, so it fulfills the low cost criteria for the development of the kit.

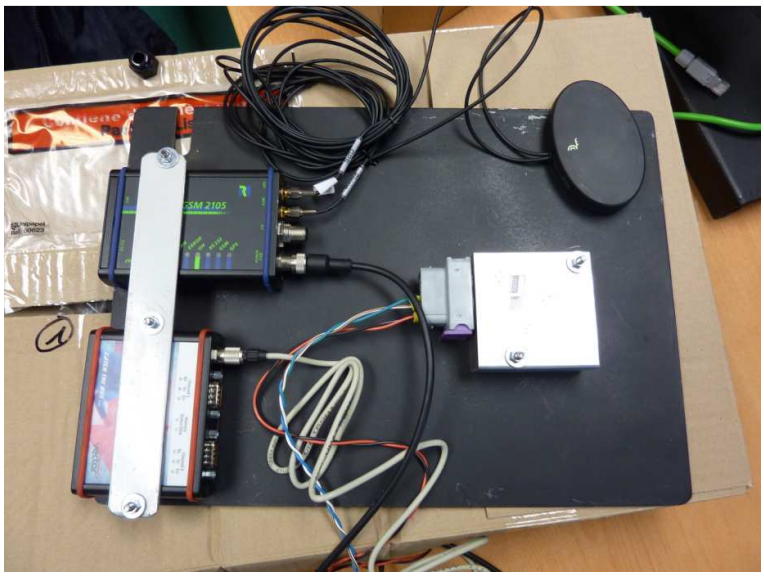

Fig. 19. Detail of the datalogging system for installation in the RCV cabin

Fig. 20. Detail of the datalogging system for installation in the RCV cabin

Fig 21. Detail of the datalogging system for installation below the body

Fig. 22. Detail of the datalogging system, pressure values acquisition

Once the hardware for data acquisition is defined, the data acquisition process has to be established.

The data shown in Table I is divided into three groups.

The first group is the data which can be measured accurately and for which no post processing is needed. It includes pressures, vehicle mass, vehicle load, rolling resistance and aerodynamic drag.

The second group is the data which can be calculated with high precision using information from manufacturers or meteorological stations. It includes vehicle frontal surface, dynamic vehicle mass and air density during the test.

The third group is the data calculated using parameters which have uncertainties and can add errors to the system but which can be corrected through post processing. This includes vehicle distance, vehicle speed, route gradient and hydraulic oil flow. In this thesis different correction algorithms are proposed for this data post processing.

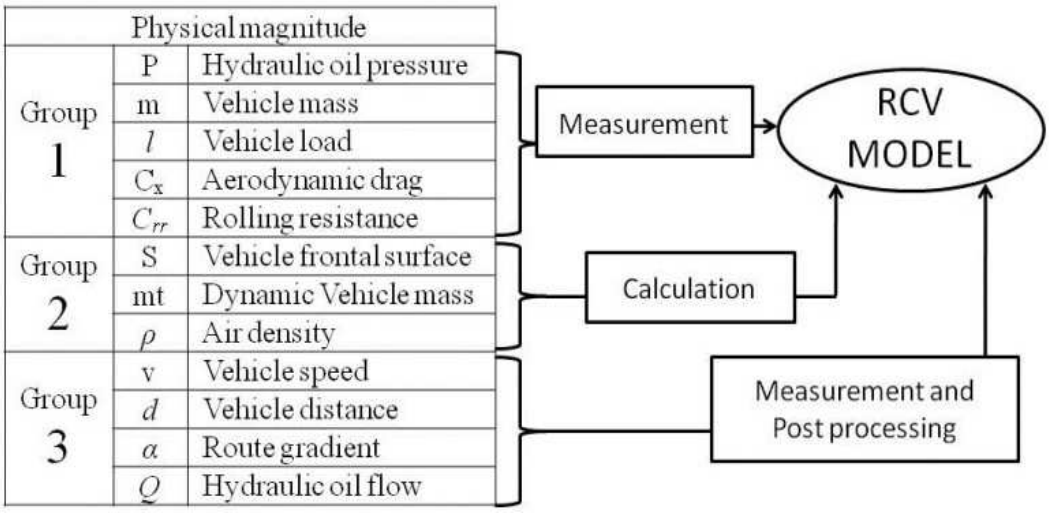

Fig. 23. Data flow to feed the mathematical model

The data from first and second group are taken and not evaluated. However, the data from the third is taken and its precision will be evaluated in this thesis in order to get an estimation of the accuracy of the correction algorithms.

3.4. Data Acquisition and Experimental Corrections for Parameters of RCV Energetic Models

In order to get the maximum accuracy on the acquired data a specific experimental work has been done for each one of the parameters which have uncertainties and can add errors to the system (included in Group 3 of Fig. 23), and for several parameters which can be measured accurately (include in Group 1 of Fig. 23) but which need a test to perform the measurement. These are:

3.4.1. Vehicle Distance and Speed Correction

The vehicle distance and speed found in the CAN bus of a truck ('wheel based speed' SPN84 and 'trip distance' SPN244, both from J1939 standard) are calculated using the wheel (or propshaft) rotation speed and an estimated effective radius of the wheel.

This technique has an associated error which is due to the variations of the real effective radius versus the estimated one. Several factors can change this real effective radius (vehicle load, tire wearing, pressure drop, etc.) and the vehicle measurement system does not have a mechanism to compensate that value in real time. There is a device (tachograph) which compensates this error using a correction factor (K), whose estimation is based on the measurement of the 'trip distance' parameter and a measurement on a calibrated roll bench. However, the K factor is not corrected in real time (each 2 years correction, according to European Community regulations).

The proposed method used in this dissertation for correcting vehicle speed data and measurement errors is to take the 'vehicle distance' value from the J1939 bus (DJ1939), get distances periodically from cartography (DMAP) [64] using geolocation, and calculate a correction factor (from now denominated as K1) in a similar way to that used when correcting the calibration of a tachograph, but in real time.

$$K1 = \frac{D_{MAP}}{D_{J1939}} \tag{16}$$

This correction factor will be used to correct the vehicle distance and speed.

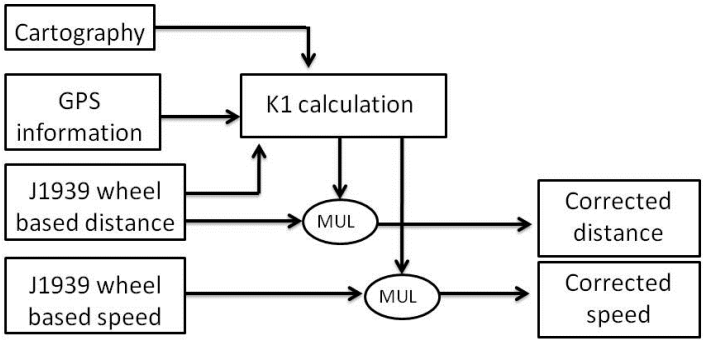

Fig. 24. Implemented algorithm to calculate the 'K1' factor and to correct the vehicle speed and displacement

Using this method, the correction factor can be updated in real time, and the effects of the real effective radius on the error will be minimized. This is important in an RCV, whose load is changing constantly in its route (loaded many times but in very small increments). This situation is very unusual in goods transport trucks, loaded and unloaded few times but with much

3.4.2. Route Gradient Correction

Deviations due to imprecise installation when fitting the inclinometer into the vehicle may introduce errors in the inclination measurement. Active suspensions in the vehicle can also introduce errors in the measurements. These deviations should also be measured and applied to the road profile correction algorithm if necessary.

To calculate the route gradient, an inertial inclinometer will be used. Because of its inertial nature, the signal read from the inclinometer will be affected by noise generated by the vehicle vibrations. This noise has to be eliminated. Only the low frequency oscillations, related to the longitudinal dynamics of the vehicle, are of interest. As a result, the higher frequency oscillations due to driveline oscillations, torsional vibrations in the gearbox etc., will be filtered. The acceleration signal is processed with a Kalman filter [7], [51], [65]-[66] to obtain a first grade estimation.

RCVs tend to have active suspensions in order to redistribute the load on each axle of the vehicle. When these controls are operating, the angle between the ground and the body can change while the vehicle is being driven. In these cases, the angle measured by the inclinometer, once filtered, has to be split into the road gradient (α) and the angle formed by the relative heights of the front and rear suspensions (β), as shown in Fig. 25.

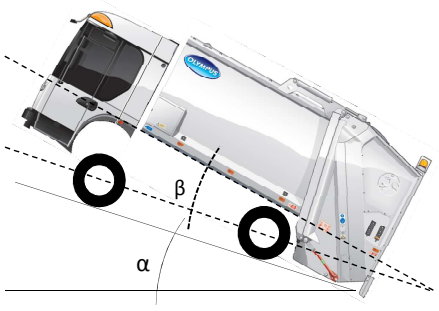

Fig. 25. Schematic model of α and β angles

The value of β can be calculated reading the relative levels of the axis available on the CAN bus (J1939 PGN 65113).

$$\beta = \operatorname{atan}\left[\frac{(RLFAL + RLFAR) - (RLRAL + RLRAR)}{2L}\right] \quad (17)$$

where:

1. RLFAL ≡ Relative Level Front Axle Left [mm].
2. RLFAR ≡ Relative Level Front Axle Right [mm].
3. RLRAL ≡ Relative Level Rear Axle Left [mm].
4. RLRAR ≡ Relative Level Rear Axle Right [mm].
1. L ≡ Wheelbase

Once the value of β is calculated, the parameter α can be estimated using the filtered accelerometer values and the calculated acceleration.

When installing the inclinometer into the vehicle, minor deviations between the sensor and the ground can add or subtract a few tenths of degrees. This value (α offset) will be corrected in a specific test.

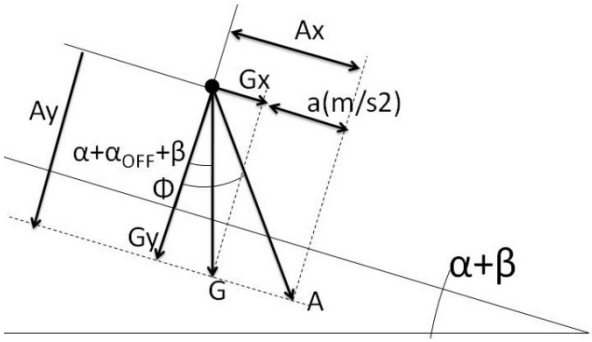

Fig. 26. Geometrical relations between acceleration vectors in the model

$$\varphi = \operatorname{atan}\left(\frac{A_x}{A_y}\right) \quad (18)$$

$$G_x = A_x - a \quad (19)$$

$$G_y = A_y \quad (20)$$

$$(\alpha + \alpha_{off}) + \beta = \operatorname{atan}\left(\frac{G_x}{G_y}\right) \quad (21)$$

where:

1. Ax, Ay≡ acceleration values read from the inclinometer [m/s^2].
2. G≡ gravity vector [m/s^2].
3. a≡ longitudinal acceleration of the vehicle [m/s^2].
4. ϕ≡ raw measured inclination.

3.4.3. Vehicle Load

To get exact values for the transported refuse mass, a certified weighing system should be used. If this kind of system is not available but the vehicle is equipped with active suspensions, the weight on each axle can be found on the CAN bus (PGN 65258), which is the case for this study.

3.4.4. Hydraulic Pressure

The chosen vehicles are equipped with hydraulically powered bodies.

To get pressure values from the hydraulic circuits of the machine, a pressure sensor for each circuit can be used. Most of the commercial industrial hydraulic blocks have test points, what means there is a line out of the block where a sensor can be inserted. This is the case for the machines chosen for this test.

3.4.5. Hydraulic Flow

To measure the hydraulic flow of the oil pump, a sensor (flow meter) could be used. As this kind of sensor needs modifications in the hydraulic lines of the machine and does not fulfill the low cost criteria, it is not selected for this test.

In the case of the selected machines, a fixed flow pump is connected directly to the engine, so that the rotational speeds of the engine and pump are the same. In the case of an ideal pump, the flow could be calculated as RPM x displacement (D) per revolution. In a real pump, the leakage has to be considered.

The flow can be calculated as follows.

$$\mathrm{Q} = \left(\mathrm{RPM} \cdot \frac{60}{2\pi} \cdot \mathrm{D}\right) - \mathrm{Leakage} \tag{22}$$

The leakage can be easily calculated using the tables supplied by the pump manufacturer, which have as input data the RPM and pressure.

3.4.6. Rolling Resistance Coefficient

To simplify the model only the tire friction will be considered, as it is the most significant component of rolling resistance. According to the result of the laboratory measurements from the manufacturer, friction is almost linear with the weight or mass of the vehicle, but very dependent on the road, wheel and tire characteristics. The model has been approximated using the laboratory measurements supplied by the tire manufacturer. The manufacturer name is confidential information.

The Table II shows the Crr coefficient measured at ISO 9948 conditions (80km/h, 8.5 bar and 3334 daN load). Tables III, IV, V show correction parameters for the variations of any of these conditions.

TABLE II

C_{RR} ACCORDING TO TEST ISO 9948

TEST ISO 9948	TIRE	LOAD (DAN)	SPEED (KM/H)	PRESSURE (BAR)	C_{RR} (KG/TON)
315/80/R22,5	Drive	3334	80	8,5	5,77
315/80/R22,5	Traction	3334	80	8,5	6,94

TABLE III

PRESSURE CORRECTION FACTORS

Pressure Correction Factor	1,13	1,1	1,07	1,04	1,02	1,00	0,98
Pressure(bar)	6	6,5	7	7,5	8	8,5	9

TABLE IV

LOAD CORRECTION FACTORS

Load correction factor	1,16	1,4	1,01	0,99
Load (daN)	1000	2000	3000	3500

TABLE V

SPEED CORRECTION FACTORS

Speed correction factor	1,06	1,04	1,02	1
Speed (km/h)	20	40	60	80

3.4.7. Aerodynamic Coefficient

The best option to estimate an aerodynamic coefficient is the use of a wind tunnel. Because of the size of a refuse truck the available wind tunnels could not be used in this study.

To estimate the aerodynamic coefficient of the vehicle a standard coastdown test is done. The vehicle is driven over a flat surface at a controlled speed and then the vehicle is put into neutral and the vehicle is slowed down because of the effect of the tires rolling resistance and aerodynamic drag.

The rate of change of speed of the vehicle is logged and the aerodynamic drag calculated.

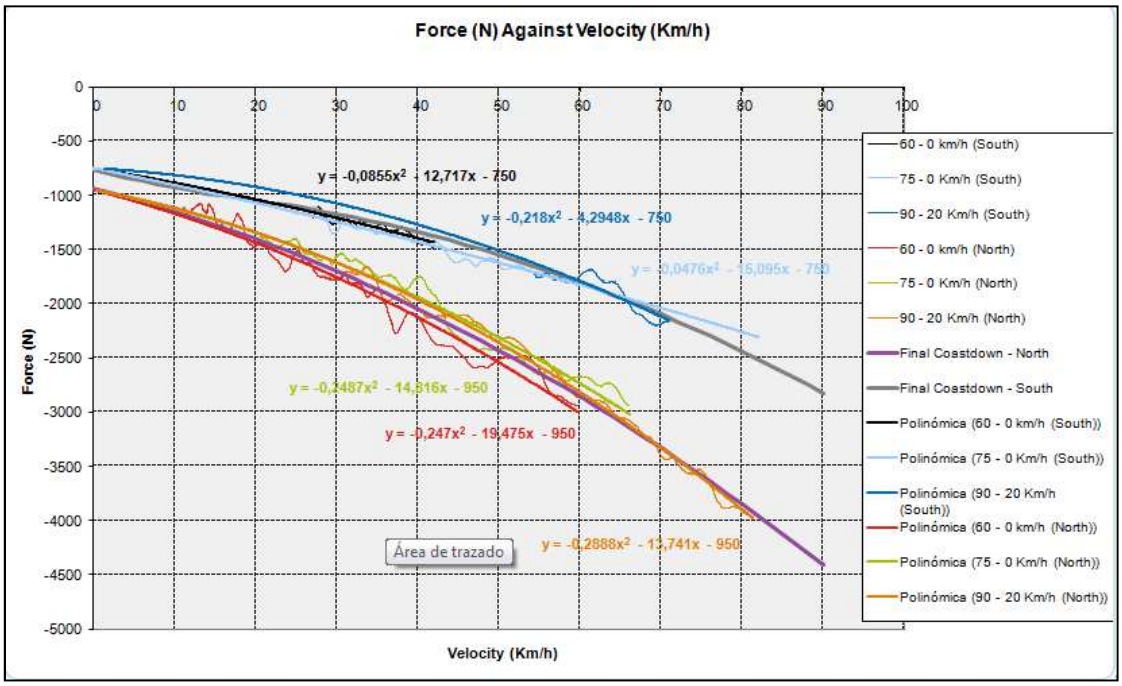

Fig. 27. Detail of the vehicle speed evolution during the Coastdown test

3.5. Post Processed Data Analysis and Models Validation

The post processed data in Fig. 23 (Group 3) is contrasted before validating the measurement system. These are: route gradient, speed/distance correction factors and body oil flow rate.

To analyze the accuracy of the post processed data, additional tests have been proposed to study the deviation of the calculated values from the measurements.

3.5.1. Route Gradient

A Renault Premium 330 DXI with a Ros Roca Olympus refuse collector body is taken for this part of the test. All the tests are performed by the same driver.

In this part of the work a new concept is introduced. The term 'calculated altitude' will be used to denominate the integration on time (from 0 to N) of the vertical decomposition of the vehicle speed.

$$\Delta H_{CALC}|_{t=0}^{t=N} = \int_0^N v \sin(\alpha) dt \tag{23}$$

The first step is to calibrate the error offset due to the installation of the inclinometer on the vehicle (α_{OFF}). To calibrate this parameter, the vehicle is driven through a round trip starting and finishing the trip at the same point. The calculated altitude of this trip is estimated and the α_{OFF} is adjusted to get zero as result.

$$\Delta H_{CALC}|_{t=0}^{t=N} = \int_0^N v \sin(\alpha + \alpha_{off}) dt = 0 \tag{24}$$

Once α_{OFF} is estimated, a specific test to determinate the accuracy of the road gradient calculation algorithm is performed. At this test, the estimated α is used to measure the calculated altitude referred to an initial point. The calculated altitude is compared to a GPS measured altitude. As GPS measurements may contain errors (related to the satellite signal reception on tunnels, mountains etc.), the GPS measurement is also compared with map data [64]. The position error of the GPS is less than 3.5m according to the device manufacturer; the map position error is less than 1m for latitude and longitude and 1.5m for altitude [64].

A route with different gradients from zero to 8% was chosen and the test vehicle is driven eight times up and down with different speed and acceleration profiles. The goal is to test the robustness of the α estimation against different road profiles, and check if its accuracy is independent of the vehicle acceleration.

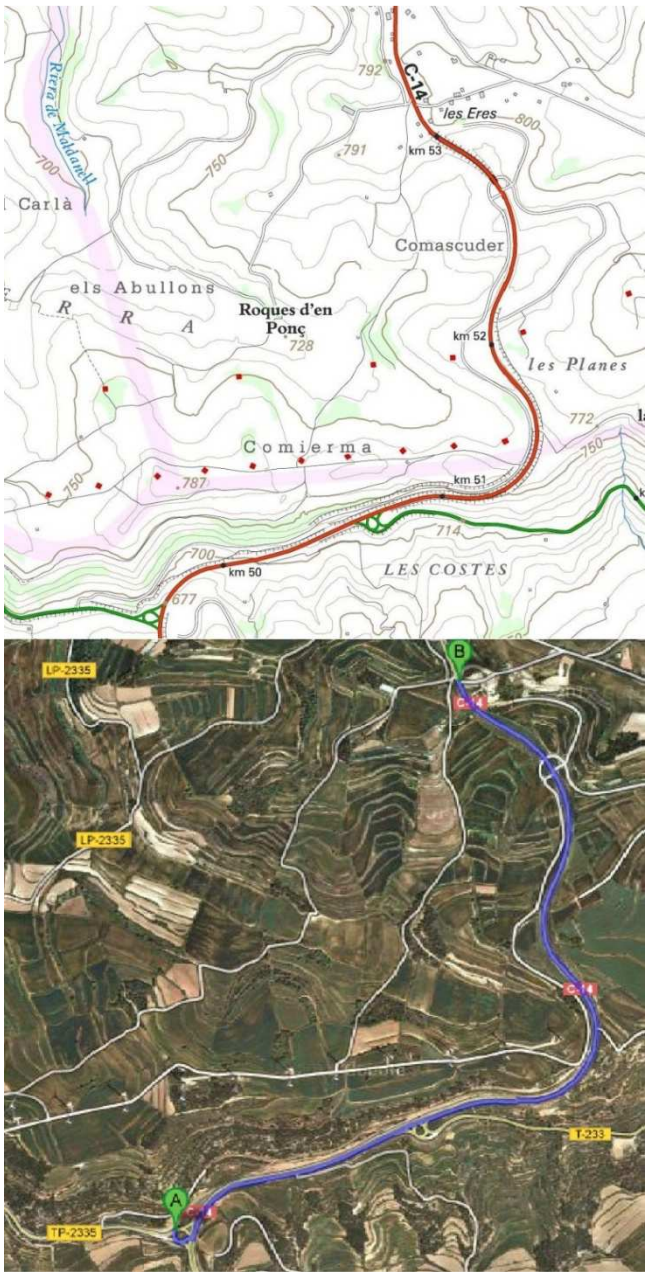

Fig. 28. Detail of the selected route for testing the post processed α. Both satellite map and contour map from [64]

A list of values is generated, in which the first dataset is the absolute altitude measured with the GPS.

The second dataset is the vehicle calculated altitude, referred to an initial instant (H|t=0).

$$\Delta H_{CALC}|_{t=0}^{t=N} = H|_{t=0} + \int_0^N v\,(t)\sin(\alpha)dt \tag{25}$$

Where the initial altitude value Ht=0 is taken from a map of the ICC [64], 0 and N are the initial and final time instants of the test, correspondingly.

Using these values two more datasets are generated in which the values for the error compared to the initial point (E_{ini}) are stored as a third dataset. An error compared to the initial point is interesting, because it shows if the calculation generates cumulative errors in altitude, showing a global deviation of the system, or not. The proposed estimation formula is:

$$E_{ini}(\%) = \frac{H_{CALC}(t) - H_{GPS}(t)}{Dist(t) - Dist(0)} \quad (26)$$

where:

1. $H_{CALC}(t)$ is the height calculated at instant 't'.
2. $H_{GPS}(t)$ is the height measured with the GPS device at instant 't'.
3. Dist(t)- Dist(0) is the total accumulated distance from time = 0 to time = t.

Also it is interesting to calculate an instantaneous error (E_{inst}), which could compare the road gradient constantly and check if there is an error associated with a local road profile or vehicle behavior.

$$E_{inst}(\%) = atan\left(\frac{H_{DGPS}(x) - H_{DGPS}(x-l)}{L}\right) - atan\left(\frac{H_{DCALC}(x) - H_{DCALC}(x-l)}{L}\right) \quad (27)$$

where:

1. $H_{DGPS}(x)$ ≡ Altitude measured with the GPS device at the distance 'x'.
2. $H_{DCALC}(x)$ ≡ Calculated altitude at the distance 'x'.
3. L ≡ calculation interval.

The vehicle is driven eight times up and down through the selected route. The result of the data logging and associated calculation analysis is shown in Figs. 29 to 44.

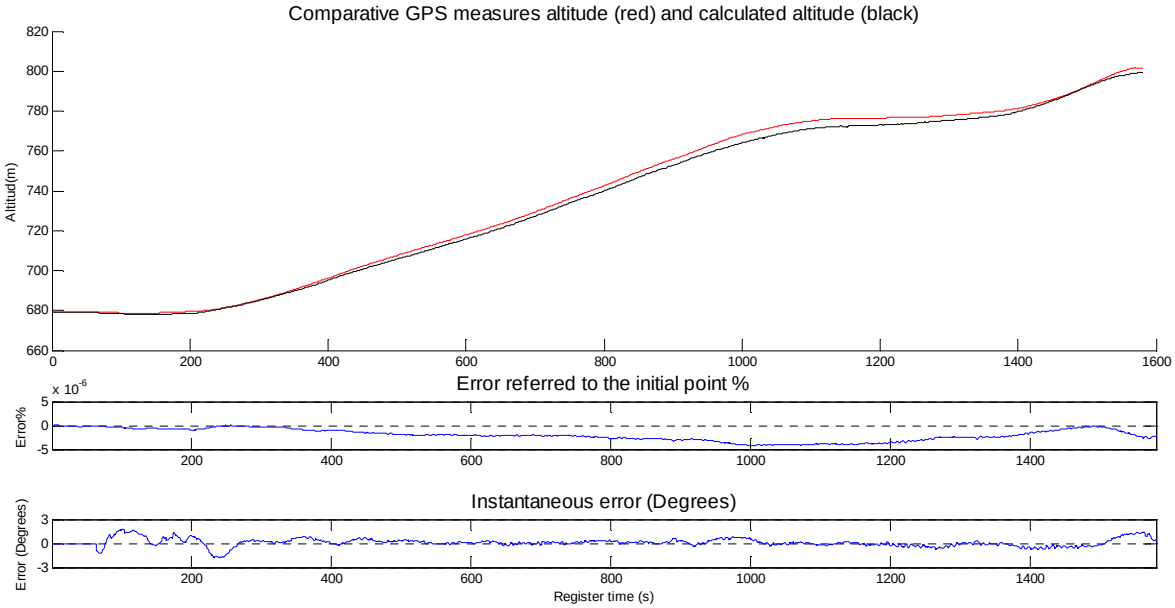

Fig. 29. Plot of the instantaneous GPS measured altitude, calculated altitude, error compared to the initial point and instantaneous error (1st route Up)

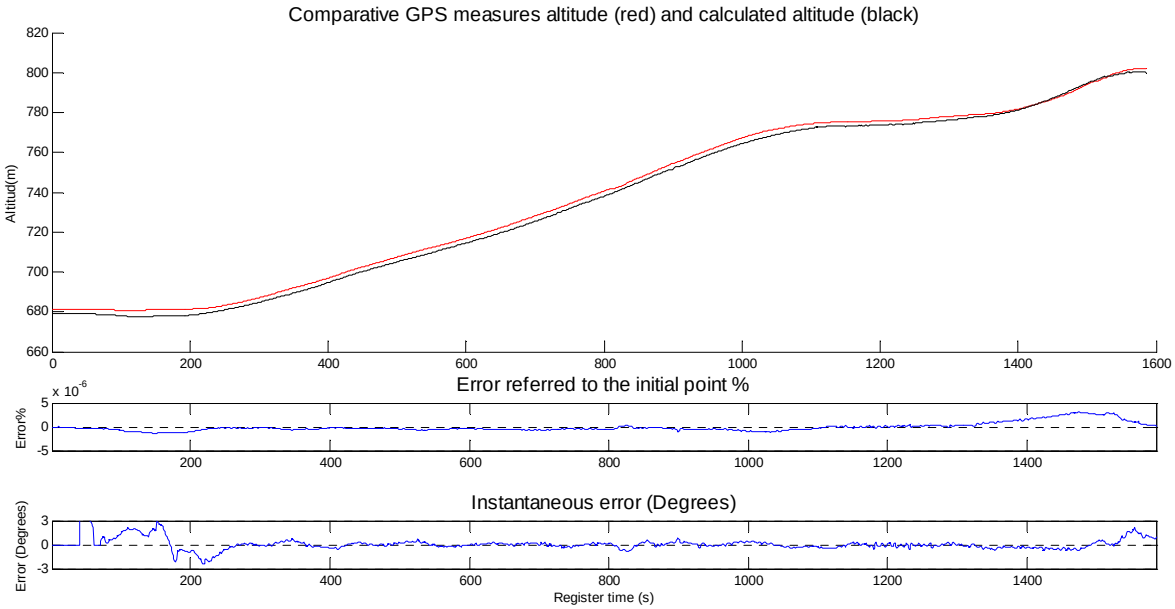

Fig. 30. Plot of the instantaneous GPS measured altitude, calculated altitude, error compared to the initial point and instantaneous error (2nd route Up)

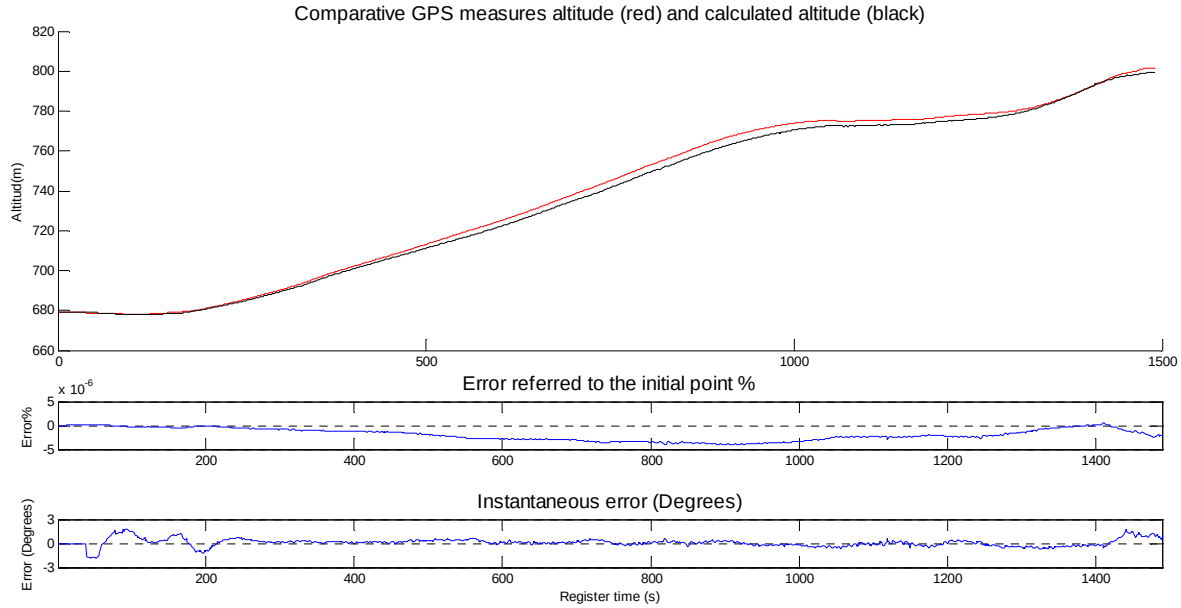

Fig. 31. Plot of the instantaneous GPS measured altitude, calculated altitude, error compared to the initial point and instantaneous error (3rd route Up)

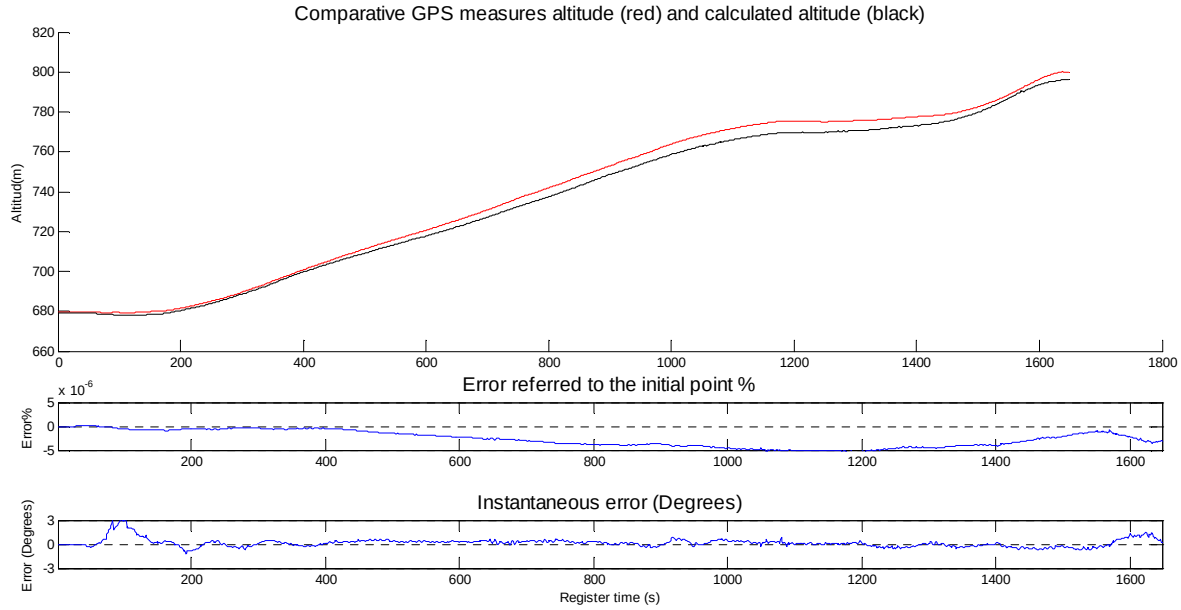

Fig. 32. Plot of the instantaneous GPS measured altitude, calculated altitude, error compared to the initial point and instantaneous error (4th route Up)

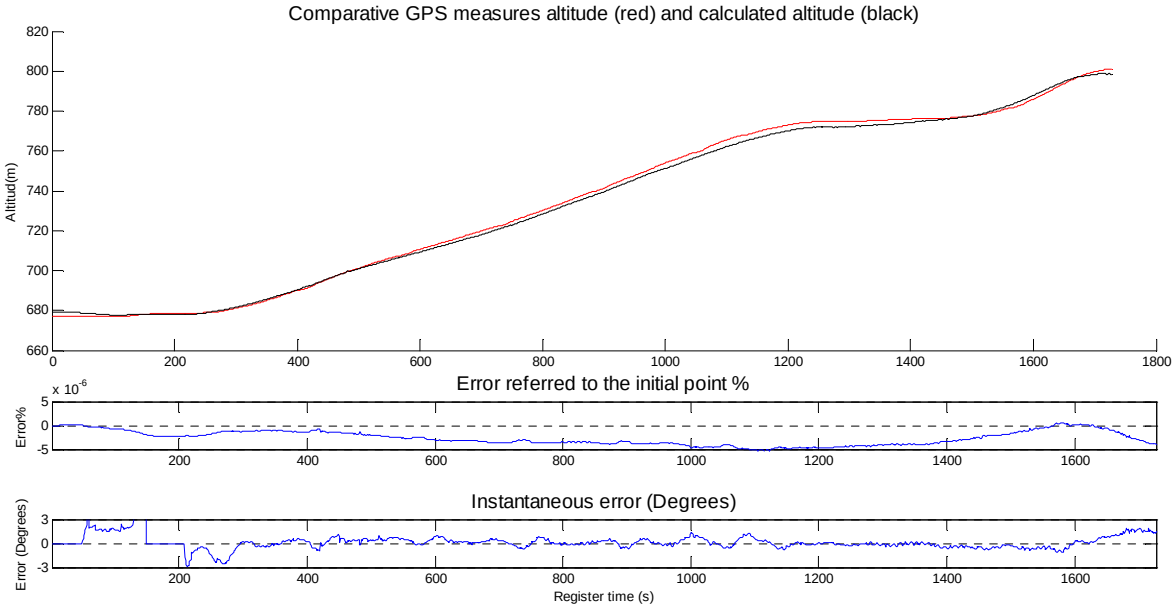

Fig. 33. Plot of the instantaneous GPS measured altitude, calculated altitude, error compared to the initial point and instantaneous error (5th route Up)

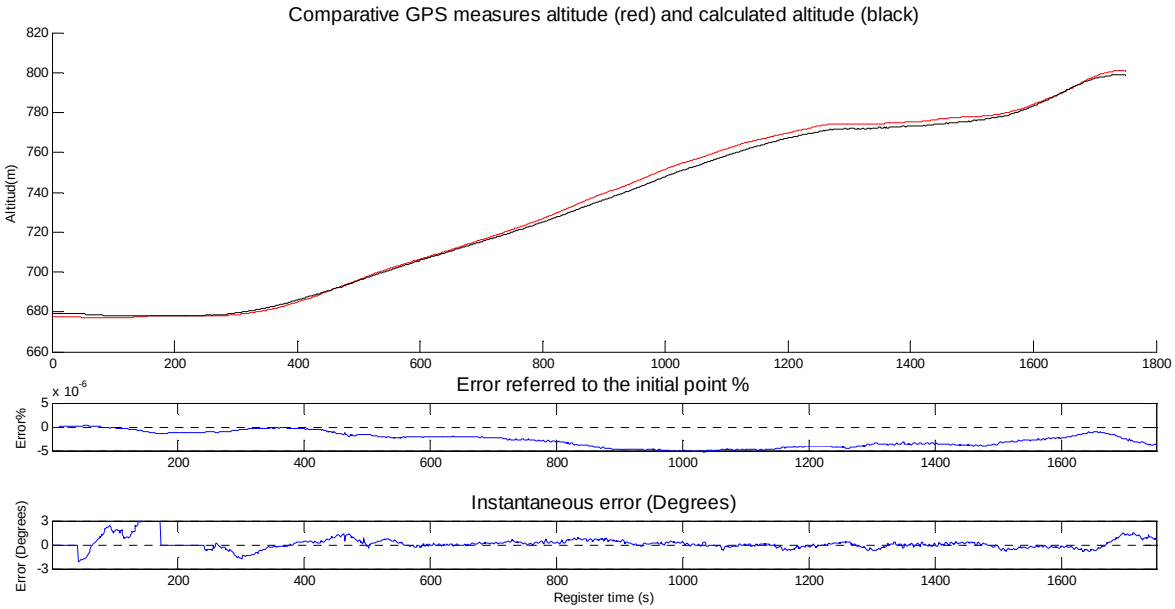

Fig. 34. Plot of the instantaneous GPS measured altitude, calculated altitude, error compared to the initial point and instantaneous error (6th route Up)

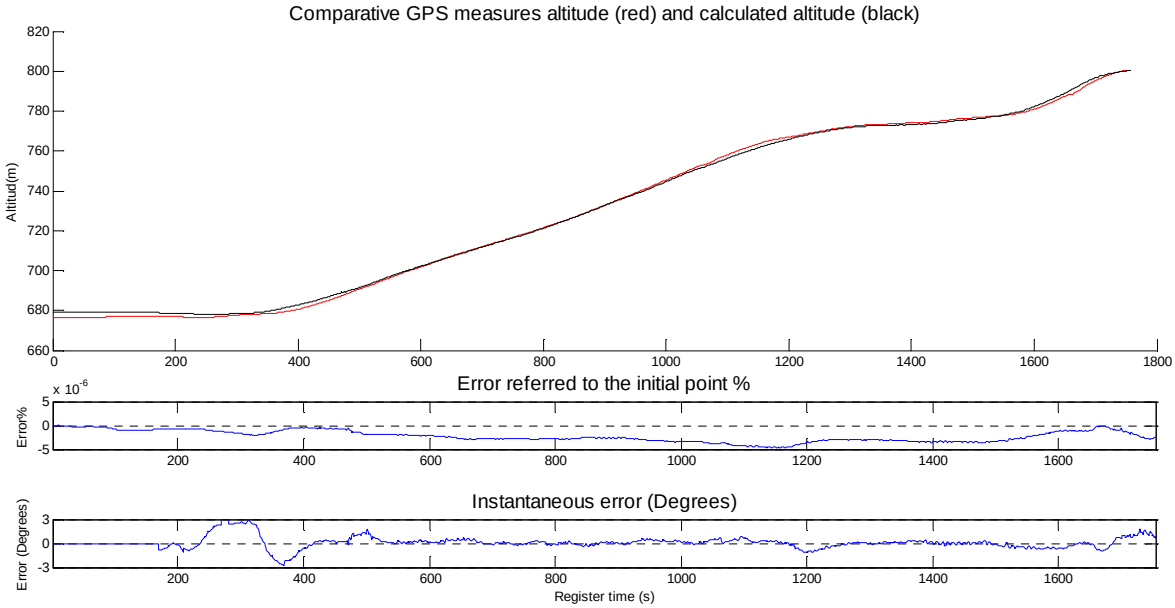

Fig. 35. Plot of the instantaneous GPS measured altitude, calculated altitude, error compared to the initial point and instantaneous error (7th route Up)

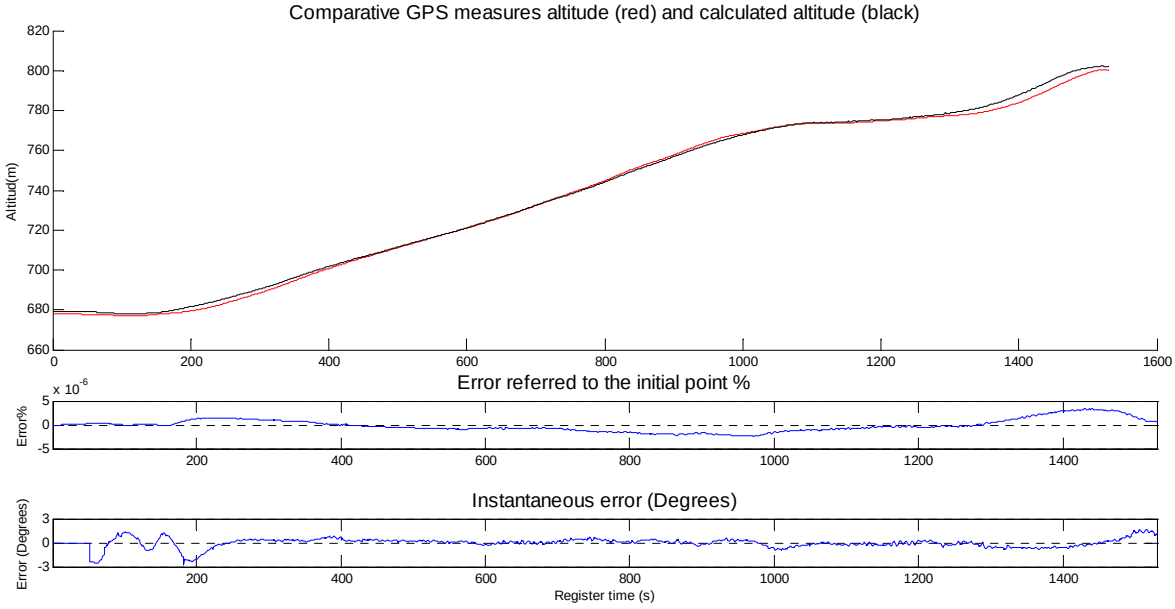

Fig. 36. Plot of the instantaneous GPS measured altitude, calculated altitude, error compared to the initial point and instantaneous error (8th route Up)

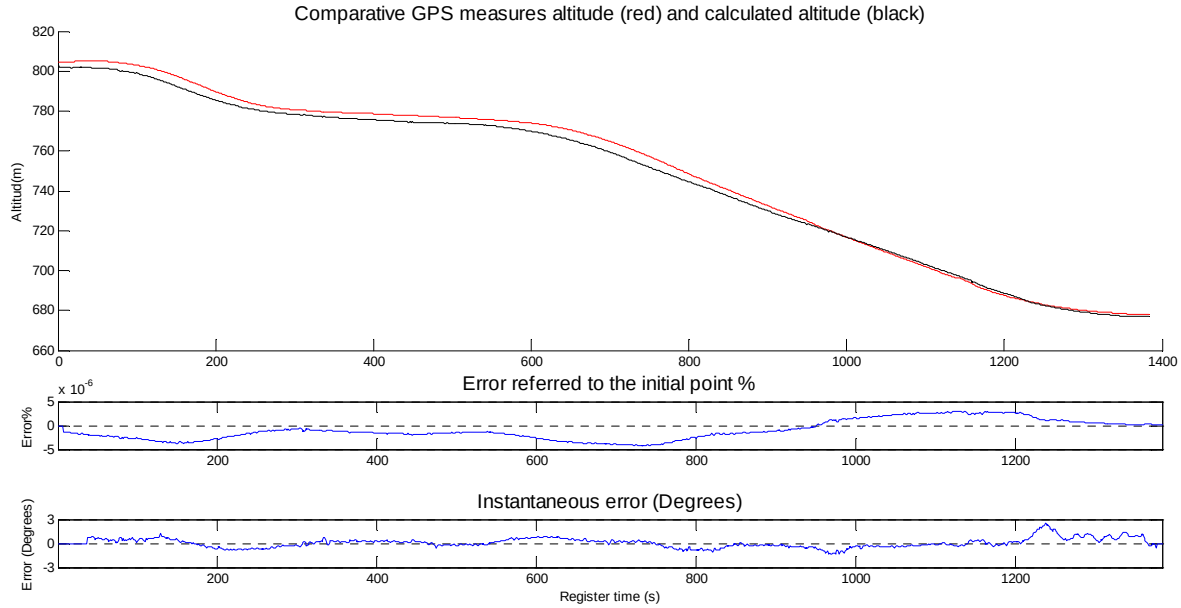

Fig. 37. Plot of the instantaneous GPS measured altitude, calculated altitude, error compared to the initial point and instantaneous error (1st route Down)

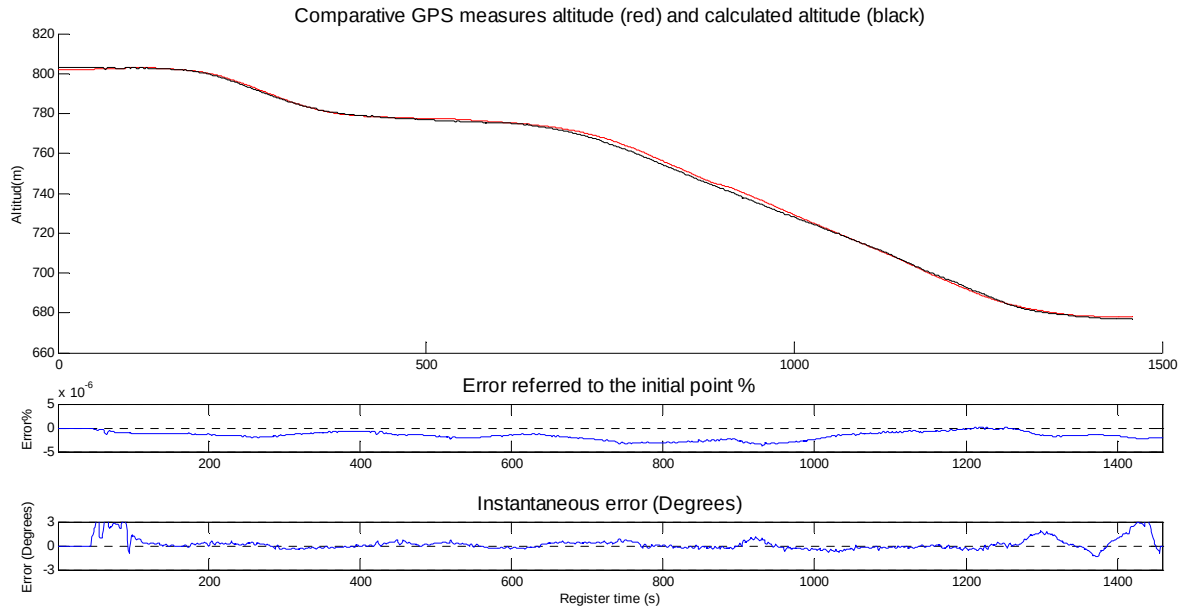

Fig. 38. Plot of the instantaneous GPS measured altitude, calculated altitude, error compared to the initial point and instantaneous error (2nd route Down)

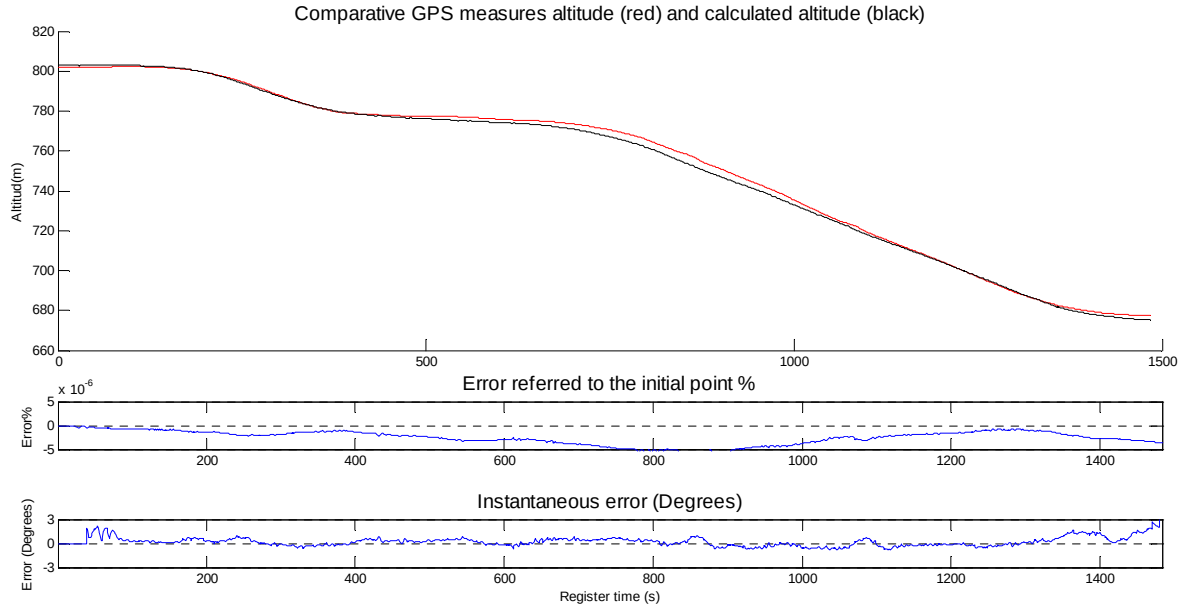

Fig. 39. Plot of the instantaneous GPS measured altitude, calculated altitude, error compared to the initial point and instantaneous error (3rd route Down).

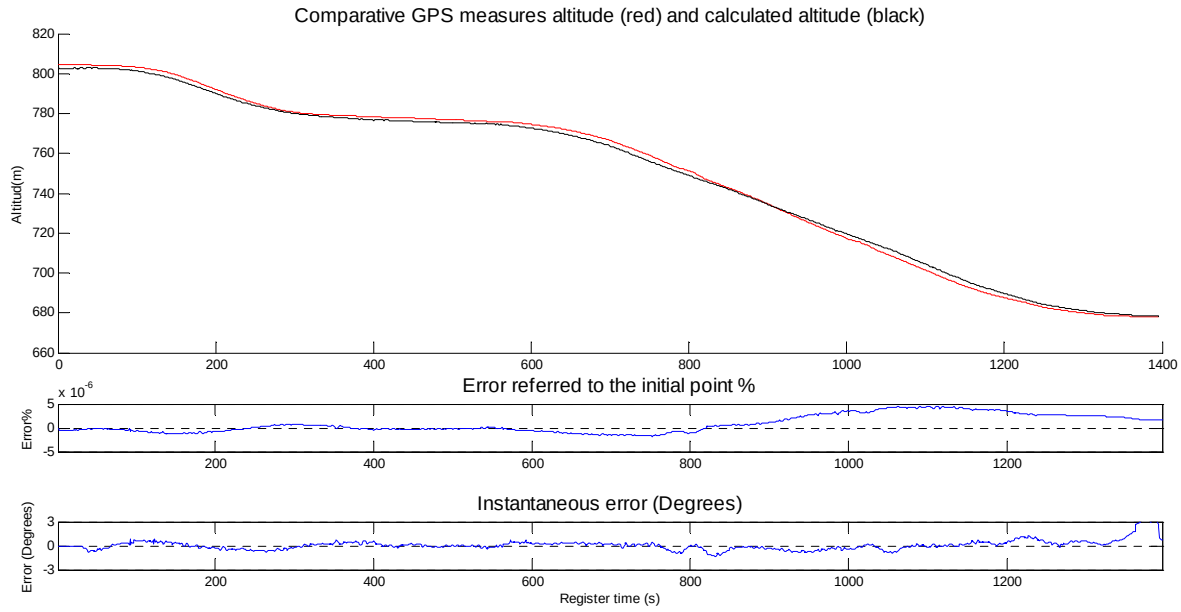

Fig. 40. Plot of the instantaneous GPS measured altitude, calculated altitude, error compared to the initial point and instantaneous error (4th route Down).

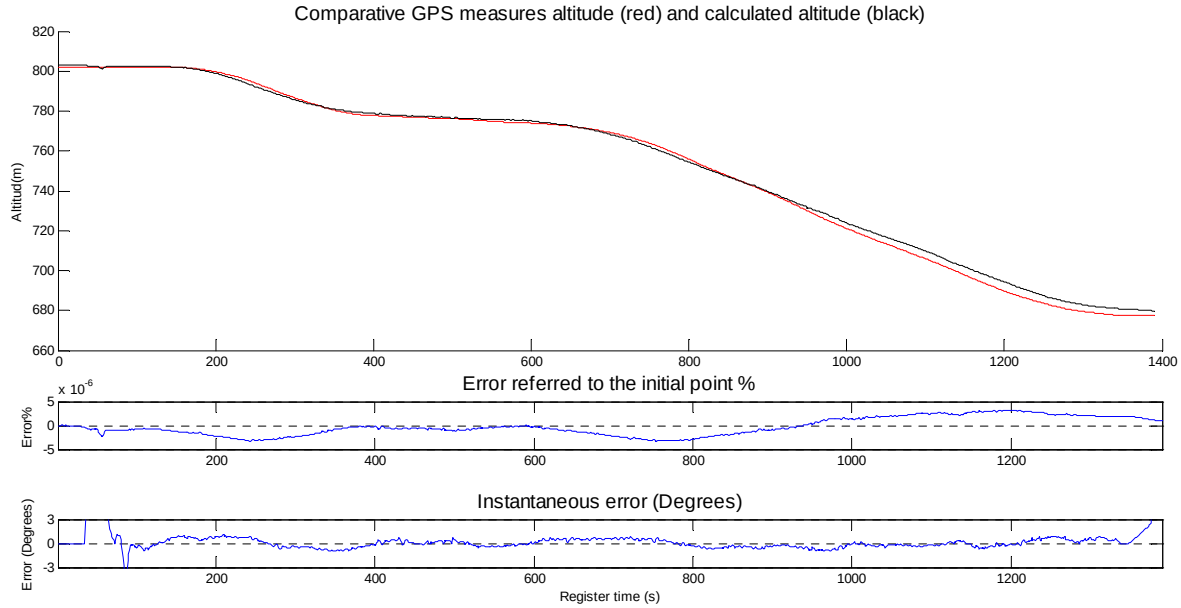

Fig. 41. Plot of the instantaneous GPS measured altitude, calculated altitude, error compared to the initial point and instantaneous error (5th route Down).

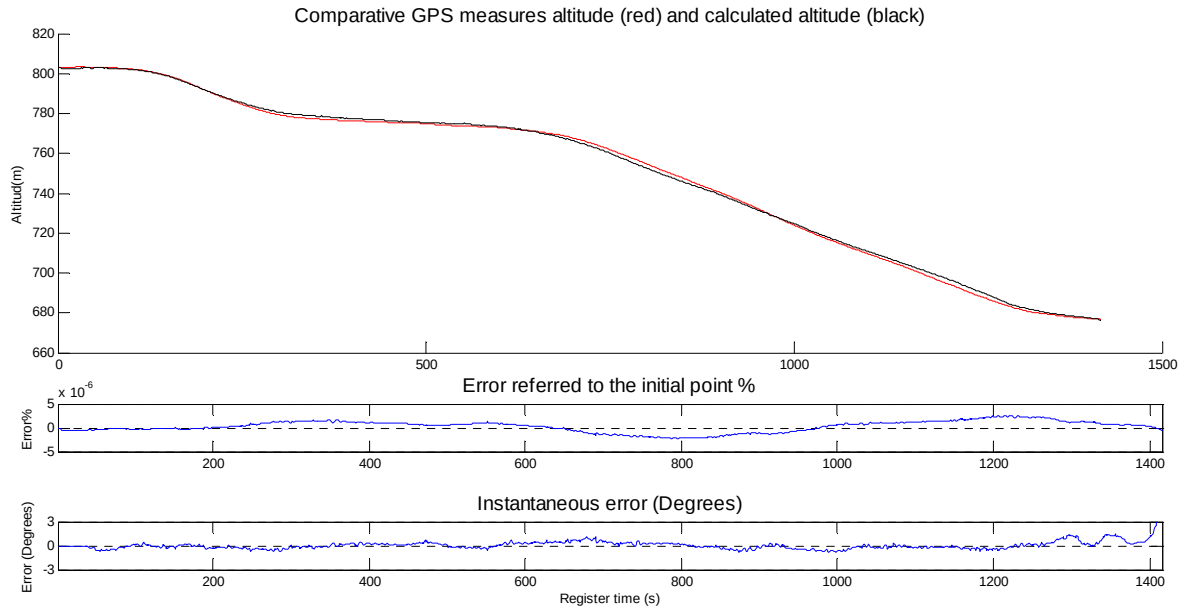

Fig. 42. Plot of the instantaneous GPS measured altitude, calculated altitude, error compared to the initial point and instantaneous error (6th route Down).

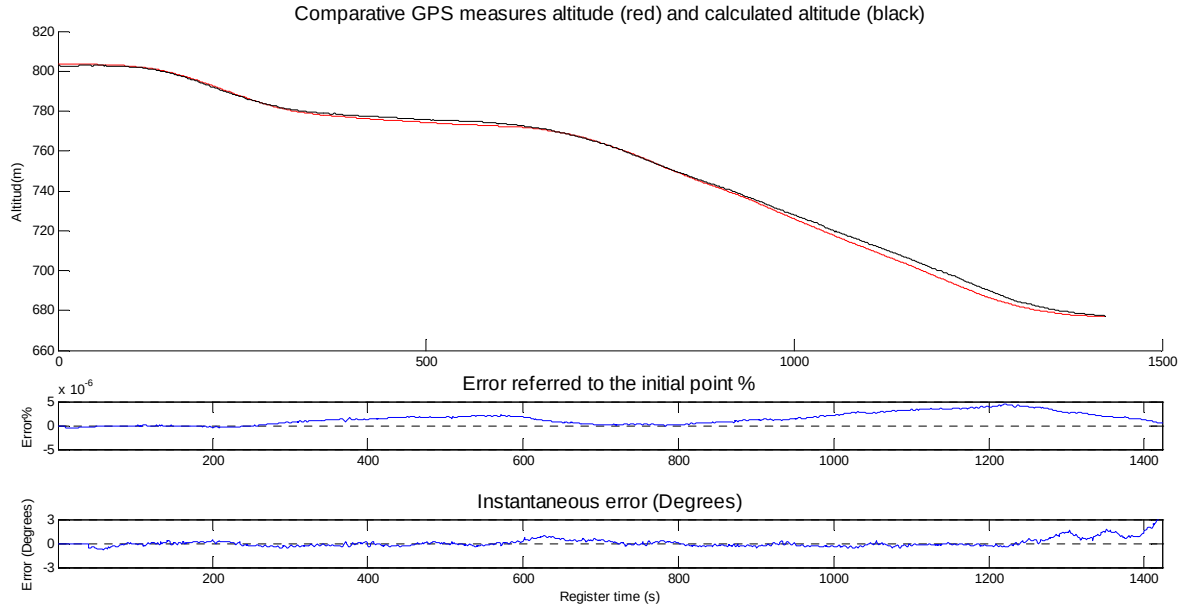

Fig. 43. Plot of the instantaneous GPS measured altitude, calculated altitude, error compared to the initial point and instantaneous error (7th route Down).

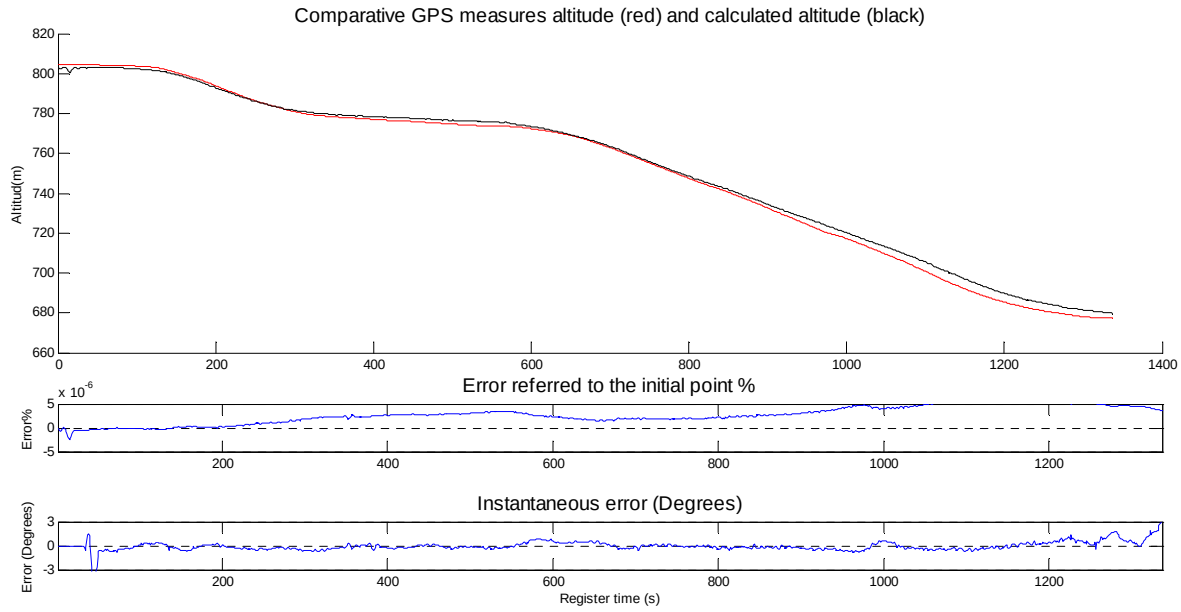

Fig. 44. Plot of the instantaneous GPS measured altitude, calculated altitude, error compared to the initial point and instantaneous error (8th route Down).

A summary of the eight routes up and eight routes down is presented in Table VI.

In this table the routes results are listed by rows ('u' for ups 'd' for downs). For each route the maximum and minimal E_{ini} values of the trip are shown in the columns three and four respectively, the mean absolute E_{ini} value is shown in the second column. In the fifth column the mean absolute E_{inst} value is shown.

Most of the routes shows maximum and minimal E_{ini} values over and below zero respectively what indicates that no cumulative errors are found. The mean absolute E_{ini} value is always close to 0% what indicates good global behavior. The mean absolute E_{inst} is always lower than 0.59 degrees and the bigger errors are usually associated to the same point of the route and not to a speed profile. The authors associate that fact to a local road irregularity not found on the GPS measurement, despite the fact that no additional tests to prove or quantify that could be done.

TABLE VI
RESULTS OF UP AND DOWN TESTS

TEST	EINI MEAN ABS	EINI MAX (%)	EINI MIN (%)	EINST (MEAN ABS °)
1 u	3.72 e-04	5.52e-04	-8.12 e-04	0.4515
2 u	3.00 e-04	0.40e-04	-7.29 e-04	0.4640
3 u	4.76 e-04	0.00e+00	-1.10 e-03	0.4432
4 u	2.79 e-04	8.50e-04	-3.28 e-04	0.4168
5 u	3.00 e-04	6.03e-04	-6.24 e-04	0.6334
6 u	1.90 e-04	4.67e-04	-4.18 e-04	0.3472
7 u	2.68 e-04	5.52e-04	-9.31 e-05	0.3517
8 u	5.19 e-04	0.40 e-04	-4.77 e-04	0.3863
1 d	3.68 e-04	8.88 e-07	-7.98 e-04	0.3500
2 d	1.23 e-04	5.81 e-04	-2.49 e-04	0.4259
3 d	3.57 e-04	1.18 e-04	-7.63 e-04	0.3441
4 d	4.99 e-04	7.16 e-06	-10.00 e-04	0.3694
5 d	4.95 e-04	1.04 e-04	-9.87 e-04	0.5940
6 d	4.91 e-04	4.42 e-05	-9.83 e-04	0.4979
7 d	4.20 e-04	8.83 e-07	-8.70 e-04	0.4635
8 d	1.97 e-04	6.19 e-04	-4.48 e-04	0.3965

3.5.2. Vehicle Speed K Factor

For this part of the test the vehicle is driven from Tarrega to La Faneca (both in the NE of Spain) and vehicle speed and distance data are acquired using the data acquisition system.

Using a map from [64], a few measured points are taken as reference points at kilometer markers 55, 60, 65, and 70. The distance between points is taken from the ICC map [64] and also

measured through the J1939. Correction parameters are calculated to compensate for the deviation in the speed/distance measurement.

In the following table the different reference points used to estimate the K1 factor are exposed with its latitude and longitude in the first three columns, the integrated distances between them and associated correction parameters are shown in the fourth and fifth column respectively.

TABLE VII
K1 FACTOR ESTIMATION

	KM	LATITUDE	LONGITUDE	DISTANCE INTEGRATED FROM J1939 (KM)	K1 FACTOR
NORTH TO SOUTH	70	41.,6276º	1,1320º		
	65	41.5827º	1,1269º	4,955	1,009
	60	41.5449º	1,1442º	4,876	1,025
	55	41.5112º	1,1803º	4,952	1,01
SOUTH TO NORTH	70	41.6276º	1,1320º		
	65	41.5827º	1,1269º	4,979	1,004
	60	41.5449º	1,1442º	4,816	1,038
	55	41.5112º	1,1803º	4,907	1,019

The average value for the K1 factor is 1.017, which means the vehicle measurement has an error of 1.7%. To correct the vehicle speed value, all measurements will be multiplied by 1.017.

To test the accuracy of the K1 factor correction algorithm, two different routes are selected to test the deviation of the K1 factor calculated in the previous section.

In order to test the repeatability of the test the first route is exactly the same as taken in the previous section. The mean value for the corrected value is 5.025 km, which means a 0.49% excess in the corrected value.

The second route selected is in the A2 highway in the area close to Tarrega, driving two times from east to west between the kilometer markers 490 and 515.

In the following table the different reference points used to test the K1 factor are presented with its latitude and longitude in the first three columns. Columns 4 and 5 show the measured (M) and corrected (C) distance of the first trip, while columns 6 and 7 seven show the measured and corrected values, respectively, of the second trip.

TABLE VIII
K1 FACTOR ESTIMATION

km	LATITUDE	LONGITUDE	1ST TRIP M (km)	1ST TRIP C (km)	2ND TRIP M (km)	2ND TRIP C (km)
515	41.671546°	1.223851°				
510	41.657087°	1.166589°	4,985	5,072	4,913	4,999
505	41.657625°	1.109332°	4,896	4,982	4,878	4,964
500	41.639275°	1.057092°	4,925	5,011	4,942	5,029
495	41.635975°	1.000170°	4,965	5,052	4,952	5,039
490	41.641180°	0.940195°	4,895	4,981	4,895	4,981

The mean value for the previous corrected value is 5.011 km what means a 0.22% excess in the corrected value.

3.5.3. Body Oil Flow

To test the accuracy of the oil flow measurements of the datalogging kit, a laboratory measurement tool (Parker Hannifin Service Master) has been installed on a vehicle. The measurements have been performed simultaneously with the datalogging kit developed in this thesis and with the laboratory tool. The RCV selected is a Ros Roca Olympus 19m3 on a Renault Premium 330DXI.

The oil flow is calculated as proposed in section 3.4.5.

The Parker system was installed just after the pump. To evaluate the accuracy of the measuring system a compactor cycle is performed and measured.

The average error during this cycle was lower than 0.67 l/min (less than 1% error compared to the total flow, 80 l/min).

3.5.4. Fuel Consumption Model Result Analysis

The mathematical model built with all the models described in section 3.2.6 of this study is defined as the ‘whole model’. This is composed by the elements belonging to the vehicle (aerodynamics, rolling, kinetic and potential energy), to the body (compactor and lifter), to the powertrain (internal combustion engine, batteries, electrical drives…) and their interactions, identifying when they act as power generators or power consumers.

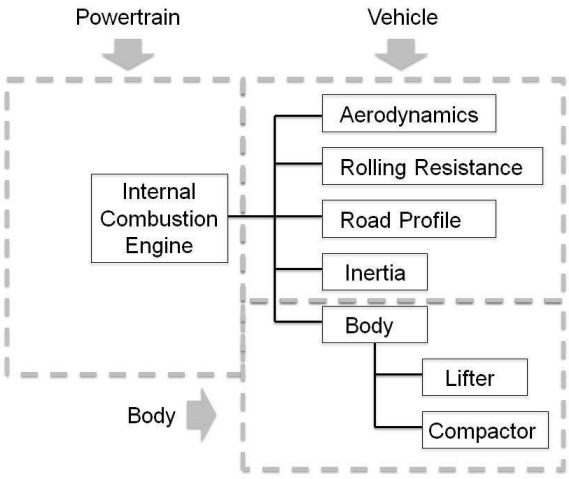

Fig 45. Diagram of the 'whole system', where all the possible energetic flows are shown

Once all the models have been defined (section 3.2.1-3.2.6) and the data input system tested and validated (section 3.3-3.5.3), the whole model is built and tested again in order to be validated as a whole. The goal is to build the model using the parameters of a real truck and run it in real routes.

The fuel consumption is calculated using the steady fuel consumption maps of the engine. Taking the engine speed from CAN J1939 and the torque calculated through the vehicle and body models, the working point of the engine is identified and the engine specific consumption (g/kWh) at that point is taken, as shown in Fig. 46. Using the specific fuel consumption and the output power, the instantaneous fuel consumption is estimated.

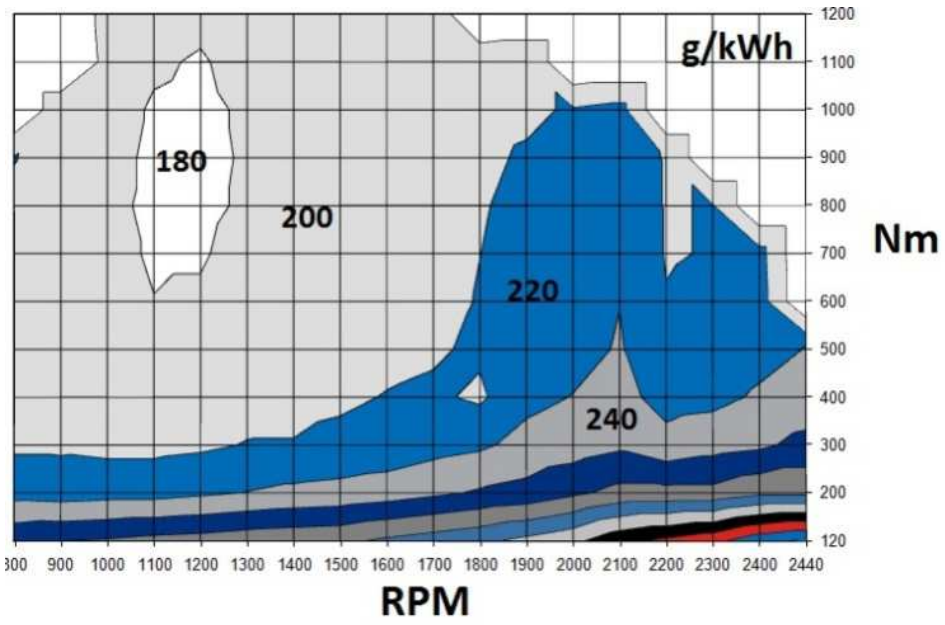

Fig 46. Fuel consumption map

Integrating all the instantaneous fuel consumption values, total fuel consumption is estimated and total fuel consumption is also measured at the fuel station. The result of both values is contrasted

to estimate the error. The calculation tool, programmed in Matlab, has been developed specifically for this research project.

An Iveco Stalis CNG 270 with a Farit FMO refuse collector body is taken for this part of the test, in which the vehicle is equipped with active suspensions. The tyre pressure is monitored daily to keep constant values during the test, AC is disabled and the machine has constant weigh during the test (minor changes related to coolant, oils etc.). The driver is not a controlled parameter. The rolling resistance coefficient (C_{rr}) is taken as a weighted average of the vehicle tires architecture and disposition, not considering changes in gravity center or road slope.

The daily routes are recorded from the beginning of August 2012 to the end of December 2012. Days with interrupted routes because of technical problems, and days with additional services different from the programmed ones, are not considered. Days with wind speed higher than 10 km/h are also dismissed.

Two sets of routes with different road profiles are selected to test the system. Flat routes are executed from 20th August to 17th September, while steeper routes are executed from October 20th to December 7th.

In Table 9 the rows show chronologically the route registers, where the fuel consumption measured at the fuel station is shown in the second column, the fuel consumption estimated using the model proposed is shown in the third column, and the estimation error is evaluated in the fourth column. None of the routes shows an error higher than 5% and the average error is 0.22%.

TABLE IX
MEASUREMENT RESULTS FOR FLAT ROUTES

DAY DD/MM/YYYY	MEASURED FUEL CONSUMPTION (KG)	CALCULATED FUEL CONSUMPTION (KG)	ERROR (%)
20_VIII_2013	38.32	36.66	-4.33
23_VIII_2012	43.01	42.88	-0.3
14_IX_2012	62.18	60.97	-1.95
16_IX_2012	44.71	45.12	0.92
17_IX_2012	59.65	61.31	2.78
20_X_2012	48.65	48.74	0.18
30_X_2012	43.41	42.52	-2.05
6_XI_2012	33.44	33.85	1.23
15_XI_2012	52.66	54.77	4.01
18_XI_2012	45.46	45.81	0.77
29_XI_2012	45.66	44.01	-3.61
4_XII_2012	53.51	54.13	1.16
7_XII_2012	43.4	43.71	0.71

3.6. Discussions and Conclusions

A new methodology to define and adjust energy consumption models of RCVs has been defined. This method is based on the classic approach for both the vehicle and body mathematical models, and specific tests to adjust all the vehicle parameters related to aerodynamics, rolling resistance, inertias, road profile and body pressure and flow.

This adjustment is done using low cost hardware, information available on the vehicle J1939 CAN bus, cartographical information and information supplied by parts manufacturers. Different algorithms to correct deviations in the measured vehicle speed and distance, oil flow, and road profile have been proposed and validated.

Specific tests to show the precision of the data post processing system have been performed and its results showed. A final test has been performed at which the fuel consumption of an RCV has been calculated and compared to the fuel consumption measured at the fuel station.

There are still a few parameters which are not taken into account by the proposed model. For example, the fuel LHV dispersion (in CNG from 43650 to 46500 kJ/kg according to [46]). In Spain the national gas company (ENAGAS) analyzes daily the supplied CNG composition and its properties, being the analysis results publicly available on internet [48]. This information could be used to generate a correction parameter. The gas analysis found in the testing period included in the section 3.5.4 of this work show minor variations in the gas properties, in the period August 20th to December 7th the minimum and maximal values of LHV have been 10.869 and 10.727 kWh/m^3(N) respectively.

Also the engine maps used to calculate the fuel consumption are taken from steady conditions instead of transient, the rolling resistance is simplified to the tire, the rest negligible, and wind speeds up to 10 km/h are accepted and not considered for the calculation.

The result of the test shows that even neglecting these parameters, high accuracy energetic consumption models (errors lower than 5%) can be built and adjusted by the use of this approach. This methodology opens the possibility of developing high quality vehicle energy use studies at low cost, being able to study also the interactions between the body consumption and powertrain energetic generation.

This method can be used to study alternative vehicle components, architectures and management strategies which could lead to a reduction of fuel consumption in vehicles. This method is highly recommended to study vehicle configurations specific for repetitive routes, such as RCV, urban buses, urban delivery trucks…

As future work should be commented that in the case of RCVs, despite representing a big automobile park (over 200.000 machines working in North America [12]), few technical documents have been found which analyze in depth the technological alternatives for these vehicles. In the case of

hybrid propulsion systems for RCVs, a specific situation is found which makes a difference in the management strategies compared to other vehicles, that is the drive cycle is repeated daily. The proposed tool contributes an easy and cheap tool to record drive cycles, which could be used to develop specific architectures and management strategies.

4.

Drive Cycle Identification Based on Algorithms

This chapter suggests two different software proposals which can be used to identify the Drive Cycle of an RCV in real time. These software architectures are based on artificial intelligence and on deterministic algorithms. Both software proposals are tested with real routes and their performance is evaluated and contrasted.

CONTENTS:

4.1. Introduction

The price of fossil fuels has been rising constantly over the last 15 years, [1]. This factor, combined with the fact that an important portion of global fossil fuel consumption is due to road traffic [49], has generated considerable interest in automotive technologies specifically aimed at reducing the consumption of fossil fuels.

Many of these technologies are related to the possibility of integrating different energy sources on-board, internal combustion engines combined with electric [18] or hydraulic [19] technologies being the most-studied. One of the challenges of these technologies is the algorithm development that will decide what portion of each type of energy will be consumed at each moment (energy split).

Knowing the future power demands of a drive cycle is advantageous for these algorithms [18]. Therefore, the development of this knowledge is the main goal of this chapter.

All the developments presented in this chapter are based on the knowledge developed in the chapter 2 of this thesis.

All the information and algorithms have been developed and executed off-line, but they could all be implemented in real time. All the information used to feed these algorithms can be found in the standard J1939 CAN bus of the vehicle and the CAN network of the body manufacturer, except for the vehicle inclination. The vehicle inclination can be estimated from the vehicle J1939 CAN bus information [50, 51], but as this is not the main scope of this project, these algorithms have been substituted by an inclinometer (as in [28]). As GPS is not a standard system on commercial vehicles, its use has been ruled out.

To finish, several studies demonstrate that a large portion of a typical driver's trip is repetitive [44]. This repetition provides the option of using these algorithms on other kinds of vehicles in the future.

4.2. Approach Based on Deterministic Algorithm

The data used to test the algorithms was acquired from April 2013 to June 2013 on a Ros Roca Cross with UPC lifter. Fifteen different routes were acquired on that period (see Table X).

The proposed logic is based on the observation of RCV routes (see chapter 2). Knowing the vehicle's drive-cycle speed profile, using body hydraulics pressure values available in the logged data and using an auxiliary algorithm to ascertain the number of times the refuse has been unloaded (N_Unloads), a deterministic algorithm has been developed. This algorithm uses mean speed values (average of the last 120 s) instead of instantaneous speed values to filter short transients which do not represent real changes in the machine status. The concept 'RCV route segment' was introduced in chapter 2.

The algorithm is incremental, so it starts with a 'RCV route segment = 1' value and decides in real time if the route segment value should be increased as a result of the analysis of different parameters.

The algorithm contains the following rules based on observation:

The mean speed at the base is always low (below 10 km/h) for safety reasons. Mean speed values (J1939 SPN 84) higher than 15 km/h, gears higher than 2 and hydraulic circuit unpowered (body ancillaries), are representative of driving out of the base, so it implies that the vehicle has started its route. This rule is used to determine when the vehicle leaves route segment 1 and starts route segment 2.

The RCV body can be powered exclusively with neutral gear engaged and mean vehicle speed equal to zero. When the hydraulic circuit is not powered, the pressure values read by the sensor are close to zero (maximum: 2 bars). Hydraulic pressures higher than 15 bars in any of the body circuits are representative of power demand. This situation implies that the vehicle is in the RCV route segments related to refuse collecting or unloading. These rules are used to determine when the vehicle is leaving route segment 2 and starting route segment 3 (also leaving 5 and starting 6).

Inside the city, the maximum legal speed is 50 km/h, which is a value rarely reached in the observed routes due to the distance from bin to bin and due to vehicle dynamics. Speeds higher than 60 km/h hydraulic circuits unpowered and gears higher than 4 are representative of driving out of the city. These rules are used to determine when the vehicle is leaving route segment 3 and starting route segment 4 (also leaving 6 and starting 7).

Unloading the RCV generates a specific pressure profile different from any other body operation. To identify this profile, a morphologic analysis software that compares the pressure profiles with a predetermined profile has been developed. The hydraulic pressure is analyzed continuously to identify when the vehicle is unloading the refuse. An increase in the N_Unload value implies that the

vehicle has been unloaded, and this situation means a change from route segment 4 to 5 (also from 7 to 8).

In Fig. 47, the algorithm that identifies the status flow is described. The route segments are shown in the big black numbers, and the rules are beside the arrows.

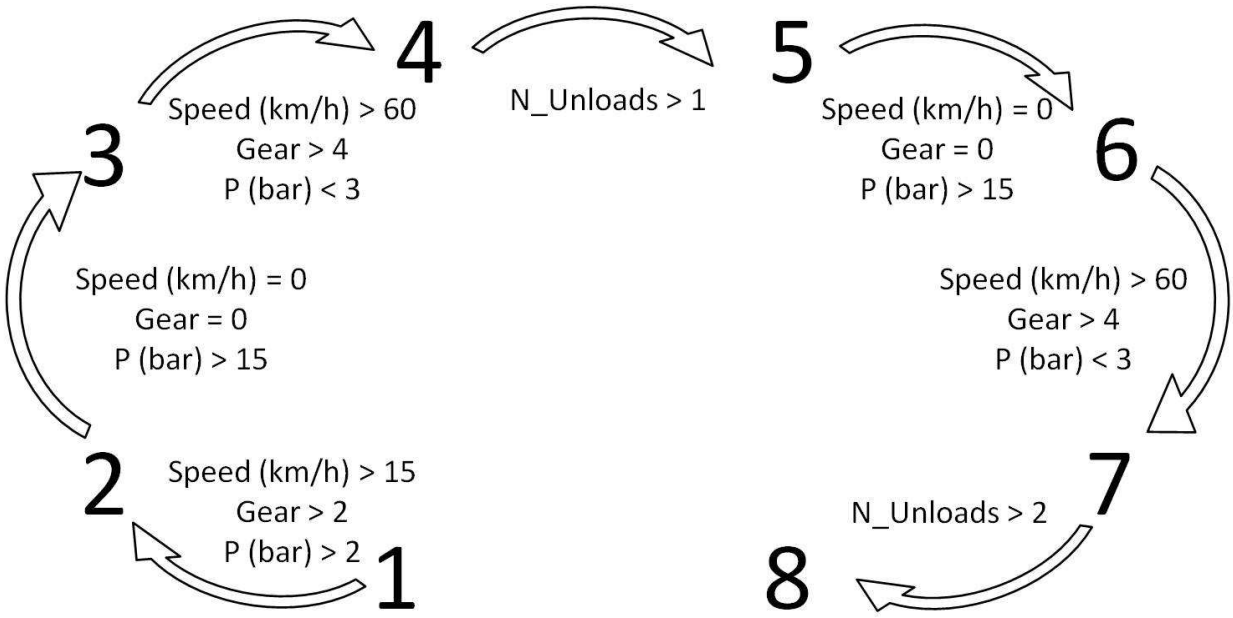

Fig. 47. RCV route segment flow on the deterministic algorithm

The accuracy of the deterministic algorithm on each logged route is discussed in detail in section 4.4. In summary it produces good results but shows problems when finding unexpected values.

Additional data could be used to improve this algorithm but the use of complex combinations of data (bin lift with compactor and vehicle speed, etc.) would be required. A person/operator assigned to the task can also be challenged during simultaneous analysis of several parameters (vehicle speed, gear engaged, distance travelled, bin lift and compactor hydraulic pressures, and the time elapsed since the last bin lift or compaction cycle). At times, the changes in parameter values used to identify the change in route segment do not always occur in the same row in the logged data.

4.3. Approach Based on Neural Networks

Testing the deterministic algorithm has shown that using a deterministic algorithm and a few variables does not provide a robust solution to such a complex problem. As there is a lot of information involved, and their interrelationships are unclear, the use of a neural network is proposed.

The physical values chosen to test the network are the same ones used by a person/operator when identifying the route segments. These are the following:

Vehicle speed: Speeds over 50 km/h are typical of transport mode and speeds below this value are typical of collecting mode.

Current gear: High ranges are typical of transport mode and low ranges are typical of collecting mode.

Distance travelled so far on the route: Useful as a reference of the degree of progression in the route.

Algorithms to generate additional data are used to generate vectors which will also feed the network. These are:

Mean speed value (considering 120 seconds): Useful to understand if the vehicle speed value is related to stationary (related to transport mode) or transient (related to collecting mode) conditions.

Time since the last bin was lifted: It shows if the vehicle is close to the last collecting point.

Number of bins collected: Useful as a reference of the degree of advancement in the route.

Number of unloads calculation: Useful to differentiate between the route segments 1 to 4, 5 to 7 and 8.

In Fig. 48, a flow diagram of the algorithm is shown:

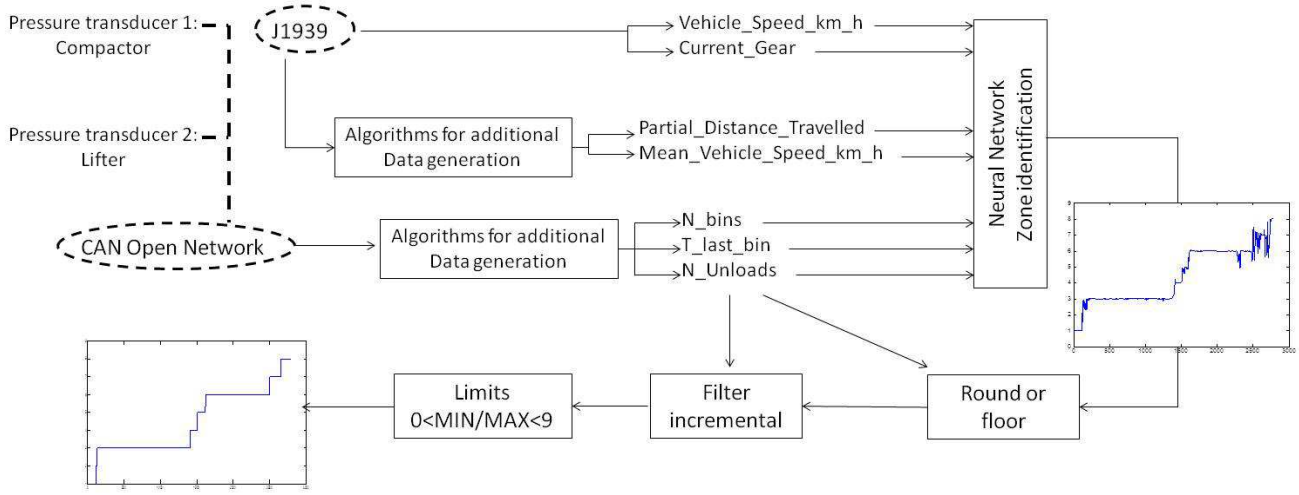

Fig. 48. Detailed data flow in the neural algorithm

The size of the network is determined by the problem to be solved. As there are 7 input parameters, 7 input neurons are chosen. For the same reason, as there are 8 different output classes (corresponding to the route segments), then there are 8 outputs giving values (0, 1), each of them. Three hidden layers of 10, 12, and 10 neurons each have been chosen experimentally. A feed-forward back-propagation network has been designed, with hyperbolic tangent sigmoid for the first four transfer functions and a linear transfer function for the output. As the output layer is linear, the values generated are close to (0, 1). Therefore, they have to be rounded. To end with the eight rounded values have to be added.

The final output of the whole system is a parameter that identifies the RCV route segment with discrete values from 1 to 8 as a function of the current values of the input parameters.

To test the neural network, a person/operator identifies route segments of the routes 1 to 4 (of the Table X). Later, these four routes and their identified route segments are used twice each to train the neural network; the routes are used in non-sequentially (1, 2, 3, 4, 2, 4, 1, 3). To reduce processing time, only one value in every 100 (so 0.1 Hz frequency) is used; so the network is tested using 21.022 records.

This work has been developed using the Matlab Neural Network Toolbox combined with the use of specific algorithms developed for this project.

4.4. Discussions and Conclusions

A set of real routes, acquired with the device proposed in section 3.3, has been used to test the accuracy of the previous commented algorithms. And a basic analysis of the logged routes considering time, distance, and collected bins during the route is carried out to determine the type of route (standard or with abnormal situations) performed. The result of this analysis is presented in Table X.

Routes from 1 to 14 represent normal situations. Route 15 is abnormal and one in which vehicle had to act as a rescue vehicle. It had to complete the route of another RCV because the initially assigned vehicle suffered a breakdown and had to come back to the base with its route unfinished and the refuse not collected.

In the following points, the RCV routes shown in Table X are considered.

A new parameter is defined to measure the accuracy of the route segment identification algorithms (deterministic algorithm and neural networks). The number of successfully identified records versus the total number of records considered is the success rate (Sr).

$$\mathrm{Sr} = \frac{\sum \text{Successful identifications}}{\sum \text{Total number of records}} \tag{28}$$

All the route segments are identified and analyzed by a person/operator. These data are considered the pattern against which the route segment identification algorithms will have to be compared.

The success rates of the deterministic and neural algorithms on each logged route are shown in Table X.

TABLE X

SUCCESS RATE OF THE DETERMINISTIC AND NEURAL ALGORITHMS

ROUTE	TOTAL DISTANCE (KM)	TOTAL TIME (MIN)	TOTAL COLLECTED BINS/CONTAINERS (N)	NEURAL SUCCESS RATE	DETERMINISTIC SUCCESS RATE
1	73.9	460.8	183	99.7	95.4
2	72.7	470.9	175	99.8	94.1
3	71.3	392.8	166	99.5	89.1
4	69.0	422.3	163	99.6	59.0
5	67.6	406.5	144	98.1	92.0
6	70.6	421.5	161	86.2	88.2
7	69.9	471.1	169	94.6	54.0
8	70.5	480.7	163	96.2	53.9
9	67.8	421.1	168	93.8	89.1
10	67.8	423.5	160	91.3	90.0
11	76.6	465.0	194	92.2	92.9
12	67.2	428.1	166	97.9	86.1
13	73.7	460.2	184	97.9	92.1
14	68.4	471.6	169	95.4	93.0
15	82.0	542.3	266	85.9	85.7

When using the deterministic algorithm, it usually produces good results but shows problems when finding unexpected values. The use of the compactor or lifter in transport modes (generating hydraulic pressure) or high-speed driving during the collection cycle (it is illegal to drive faster than 50 km/h in the city, but the logged data show values up to 80 km/h) generates errors in routes 4, 7, and 8.

The output of the tested neural network is far more robust than the output of the deterministic algorithm. Not only can it overcome the occurrence of unexpected values, but it also attains better results in all the studied routes except route 11. Despite the fact that the neural network gets lower success rate on route 11, its value is still higher than 92%.

When analyzing route 15, in which the vehicle had to act as a rescue vehicle, adding distance, time and bin/container collection to the daily service. It can be seen that the success rate of the neural algorithm remains high (over 85%). We can draw the conclusion that the neural algorithm can guarantee accuracy when changes in the basic route are introduced.

5.
Energy Left Estimation

This chapter proposes a novel method to estimate the energy left to finish an RCV route. If the energy management algorithm of a hybrid vehicle can account for future energy demand, then it can be arranged in such a way that the non-fossil-fuel energy sources are fully depleted at the end of the drive cycle.

CONTENTS:

5.1. Introduction

Knowing the future power demands of a drive cycle is advantageous for hybrid powertrains. One of the points of interest is the estimation in real time of the energy needed to finish the present drive cycle (Energy Left E_L). If E_L is considered when developing the powertrain management strategy of an HEV the batteries can be planned for consumption on arrival at the base, thus replacing the consumption of fossil fuels.

Several authors have proposed the use of on-board GPS systems that record parameters of repetitive drive cycles. As the vehicle is run daily on the same route, the previously generated information is used to predict these parameters in real time for the current drive cycle [19].

Other authors infer road type and traffic congestion level from the power demand and vehicle speed [22]-[24].

Many authors have also developed predictive control based on known drive cycles, instantaneous position supplied by GPS, and knowledge of statistical traffic flow [20].

In this chapter of the thesis, a novel system is proposed in which the energy needed to finish the current trip and the drive cycle of a vehicle are estimated. The results of this study can be applied to vehicles which run daily on similar routes, such as buses, RCVs or delivery vehicles. The experimental data used for this work has been acquired from RCVs.

5.2. Theoretical Approach

In this part of the thesis, a novel technique for real time estimation of the energy needed to finish a route is presented. This value is estimated from observation of previous drive-cycle consumptions on the same route, and the energy consumption estimated real time using methods presented in a previous work [28] in which a methodology to develop and validate energy models of RCV was developed. These models showed an energy-consumption estimation error lower than 5% compared empirically with measurements performed when refueling the vehicle. Using these models, the instantaneous power consumption is estimated as:

$$P(t) = \left[\frac{1}{2}\rho(SC_x)\right]v(t)^3 + [C_{rr}(m+l) + mg(\sin\alpha)]v(t) + m_t\frac{v(t)-v(t-\Delta t)}{\Delta t}v + Q(t)P(t) \quad (29)$$

TABLE I
PARAMETERS NEEDED TO CHARACTERIZE A ROUTE

SYMBOL	QUANTITY	UNITS
v	Vehicle speed	m/s
α	Route gradient	radian
l	Vehicle load	kg
Q	Hydraulic oil flow	m3/s
P	Hydraulic oil pressure	Pa
S	Vehicle frontal surface	m2
C_x	Aerodynamic drag coefficient	Dimensionless
m	Vehicle mass	kg
m_t	Dynamic Vehicle mass	kg
C_{rr}	Rolling resistance Coefficient	kg/kg
ρ	Air density	kg/m3

Following the methodology presented in [28], the parameters of Table I related to the vehicle have been adjusted empirically using the data acquisition system presented in chapter 3 and cartography.

Based on this algorithm, the energy that would be needed to finish the route (energy left 'E_L') can be estimated.

If E_L is considered when developing the powertrain management strategy of a vehicle with different energy sources on-board (ex. hybrids), the non-fossil energy source on-board (batteries, hydraulic accumulators, fuel cells) can be planned for consumption on arrival at the base, replacing the consumption of fossil fuels.

The perfect E_L estimation would reach zero when parking the vehicle at the base at the end of the route. This is of particular interest in fleet vehicles in which the non-fossil energy source (ex. batteries) could be recharged overnight while the vehicle is parked. Certain energy-storage devices may need specific strategies to keep long life cycles, such as minimum charges on batteries or minimum

voltages in supercaps. In this work, E_L that equals to zero must be understood as the minimum of the useful energy of the energy storage system.

In vehicles that use this strategy, finishing a route with $E_L>0$ means arriving at the base under normal driving conditions, with non-fossil energy still available.

On the other hand, arriving at the base with a high E_L value means inefficiencies in the hybrid power-train management as some of the fossil energy consumed during the drive cycle could have been replaced by non-fossil energy.

There are limits to the accuracy with which such predictions can be made.

The proposed method for calculating E_L at a certain instance 't' is to take the expected fuel consumption of the route (named as E_{ROUTE}) and to subtract the consumed energy estimated in real time.

$$E_L(t) = E_{ROUTE} - \int_0^t fc_{iso}(RPM, \tau) \cdot P(t)\, \partial t \quad (30)$$

The instantaneous power consumption P(t) is estimated using (29). In case of an ICE-based power train, the engine fuel consumption (fciso [g/kWh]) is estimated by using the RPM (J1939 SPN 190) and estimated torque coordinates, and then looking up the fuel consumption on an iso-consumption engine map [28]. In case of electric power train, the energy consumption (kWh) is estimated by correcting the instantaneous power consumption (29) by using efficiency maps (motors, energy sources, inverters, etc.) and integrating values on the whole route.

If a vehicle was to consume the same amount of energy every time it was driven through the same route, estimates of the remaining energy required for the route could be very accurate, but as shown previously, the energy consumed on a route varies.

To find valid values for E_{ROUTE}, a statistical analysis is performed taking data from the daily records of the vehicle during the refuse-collection service. The total number of routes analyzed is 50. They fulfill a Gaussian law with an average value of 65.28 liters of diesel (μ=594.78 kWh, σ=34.90 kWh).

$$N(\mu=594.78\ kWh,\ \sigma=34.90\ kWh) \quad (31)$$

'Ratio' is defined in this work as the proportion of routes in which there is non-fossil energy still available ($E_L>0$) at the end of the route.

Using this statistical law (31) and using its cumulated distribution function, a bilateral relation can be established, in which a certain E_{ROUTE} value corresponds to a Ratio, and a Ratio corresponds to its associated E_{ROUTE} value.

Two examples are shown. In the first one, the Ratio selected is 50%, as a result E_{ROUTE} is μ (594.78 kWh). The routes contained in the black area would finish with EL higher than zero; the routes contained in the white area would finish with E_L lower than zero.

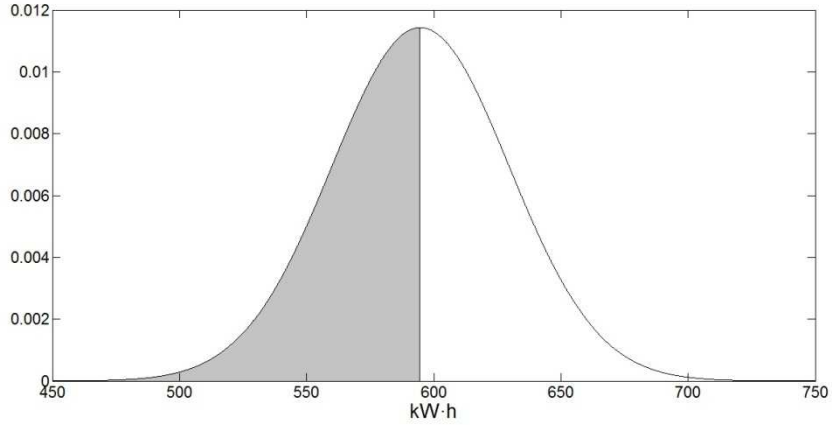

Fig. 49. First example, ratio 50% implies E_{ROUTE} equal to μ

In the second example, the E_{ROUTE} selected is 650 kWh, as a result, the ratio is 94.3%.The population in the black area would finish its route with E_L higher than zero, the population in the white area would finish its route with E_L lower than zero.

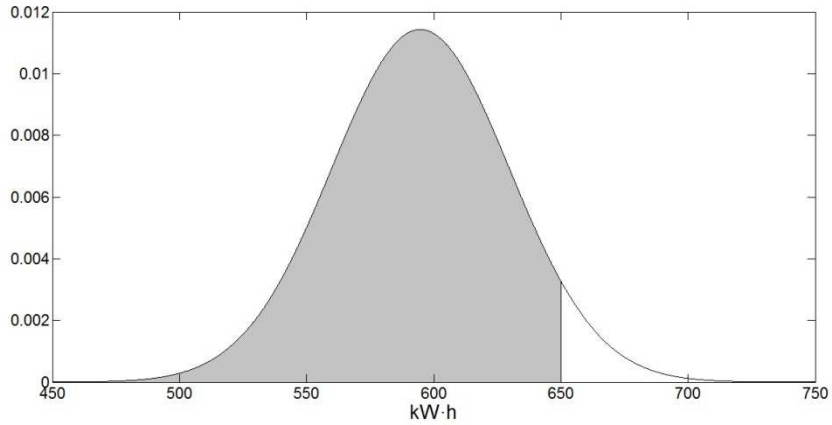

Fig. 50. Second example, E_{ROUTE} equals to 650 kWh implies ratio equal to 94.3%

When the daily consumption is lower than the E_{ROUTE} defined, the vehicle will finish its route in normal conditions. When the daily consumption is higher than the E_{ROUTE} defined, the vehicle will not finish its route in normal conditions and will have a penalty. Depending on what parameter is to be optimized (ex. minimize fossil-fuel consumption), the penalty will have to be defined (ex. the vehicle arrives late at the base because of running with low power and the crew has to be overpaid for extra time).

Working with this vehicle development concept, the impact of running out of batteries has to be studied, because the impact will differ with different vehicle architectures. In general, if the ICE is big

enough, the impact will be minimal, but when the ICE is not powerful enough to propel the vehicle at expected speeds, road speed will be reduced. In critical cases, a tow truck would be needed.

There will be an incentive for fossil energy saved daily, and a penalty for vehicles (or vehicle drivers) not finishing their routes in normal conditions.

This argument could be applied to other factors which could be optimized such as CO_2.

The savings of this fleet operation mode can be calculated as:

$$\text{Savings} = K_{SAV} \cdot \text{Ratio} \cdot N_{TRIPS} \tag{32}$$

where K_{SAV} is the unitary saving related to the substitution of fossil fuels (as an example for electric energy stored in a battery), and N_{TRIPS} is the total amount of services affected by this working concept.

The cost associated to the vehicles not finishing its routes can be calculated as:

$$\text{Overcost} = K_{OCOST} \cdot (1 - \text{Ratio}) \cdot N_{TRIPS} \tag{33}$$

Where K_{OCOST} is the cost related to the vehicles not finishing routes in good condition. This could be interpreted as the cost of a tow truck, its CO_2 emissions or its fossil-fuel consumption.

This fleet working mode is interesting while the benefit is positive; the benefit is defined as:

$$\text{Benefit} = \text{Savings} - \text{Overcost} \tag{34}$$

$$\text{Benefit} = K_{SAV} \cdot \text{Ratio} \cdot N_{TRIPS} - K_{OCOST} \cdot (1 - \text{Ratio}) \cdot N_{TRIPS} \tag{35}$$

$$\text{Benefit} = N_{TRIPS}\big((K_{SAV} + K_{OCOST})\text{Ratio} - K_{OCOST}\big) \tag{36}$$

Considering E_{99} as the E_{ROUTE} value which corresponds to all vehicles (approximated by 99.999%) finishing their routes with $E_L>0$, the relation between E_{ROUTE} and K_{SAV} is:

$$E_{ROUTE} = E_{99} - K_{SAV} \tag{37}$$

The goal is to find the optimal benefit, sizing K_{SAV} (unitary saving) as a function of K_{OCOST}. As K_{SAV} and Ratio are related through the normal law (31) K_{OCOST} will also define the Ratio value. Based on the complementary Gaussian error function and Taylor series, an expression which identifies the relation between K_{OCOST} and K_{SAV} is presented in (52).

Ratio being the cumulative distribution function of N:

$$\text{Ratio} = \int_{-\infty}^{E_{99}-K_{SAV}} \frac{1}{\sigma\sqrt{2\pi}} e^{-\frac{1}{2}\left(\frac{x-\mu}{\sigma}\right)^2} \partial x \tag{38}$$

Due to the normal law property:

$$(1 - \text{Ratio}) = \int_{E_{99}-K_{SAV}}^{\infty} \frac{1}{\sigma\sqrt{2\pi}} e^{-\frac{1}{2}\left(\frac{x-\mu}{\sigma}\right)^2} \partial x = \frac{1}{\sigma\sqrt{2\pi}} \int_{E_{99}-K_{SAV}}^{\infty} e^{-\left(\frac{x-\mu}{\sqrt{2}\sigma}\right)^2} \partial x \tag{39}$$

Variable change:

$$\tau = \frac{x-\mu}{\sqrt{2}\sigma} \;;\; \partial\tau = \frac{\partial x}{\sqrt{2}\sigma} \rightarrow \sqrt{2}\sigma\, \partial\tau = \partial x \;;\; x = \infty \rightarrow \tau = \infty \tag{40}$$

$$x = (E_{99} - K_{SAV}) \rightarrow \tau = \left(\frac{E_{99}-K_{SAV}-\mu}{\sqrt{2}\sigma}\right) \tag{41}$$

After the variable change:

$$(1 - \text{Ratio}) = \frac{\sqrt{2}\sigma}{\sigma\sqrt{2\pi}} \int_{\frac{E_{99}-K_{SAV}-\mu}{\sqrt{2}\sigma}}^{\infty} e^{-\tau^2}\, d\tau = \frac{1}{\sqrt{\pi}} \int_{\frac{E_{99}-K_{SAV}-\mu}{\sqrt{2}\sigma}}^{\infty} e^{-\tau^2}\, d\tau \tag{42}$$

According to the 'Gaussian error function' and the 'complementary Gaussian error function':

$$(1 - \text{Ratio}) = \frac{1}{2} \cdot \text{erfc}\left(\frac{E_{99}-K_{SAV}-\mu}{\sqrt{2}\sigma}\right) = \frac{1}{2}\left(1 - \text{erf}\left(\frac{E_{99}-K_{SAV}-\mu}{\sqrt{2}\sigma}\right)\right) \tag{43}$$

Using the Taylor series:

$$\text{erf}\left(\frac{E_{99}-K_{SAV}-\mu}{\sqrt{2}\sigma}\right) = \frac{2}{\sqrt{\pi}} \sum_{n=0}^{\infty} \frac{(-1)^n \left(\frac{E_{99}-K_{SAV}-\mu}{\sqrt{2}\sigma}\right)^{(2n+1)}}{n!(2n+1)} \tag{44}$$

$$\text{Ratio} = 1 - \frac{1}{2}\left(1 - \frac{2}{\sqrt{\pi}} \sum_{n=0}^{\infty} \frac{(-1)^n \left(\frac{E_{99}-K_{SAV}-\mu}{\sqrt{2}\sigma}\right)^{(2n+1)}}{n!(2n+1)}\right) \tag{45}$$

$$\text{Ratio} = \frac{1}{2} + \sum_{n=0}^{\infty} \frac{(-1)^n \left(\frac{E_{99}-K_{SAV}-\mu}{\sqrt{2}\sigma}\right)^{(2n+1)}}{\sqrt{\pi}\, n!(2n+1)} \tag{46}$$

To find the optimal benefit as a function of K_{SAV}:

$$\frac{\partial \text{Benefit}}{\partial K_{SAV}} = N_{TRIPS}\left((K_{SAV} + K_{OCOST})\frac{\partial \text{Ratio}}{\partial K_{SAV}} + \text{Ratio}\right) = 0 \tag{47}$$

$$\frac{\partial \text{Ratio}}{\partial K_{SAV}} = \sum_{n=0}^{\infty} \frac{(-1)^n (2n+1) \left(\frac{E_{99}-K_{SAV}-\mu}{\sqrt{2}\sigma}\right)^{(2n)} (-1)}{\sqrt{2}\sigma\sqrt{\pi}\, n!(2n+1)} \tag{48}$$

$$\frac{\partial \text{Ratio}}{\partial K_{SAV}} = \sum_{n=0}^{\infty} \frac{(-1)^{n+1} \left(\frac{E_{99}-K_{SAV}-\mu}{\sqrt{2}\sigma}\right)^{(2n)}}{\sqrt{2}\sigma\sqrt{\pi}\, n!} \tag{49}$$

$$\frac{\partial \text{Benefit}}{\partial K_{SAV}} = N_{TRIPS}\left((K_{SAV} + K_{OCOST})\frac{\partial \text{Ratio}}{\partial K_{SAV}} + \text{Ratio}\right) \tag{50}$$

$$\frac{\partial \text{Benefit}}{\partial K_{SAV}} = N_{TRIPS}\left((K_{SAV} + K_{OCOST}) \sum_{n=0}^{\infty} \frac{(-1)^{n+1} \left(\frac{E_{99} - K_{SAV} - \mu}{\sqrt{2}\sigma}\right)^{(2n)}}{\sqrt{2}\sigma\sqrt{\pi}\, n!} + \frac{1}{2} + \sum_{n=0}^{\infty} \frac{(-1)^n \left(\frac{E_{99} - K_{SAV} - \mu}{\sqrt{2}\sigma}\right)^{(2n+1)}}{\sqrt{\pi}\, n!\, (2n+1)}\right) = 0 \tag{51}$$

As $N_{TRIPS} \neq 0$:

$$\frac{1}{\sqrt{\pi}}\sum_{0}^{\infty}(-1)^{n}\left[\frac{-(K_{SAV}+K_{OCOST})\left(\frac{E_{99}-K_{SAV}-\mu}{\sqrt{2}\sigma}\right)^{2n}}{\sqrt{2}\sigma n!}+\frac{\left(\frac{E_{99}-K_{SAV}-\mu}{\sqrt{2}\sigma}\right)^{2n+1}}{n!(2n+1)}\right]+\frac{1}{2}=0 \quad (52)$$

As there is no analytic solution, the K_{SAV} has to be identified for a given K_{OCOST} value by iteration. Once the K_{SAV} is estimated, E_{99} and Ratio can be estimated from (52).

A few examples showing how this method could be implemented are presented, considering that the vehicle works 365 days per year.

On the first example, we will consider an electric vehicle with batteries and fuel cells as range extender. This vehicle needs a special service (technical service replaces batteries, takes a fast battery charger to the truck…) if the battery is depleted. The average consumption in its daily route is (μ= 594.78 kWh, σ=34.90 kWh, E_{99}=750 kWh). The optimization target parameter is the energy consumption. If the fleet vehicle needs the special service when E_L<0 and it has an average consumption of 15 liter per service (K_{OCOST}= 140.1 kWh), K_{SAV} should be 81.5 kWh and E_{ROUTE}= 668.5 kWh (Ratio 98.27%). Compared to a traditional hybrid power-train management strategy (SOC constant), working with E_{ROUTE}= 668.5 kWh would generate a yearly saving:

$$\text{Benefit} = 365\big((81.5 + 140.1) * 0.9827 - 140.1\big) = 28384\ \text{kWh}$$

The vehicle would finish its route in normal conditions 358 times per year.

The second example is similar to the first one, but the services company does not accept more than three stops per year because of this working concept (Ratio 99.18%) even if this value does not match what is optimal in terms of fuel consumption.

The savings per year would be:

$$K_{SAV} = E_{99.99} - E_{ROUTE} = 750 - 678.5 = 71.5\ \text{kWh}$$

$$\text{Benefit} = 365\big((71.5\ + 140.1) * 0.9918 - 140.1\big) = 25464\ \text{kWh}$$

The vehicle would finish its route in normal conditions 362 times per year.

The third example is similar to the first one but for the special service, a tow truck would be needed and the optimization target is economic cost. The cost of a tow truck considered is 450 euros (standard cost in Barcelona in 2014). There is no K_{SAV} value which can generate a positive benefit, so this working concept could not be applied.

On the forth example, we will consider a series hybrid vehicle with internal combustion engine and battery. Its ICE cannot deliver the maximum power that the power train may demand, so if the batteries are depleted, the vehicle would drive at reduced speed. Each hour fraction, the crew arrives late at the base and has to be paid as a whole hour.

As this would occur just at the end of the trip, it has been considered that the delay would be shorter than one hour, and we will consider the cost of one full hour as penalty (75 euros which is the cost of 583.7 kWh). K_{SAV} should be 17.5 kWh and E_{ROUTE} = 732.5 kWh (Ratio 99.99%).

Compared to a traditional hybrid power-train management strategy (SOC constant), working with this concept and E_{ROUTE}=732.5 kWh would generate savings per year:

$$\text{Benefit} = 365\big((17.5 + 583.7\,) * 0.9999 - 583.7\ \big) = 6360\ \text{kWh}$$ of fossil fuel, 558.5 diesel kg

The vehicle would not finish its route in normal conditions 1 day for every 28 years.

The estimations presented in the current section are related to optimizations for a given vehicle driving daily on the same route. These optimization algorithms could also be used in real time and on-board the vehicle, providing specific developments. As it has been presented in this dissertation, the vehicle can use these algorithms in real time, but it needs of a previous work which has been developed by the researchers.

What makes the method interesting is the fact that the previous work necessary to define the normal law (31) can be easily implemented on the control system of the vehicle, estimating the daily consumption with (29).

This opens the option to generate systems with the possibility to auto-learn constantly on the repeated routes and adjust the control systems to deplete the battery on a daily basis.

5.3. Discussions and Conclusions

Some vehicles (such as RCVs, buses or delivery trucks) follow the same route daily, performing drive cycles which are not entirely the same but still very similar in many aspects.

This route repetition can be understood as an information source which can provide knowledge real time about the future power and energy demands for drive cycles being executed on repeated routes. Several authors have also demonstrated that most of the kilometers or distances travelled by a standard driver belong to a small number of routes [44] which would open the application of these concepts to other machines.

The proposed algorithm is an analytic algorithm which can estimate the energy necessary for the vehicle to finish daily work. Based on this information, the power train management strategy can deplete the energy storage system of a hybrid vehicle before the end of its trip, thus, optimizing the substitution of fossil fuel by electricity. This algorithm can also be used to reduce other parameters such as pollutant emissions, or fleet operations costs.

6.
Drive Cycle Analysis of the Performance of ICE

This chapter analyses the working modes of an ICE on real RCV drive cycles by the use of data logged during regular services. It contrasts the engine working points and efficiency maps, and it also estimates the average power consumption of an RCV, comparing it to the instantaneous power at each moment during the whole drive cycle. Based on the conclusions of this analysis, hybrid powertrain architectures are proposed.

CONTENTS:

6.1. Introduction

Standard vehicle powertrains are developed taking into account that they have to work in a wide variety of drive cycles, and the performance of the powertrain has to be satisfactory in each of them. Usually the same vehicle is sold in different places in which the weather, the altitude above sea level or the population distribution of the area conditions the vehicle's drive cycle.

High places are characterized by low atmospheric pressure (e.g. Andean regions), the north of Europe is characterized by low temperatures in winter, urban areas are characterized by drive cycles with a lot of transients and low mean speeds and rural areas are characterized by minor transients and higher mean speeds. When developing hybrid powertrains all these conditions have to be considered.

When considering RCVs this situation is different. As shown in chapter 2 of this thesis, the drive cycle of an RCV always follows a similar profile. As a result the working points of an ICE (understood as RPM and torque coordinates) will also have a similar distribution.

In the present chapter of this thesis the working points of an RCV ICE on real routes have been analyzed and contrasted with a BSFC map, to determine whether the engine is working at high efficiency points or not. Also the average power delivered by the engine via the drive cycle is estimated and compared to the instantaneous power in order to analyze the downsizing potential in the case of hybridization.

6.2. Drive Cycle Analysis of the Efficiency of ICE in RCV

To understand the efficiency improvement potential of the powertrain hybridization, two algorithms have been developed to analyze the operation of the internal combustion engine in a standard RCV powertrain. The studied ICEs are a 220-kW diesel unit and a 200-kW CNG unit.

The first algorithm registers the torque (J1939 SPN 513) and RPM (J1939 SPN 190) of the ICE, acquiring data at 10 Hz during the whole working route. By plotting the logged data on a graphic (see Figs. 51-55), the density of samples at each RPM (abscissa) and torque (ordinate) can be observed. The coloured areas in red mean a high density sample, while the coloured areas in blue mean a low density sample.

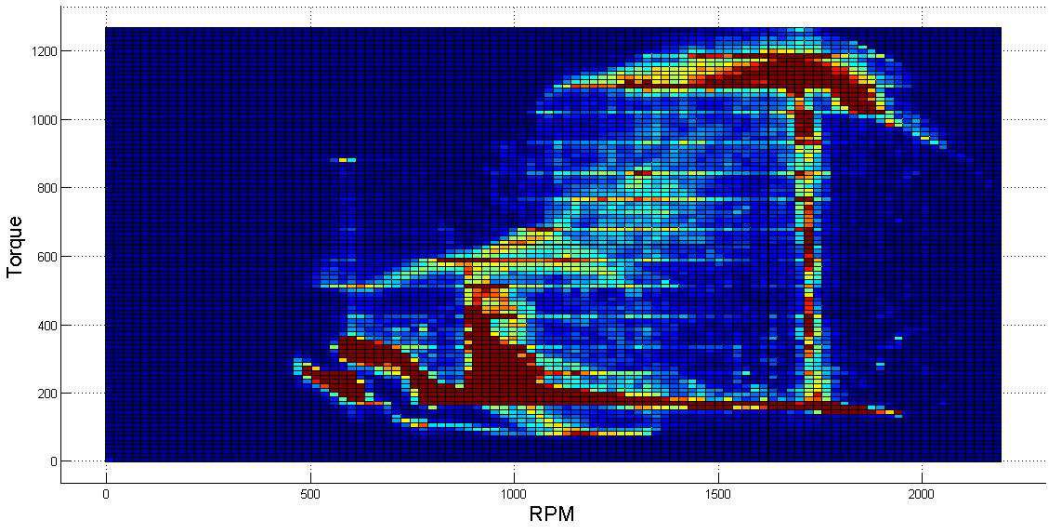

Fig. 51. Densities of samples 1

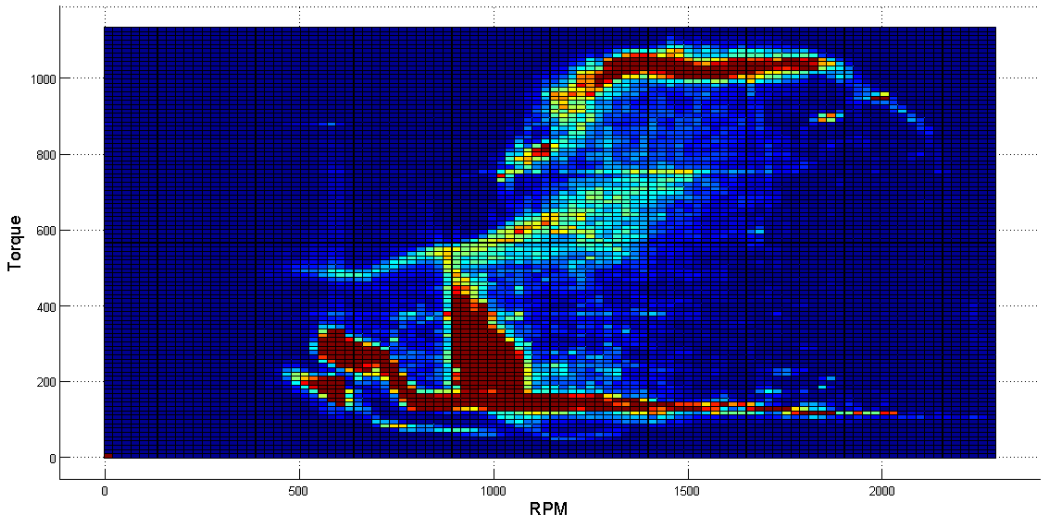

Fig. 52. Densities of samples 2

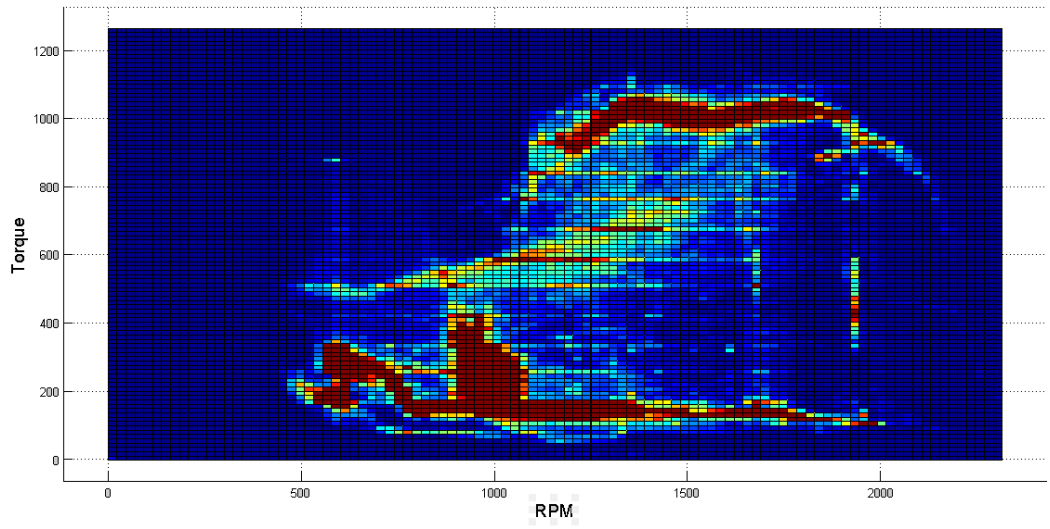

Fig. 53. Densities of samples 3

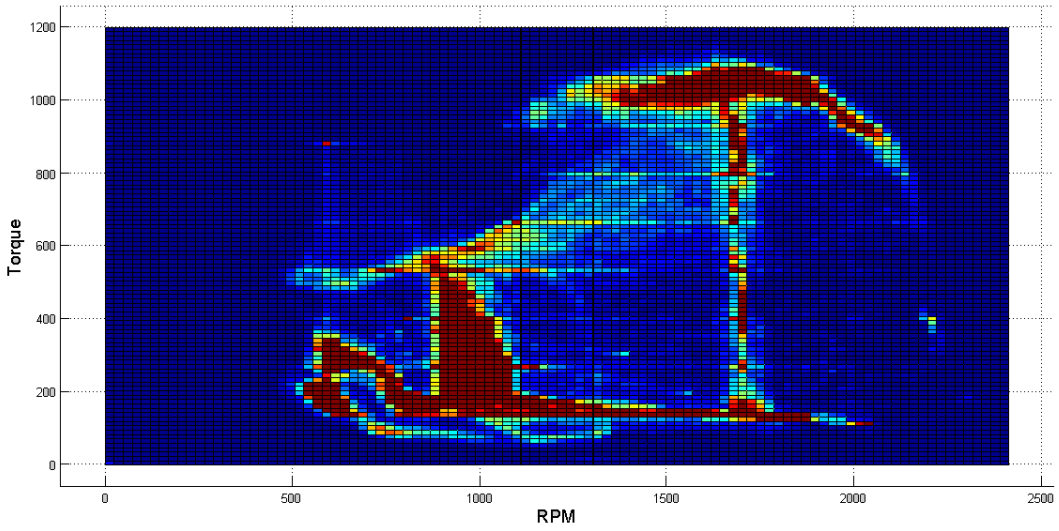

Fig. 54. Densities of samples 4

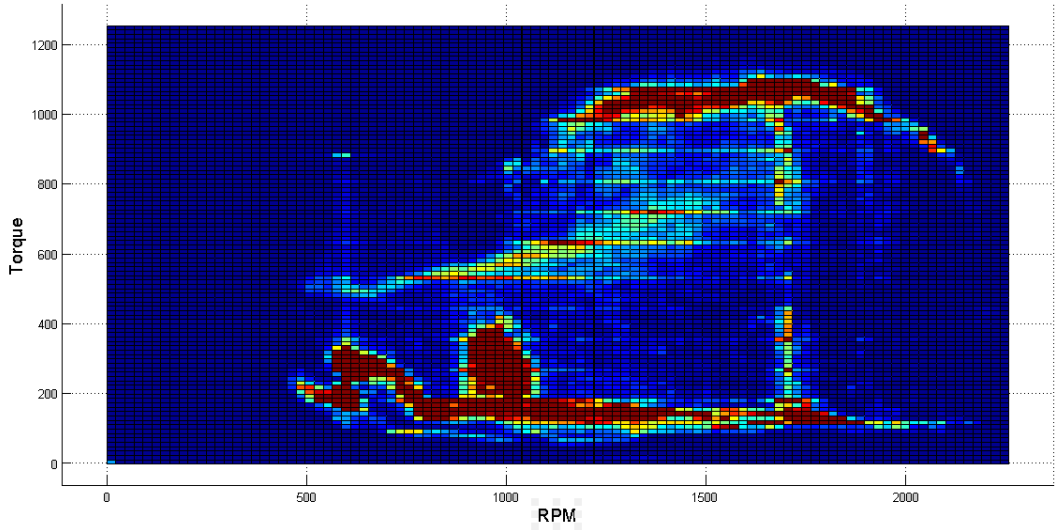

Fig. 55. Densities of samples 5

In Figs. 51-55, three areas containing a higher density sample can be clearly identified. These three areas have been marked with red balloons on Fig. 56:

The first area, labelled as 1, belongs to the samples when the ICE has been at idling (vehicle stopped due to traffic or waiting to collect refuse). This area has the highest number of samples of all identified areas.

The second area, labelled as 2, belongs to the samples when the vehicle is stopped but the body ancillaries are working. No traction power is needed but power to energize the body is consumed. This is the area with the second highest number of samples.

The third area, labelled as 3, belongs to the interval of time when the vehicle is being driven from one stop to another. Usually this manoeuvre is performed at full throttle. This is the area with the third highest number of samples.

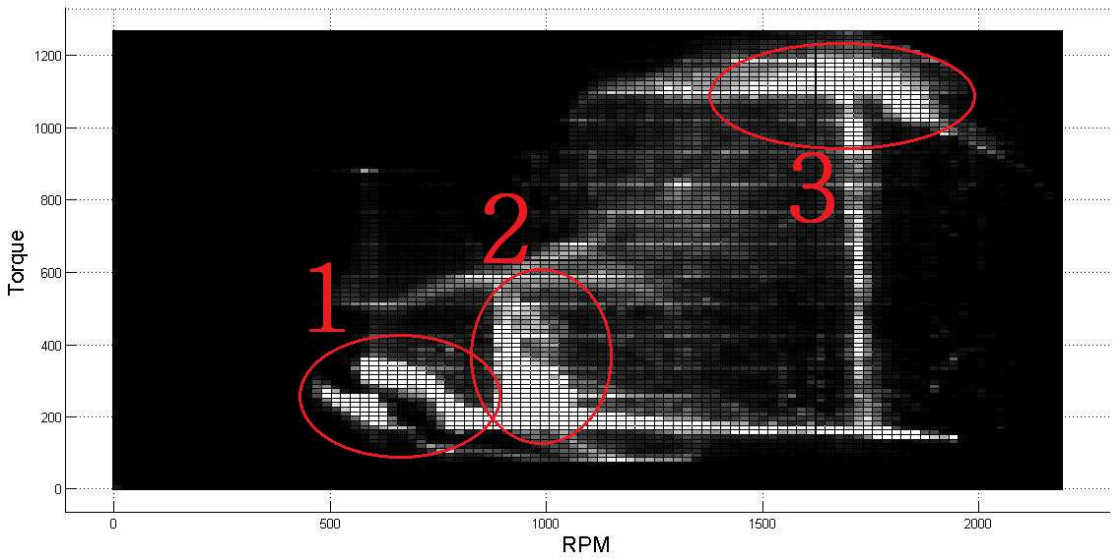

Fig. 56. Some identified areas with high density of samples

In Fig. 57, the efficiency map of the diesel engine of a typical RCV is shown. The isoconsumption trajectories/lines can be appreciated with the associated fuel consumption curves. A wide red curve can also be observed over the efficiency map. This curve is the optimal consumption line, and it shows the torque at which the ICE has its best efficiency for each regime.

Comparing the areas with high density samples (Fig. 56) with an efficiency map (BSFC in g/kWh, Fig. 57), it must therefore be concluded that the ICE of a standard RCV working on a regular refuse-collecting route tends to work far from the high efficiency points.

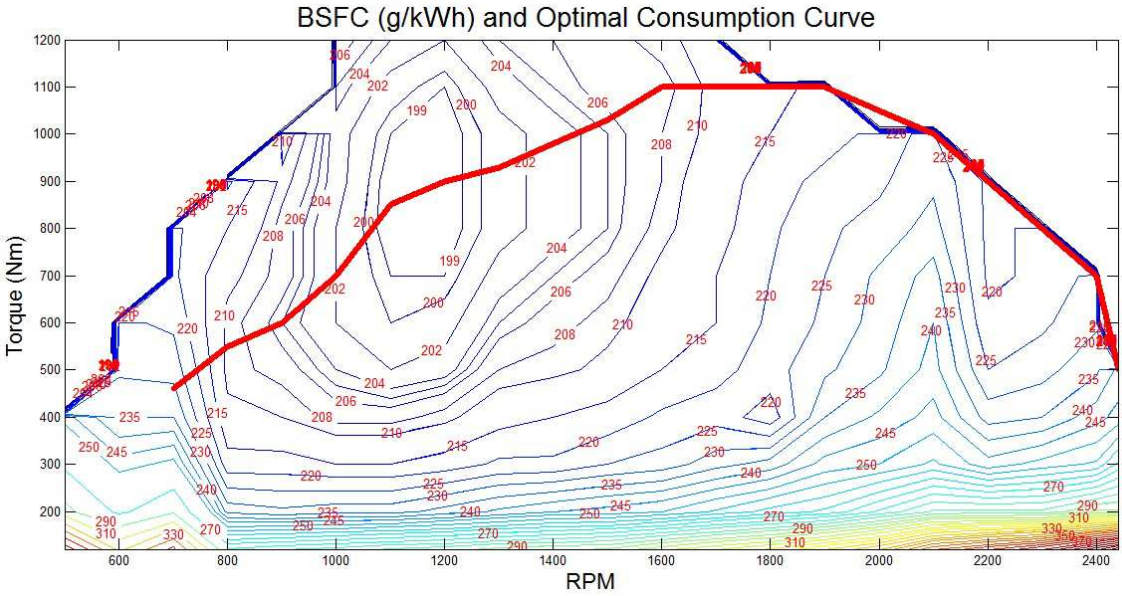

Fig. 57. BSFC (g/kWh) of a 220-kW diesel engine

6.3. Drive Cycle Analysis of the Average Power of ICE in RCV

The second developed algorithm to analyze the ICE operation estimates the instantaneous engine power and also its average value from the previously mentioned engine RPM and torque, during the whole collecting cycle and plots both versus time. In Figs. 58-59, the instantaneous power (in blue) and its average value (in red) can be observed for a whole refuse-collecting drive cycle.

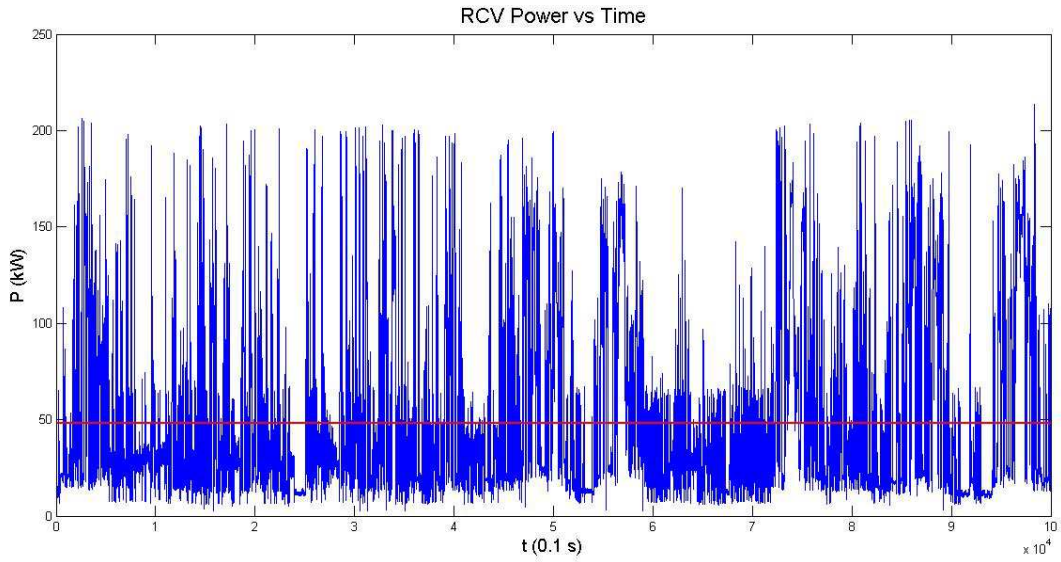

Fig. 58. Instantaneous power (in blue) and average power (in red) [kW] for an RCV drive cycle

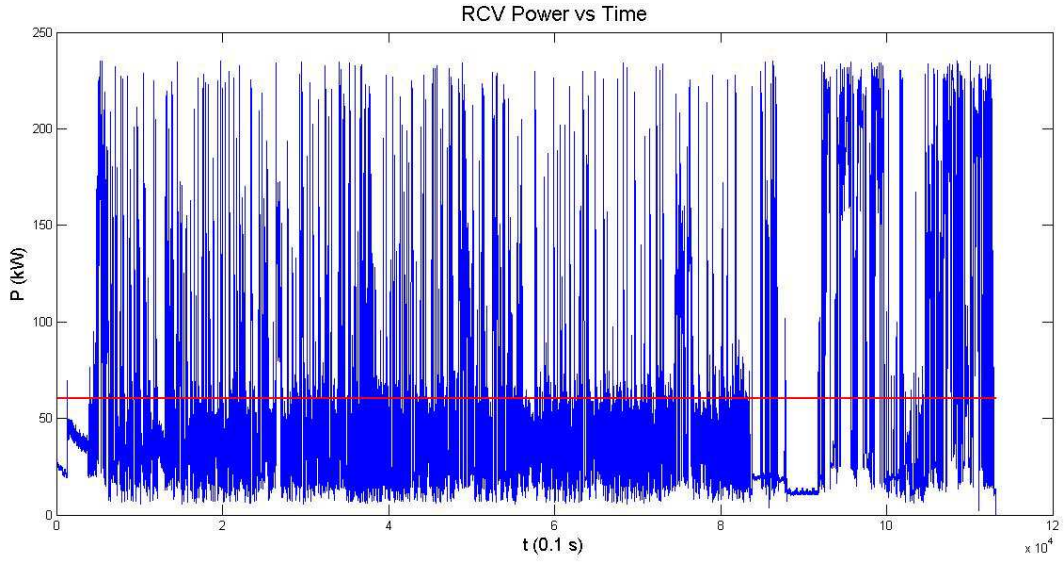

Fig. 59. Instantaneous power (in blue) and average power (in red) [kW] for an RCV drive cycle

Despite the fact that maximum peak power values are over 200 kW, the average value of power is from 40 kW to 70 kW for the complete set of analyzed routes.

6.4. Conclusions

The main conclusions of this chapter are that the ICE hardly ever works at high efficiency points and it is oversized for most of the drive cycle. A series hybrid vehicle can maintain its engine working at high efficiency points independently of the total instantaneous power demanded by the powertrain or its speed. This has demonstrated that a series hybrid vehicle is more efficient in similar drive cycles such as urban buses [55]. For this reason, it is decided in this research work that a series hybrid vehicle be chosen as powertrain architecture.

7.

Topological Analysis for Hybrid-Hydraulic Powertrain

In this chapter hybrid hydraulic powertrain architecture is proposed and modeled. The proposed powertrain model is executed using two different control algorithms, with and without predictive strategies, with data obtained from real routes.

CONTENTS:

7.1. Introduction

Compared with electric hybridization, hydraulic hybridization offers higher power density but lower energy density [2]. Hydraulic hybridization seems to be the technical option best suited to vehicles with high power flows, such as heavy machinery. On the other hand, electric hybridization seems to be the most appropriate technical option for cars. Refuse-collection vehicles and urban buses remain in an intermediate situation.

The main scope of this chapter is not to improve knowledge of hybrid hydraulic systems, which have been studied by other authors [2], [19], [29]-[34] in the past, but to study the impact of the use of this type of powertrain in RCVs.

The industrialization of a hybrid-hydraulic powertrain is not novel. From an application point of view, commercial proposals to hydraulically hybridize a powertrain in parallel [52], in series [53], [54] or by using two powertrains applied to different vehicle wheels [54] are available on the market.

7.2. Powertrain Models

The proposed powertrain architecture in this work is composed of three main elements: a hydraulic accumulator as the energy storage system (ESS), an ICE as the energy generation system (EGS), and a hydraulic motor/pump as the energy consumption/generator system (ECS).

In Fig. 60, the proposed topological design in this work is introduced. The cardan of the vehicle is linked to the hydraulic motor of the vehicle through the gearbox which remains the same as in the original vehicle (with ICE).

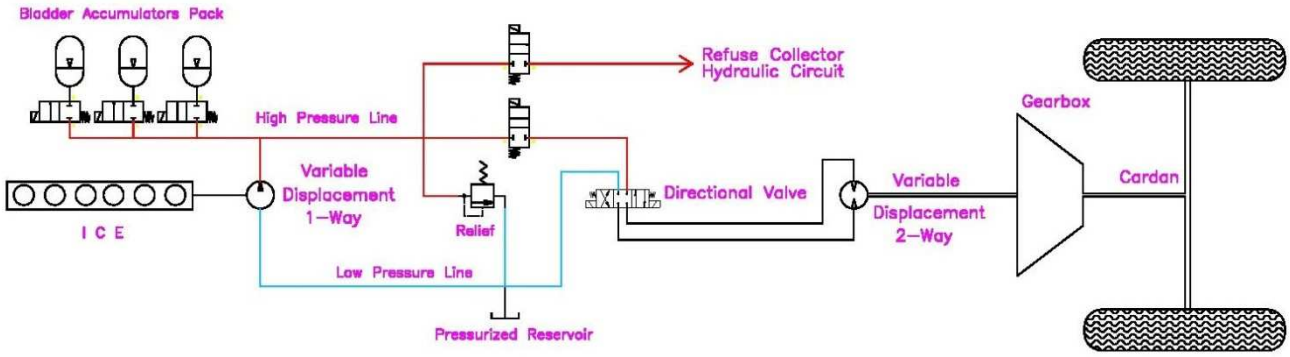

Fig. 60. Series architecture of the proposed hybrid hydraulic powertrain

Depending on the position of the directional valve, the 'Variable Displacement 2-Way' element, the hydraulic motor will act as motor or as pump, consuming power from the 'High Pressure Line' or adding power to the 'High Pressure Line'. This schema does not intend to be an exhaustive design but a conceptual proposal which will help to understand the hybrid powertrain architecture.

7.2.1. Hydraulic Motor an Pump Model

The motor/pump model proposed (referred on Fig. 60 as 'Variable Displacement 1- or 2-Way') is an electronically controlled variable displacement pump [56]. The main reason for working with this technologic concept is that the hydraulic motor can match any pressure at the high pressure rail with any torque needed at the input axe of the gearbox, just modifying the displacement of the pump (of course, there will always be limits on the pump displacement). At the same time, its efficiency is higher at a wider RPM range compared with the traditional concept of variable displacement pumps [56].

The efficiency maps proposed for the hydraulic motors (Figs. 61-62) are replotted from [56] and reproduced in this form by permission of [57]. In the associated model, the efficiency of the motor and motor/pump is taken directly from these maps or interpolated for intermediate displacement values.

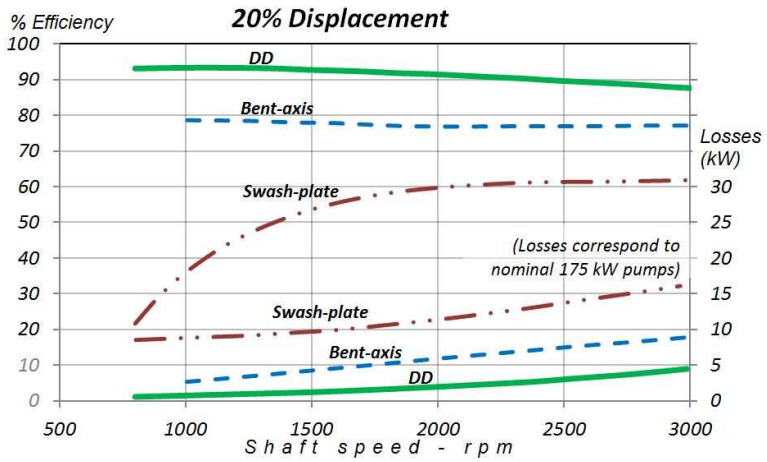

Fig. 61. Efficiency of the variable displacement pump at 20% displacement

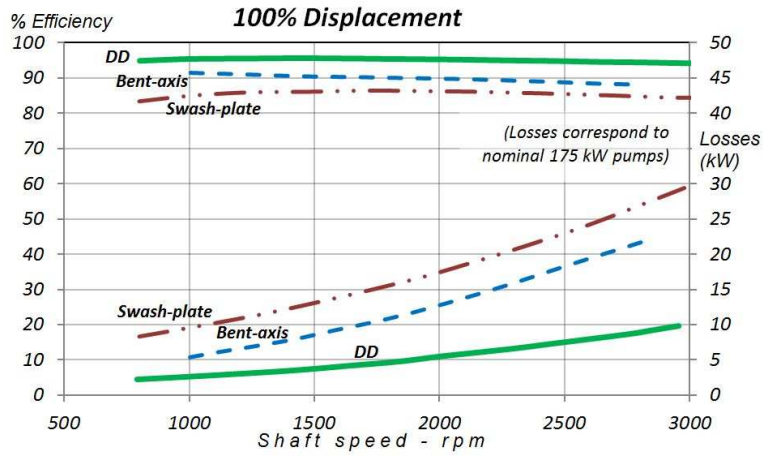

Fig. 62. Efficiency of the variable displacement pump at 100% displacement

7.2.2. Hydraulic Accumulators

The model of the hydraulic accumulator is inspired in the work published in [2]. More complex and accurate models [30] have not been considered because, as mentioned previously, the main goal of this work is not to have an exhaustive hydraulic model but to estimate the impact of a hydraulic powertrain on an RCV.

The size of the accumulators has been estimated fulfilling the manufacturer requirements [58].

The whole proposed system is a bladder accumulator, whose behaviour is supposed to be adiabatic, filled with nitrogen. The expression used to calculate the accumulator sizing is:

$$V_0 = \frac{\Delta V}{\left(\frac{P_0}{P_1}\right)^{0.714} - \left(\frac{P_0}{P_2}\right)^{0.714}} \tag{53}$$

where:

1. P0: Gas pre-charge pressure.
2. P1: Lower working pressure.
3. P2: Higher working pressure.
4. ΔV: Volume at P2 – volume at P1.
5. V0: Effective gas volume.

The expression used to estimate the inner pressure from the accumulated volume is:

$$P_x = P_1 \left(\frac{V_1^{1.4}}{V_x^{1.4}}\right) \tag{54}$$

and the expression used to estimate the energy stored in a compression between any two states 1 and 2 is:

$$E(kJ) = \frac{P_1 \cdot V_1^{\gamma}}{1000} \left(\frac{V_2^{1-\gamma} - V_1^{1-\gamma}}{1-\gamma}\right) \tag{55}$$

The efficiency of this system is always difficult to estimate because it depends on the heat exchange with the environment. As the vehicle speed and the ambient temperature change, the convection coefficient is difficult to estimate. In this work, the efficiency of the hydraulic accumulator used for calculations is 0.9 [2]. This is implemented in the model applying the corresponding pressure loss on the discharge phase of the accumulator [2], as represented in Fig. 63.

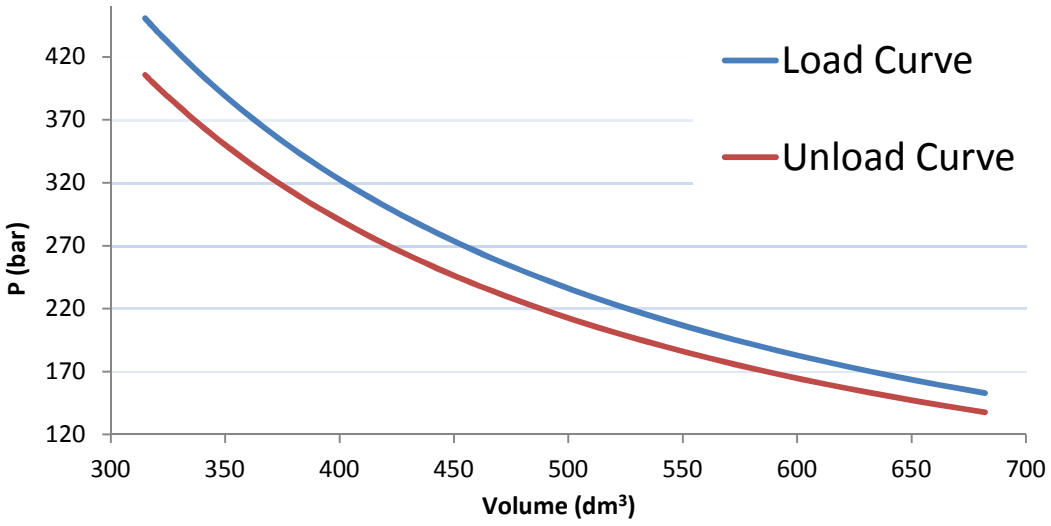

Fig. 63. Graphic representation of the load and unload curve of the bladder accumulator (adiabatic with 90% efficiency)

7.2.3. Body Hydraulic System

The model of the body of the RCV used for estimations is a Ros Roca Cross Body with a Ros Roca UPC lifter (both hydraulically powered). In this work, the body ancillaries' energetic consumption is simplified to its pressure and flow consumption. The pressure is taken from a pressure sensor installed on the hydraulic line at the output of the oil pumps as in [28]. The flow is estimated considering the RPM of the engine (J1939 SPN 190); the displacement of the pump and its leakage. The leakage is estimated as in [28] using the maps provided by the pump manufacturer.

$$\mathrm{Q} = \left(\mathrm{RPM}\frac{60}{2\pi}\mathrm{D}\right) - \mathrm{Leakage} \tag{56}$$

7.2.4. Internal Combustion Engine

In this model, the engine element is reduced to the optimal consumption curve of the BSFC map (see the red line in Fig. 57) which will estimate the fuel consumption, the torque, and RPM in the function of the demanded power (see Table XI).

TABLE XI
PARAMETERS OF THE OPTIMAL CONSUMPTION CURVE OF THE ICE

Power(kW)	33.7	46	56.5	73.3	97.9	113	127	144	162	184	196	207
Speed (RPM)	700	800	900	1000	1100	1200	1300	1400	1500	1600	1700	1800
BSFC(g/kW·h)	213	209	205	202	198	198	201	203	205	207	211	213
Torque (Nm)	460	550	600	700	850	900	930	980	1030	1100	1100	1100

The fuel necessary to restart the engine when it is off has been parameterized and introduced in the simulation of the powertrain. As no specific literature for heavy duty engines has been found, this parameter has been taken from a smaller engine [67] and its value corrected based on the displacement ratios (estimated to be 10.5 g for this study).

7.3. Control Strategies

The control strategy proposed in the present section depends on two different concepts. The first is the ICE control strategy which is presented in section 7.3.2. The second is the Route prediction system which is commented in 7.3.1. and generates information (SOC_{Limit}, SOC_{100}, P_{mean}) for a higher layer control strategy which can change the parameters of the ICE control strategy in real time.

7.3.1. Route Prediction System

RCV routes are characterized by two main working modes.

The first mode is the vehicle transport mode, in which the drive cycle is characterized by higher speeds and slower power transitions; this mode corresponds to the travel from the base to the urban zone and vice-versa, or from the urban zone to the landfill/transfer station and vice-versa. In this mode, the engine is usually working in the area marked as '3' in Fig. 56.

The second mode is the refuse-collecting mode (performed in the urban zone). In this mode, the vehicle is accelerated and slowed aggressively from one bin collection to the next one. When the vehicle is stopped, the ancillaries are actuated. In this mode, the working points of the engine change constantly among the areas '1', '2', and '3' of Fig. 56.

In chapter 2, detailed information about the drive cycles in an RCV can be found. In chapter 4 an algorithm based on artificial intelligence (AI) is also proposed to identify if the vehicle is working in 'collecting mode' or 'transport mode', each working mode has associated values for SOC_{Limit}, SOC_{100}, P_{mean} values. In the present chapter, this information is assumed available.

7.3.2. ICE Control Strategy

Based on the state of charge (SOC) of the accumulators and the 'Engine Status', the ICE control strategy (Fig. 64 and Equations 57 to 61) is defined by a deterministic algorithm. The ICE control is inspired in [30] but parameterized, meaning that these parameters (SOC_{Limit}, SOC_{100}, P_{mean}) can be changed during the drive cycle depending on a higher layer control strategy, which depends on the Route prediction system.

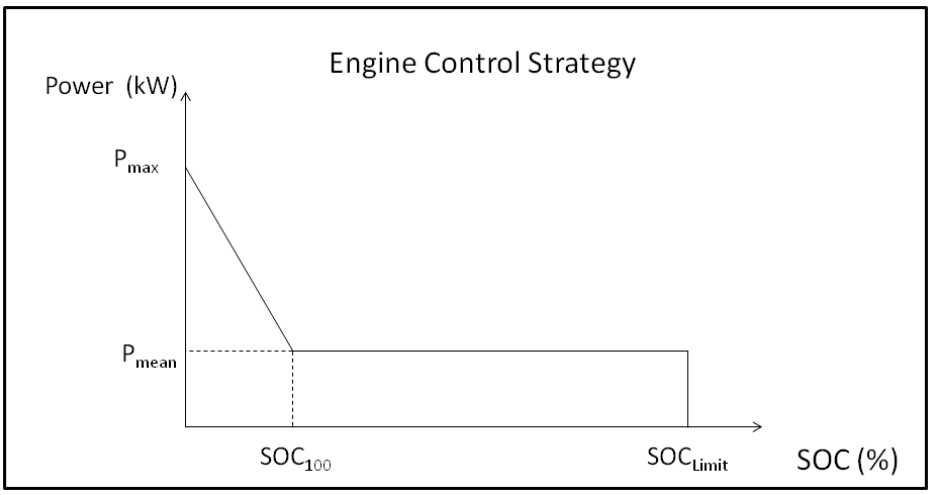

Fig. 64. Control Strategy for the Internal Combustion Engine

At the abscissa axis, the state of charge (SOC %) of the ESS is shown; at the ordinate axis, the power demanded to the engine is shown.

The ICE has two operating modes: running and stopped. When the SOC reaches SOCLimit, its mode becomes stopped and it will be switched again to running mode only if the SOC falls below SOC_{100}. When the ICE is stopped, it has no consumption and each time the ICE is started, it consumes the fuel amount specified in the ICE model (section.7.2.4.).

When the engine is running, it follows the following rules:

If the SOC of the ESS is between two values (SOC_{100} and SOC_{Limit}), the power demanded from the ICE is the average value of a drive cycle, or part of a drive cycle (P_{mean}).

If the SOC of the ESS is below SOC_{100}, the power demanded from the ICE will increase proportionally to the distance to SOC_{100}, reaching the maximum nominal power (P_{max}) of the ICE when the SOC is zero.

The following equations summarize the control algorithm used for the engine control:

$$\text{if Engine Status} = \text{ON}$$

$$\text{if SOC} \leq \text{SOC}_{100} \quad \rightarrow \text{P(kW)} = \text{P}_{\text{mean}} + (\text{P}_{\text{max}} - \text{P}_{\text{mean}}) \left(\frac{\text{SOC}_{100} - \text{SOC}}{\text{SOC}_{100}}\right) \tag{57}$$

$$\text{if SOC}_{100} < SOC \leq \text{SOC}_{\text{Limit}} \rightarrow \text{P(kW)} = \text{P}_{\text{mean}} \tag{58}$$

$$\text{if SOC} > SOC_{\text{Limit}} \quad \rightarrow \text{P(kW)} = 0 \text{ and Engine Status = OFF} \tag{59}$$

$$\text{if Engine Status} = \text{OFF}$$

$$\text{if SOC} \leq \text{SOC}_{100} \quad \rightarrow \text{P(kW)} = 0 \text{ and Engine Status} = \text{ON} \tag{60}$$

$$\text{if SOC} > \text{SOC}_{100} \quad \rightarrow \text{P(kW)} = 0 \text{ and Engine Status = OFF} \tag{61}$$

7.4. Component Sizing

In this work, the parameters SOC_{100} and SOC_{Limit} have been set to 30% and 70%, respectively. The P_{mean} parameter will be controlled in two different ways, which will define two control strategies.

In the first powertrain control strategy, it is supposed that the AI system, which identifies the current driving mode (vehicle transport and refuse-collecting drive cycle), is unavailable. As the average power of the whole drive cycle is between 40 kW and 70 kW in the previously analyzed cycles, and in this spectrum, the highest efficiency is found at 70 kW, this value is chosen as P_{mean}.

In the second powertrain control strategy, the AI system is available. The average power during the refuse-collecting mode is about 17 kW to 25 kW and the average value during the vehicle transport mode is about 90 kW to 120 kW. Using the same criteria previously mentioned, the P_{mean} is set to 25 kW during the refuse-collecting mode and to 100 kW during the transport mode.

As the bladder accumulators (ESS) are cheap components compared with the cost of an ICE or an RCV body, its cost has not been considered for the powertrain dimensioning, knowing that the main limitation of an RCV is its volume (the volume occupied by these components cannot be used to transport refuse which affects machine productivity):

Given that the bladder pack would be placed between the chassis cabin and the body, and the refuse body will have to be moved backwards, all this room will be filled with bladders, resulting to a final volume of 700 liters (7 bladders multiplied by 100 l/bladder). Pressures P0, P1, and P2 would be 153, 170, and 450 bar, respectively, which are the usual values for hydraulic circuits and are useful for the selected motor.

The hydraulic motor and pump have been sized according to the needs of an RCV powertrain as the one studied in this dissertation (maximum torque 1200 Nm and maximum speed 2450 RPM), which are the standard values for this type of technology. Commercial proposals with similar figures can be found in the market.

As the energy stored in hydraulic bladders is minimal (7760 kJ considering the previously mentioned volumes and pressures), a downsizing criteria cannot be applied to the internal combustion engine, and it has to deliver the same amount of power of the original ICE. As a result, the original ICE remains the same.

7.5. Calculation Engine

The calculation engine of this chapter has been developed in Matlab.

Using data from real routes acquired from April 2013 to June 2013 (on a Ros Roca Cross with UPC lifter), two vectors (RPM and power) containing samples at 0.1 Hz during the whole collecting work (about 7 to 8 hours), have been generated daily for 15 days.

In the calculation engine, the ICE RPM and torque values were extracted from the logged and post-processed data.

Two different hardware architectures have been simulated, a standard ICE and a hybrid series powertrain.

For the standard ICE, at each time sample (at 0.1 s), the algorithm estimates:

The instantaneous power generated by the ICE, based on the logged data.

Based on the power and RPM, it searches the BSFC.

Multiplying the two previous values (power (kW) and BSFC (g/kWh)), it estimates the instantaneous consumption, which is integrated on the whole route to get the total fuel consumption.

To estimate both powertrains in the maximum possible equity conditions, the intervals of time when the powertrain is not generating useful energy (idle) have been set to zero consumption. This is representative of a start/stop vehicle.

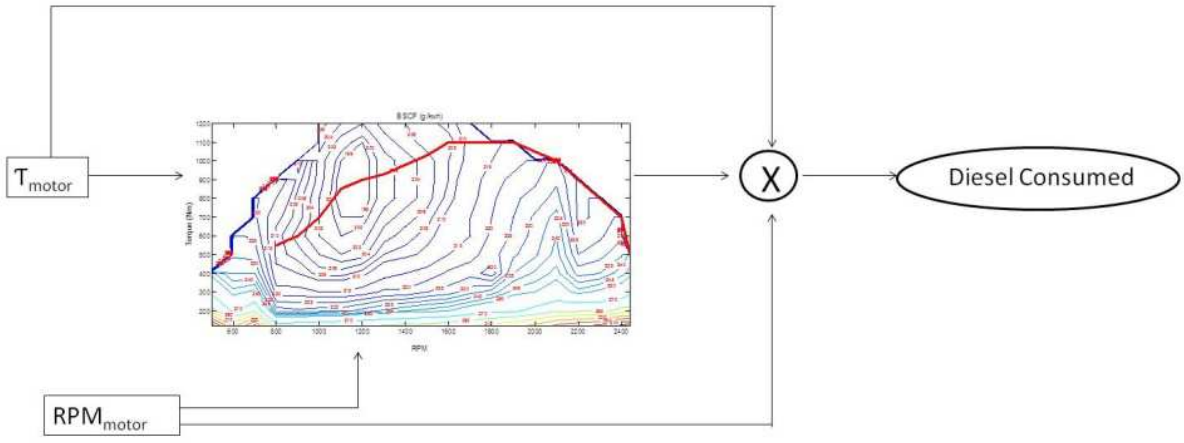

Fig. 65. Detail of the ICE fuel estimation flow

For the hybrid hydraulic powertrain, at each time sample (at 0.1 s), the algorithm:

Estimates the instantaneous power generated by the ICE, based on the SOC of the ESS in the previous instant. Based on the motor torque and the rail pressure, the displacement of the pump and the oil flow are estimated.

Estimates the instantaneous power consumption of the motor, based on the logged data. Using the instantaneous motor torque, the hydraulic rail pressure and the variable displacement of the pump, the pump displacement and the oil flow are estimated.

If the addition of the two previous values is negative, it means that there is lack of power that is supplied by the ESS. If it is positive, the power excess is stored on the ESS.

Fig. 66 summarizes how the simulation process of the powertrain is implemented. Logged files corresponding to real routes are used to feed the algorithm which is executed in quasistatic mode. As the acquisition frequency was adjusted to 10 Hz, the file contains one register for each 0.1 s of the route.

The input parameters of the algorithm are displayed in boxes. The output parameters are showed in balloons.

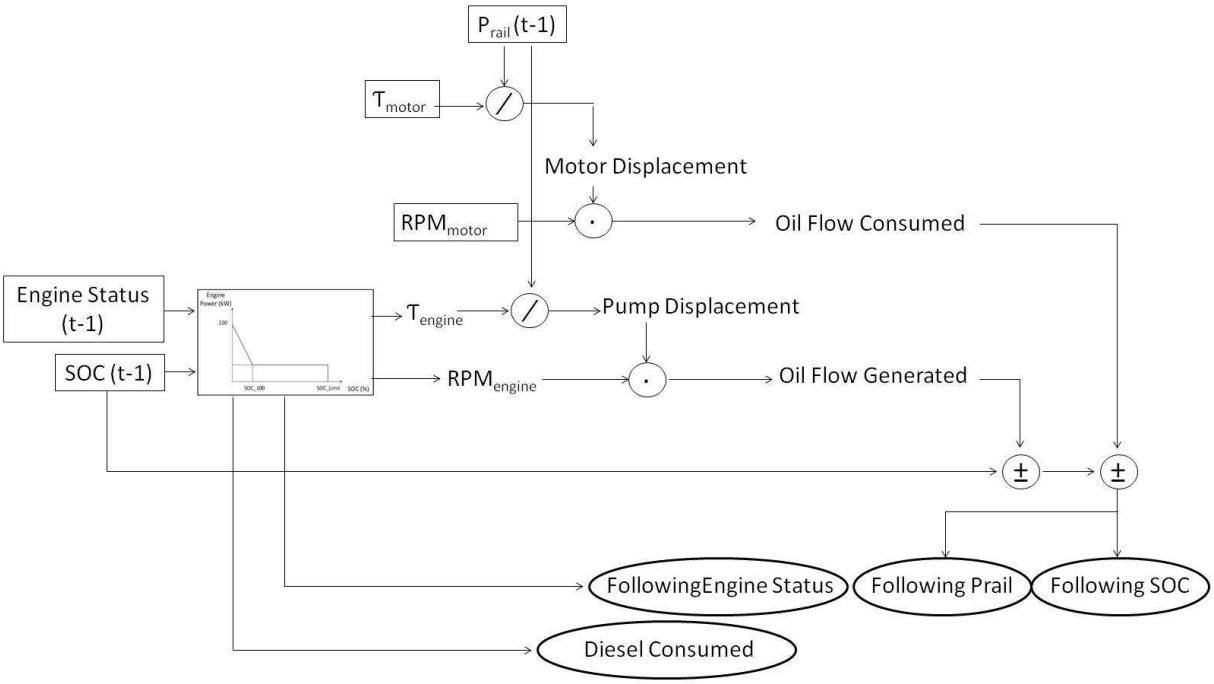

Fig. 66. Diagram of the calculation engine

The pressure at the high pressure line 'Prail' and the motor torque 'Tmotor' define the displacement of the hydraulic motor:

$$\mathrm{D}\left(\mathrm{cm}^3/_{\mathrm{rev}}\right) = \frac{\tau_{\mathrm{motor}}(\mathrm{Nm})}{\mathrm{P_{rail}(Pa)}} \tag{62}$$

The displacement and the RPM of the motor define the 'Oil Flow Consumed' from the high pressure line.

$$\mathrm{Q}\left(\mathrm{m}^3/_{\mathrm{s}}\right) = \mathrm{RPM_{Motor}} \cdot \mathrm{D}\left(\mathrm{cm}^3/_{\mathrm{rev}}\right)\frac{1}{60\cdot 10^6} \tag{63}$$

The pump displacement and the pump flow are estimated in the same way.

As mentioned previously, the simulation is executed in quasistatic mode so no transients on the engine, pumps or motor are considered. No models for the losses on the hydraulic lines have been considered.

The body ancillaries are designed to work at constant flow so they cannot be fed from the bladders, which would feed the ancillaries following an adiabatic discharge curve which determines pressures instead of flows. When the vehicle is stopped and the ancillaries need power, they will be fed from the engine and pump at the nominal flow.

Based on the power generated by the engine and its BSFC map, the instantaneous fuel consumption is estimated. The whole route consumption is approximated by integration.

7.6. Simulations Results and Conclusions

Table XII summarizes the results of the simulations with different powertrains. In the first column, the route number is displayed. In the second column, the result of the ICE consumption in kg for each route is shown. In the third column, the result of the Hybrid Hydraulic powertrain with no AI adaptation to the different driving modes can be found. In the fourth and last column, the result of the Hybrid Hydraulic powertrain with AI adaptation is presented.

TABLE XII
FUEL CONSUMPTION (KG) OF THE DIFFERENT ARCHITECTURES

ROUTE	ICE (FUEL KG)	HYBRID HYDRAULIC POWERTRAIN WITHOUT ZONE DENTIFICATION (FUEL KG)	HYBRID HYDRAULIC POWERTRAIN WITH ZONE IDENTIFICATION (FUEL KG)
1	34.51	30.86	29.59
2	33.05	29.93	28.76
3	33.08	31.37	30.40
4	29.49	26.16	25.06
5	29.53	27.13	25.85
6	31.25	28.45	27.30
7	30.98	25.80	25.15
8	31.67	26.59	25.52
9	30.76	27.38	26.37
10	30.81	27.62	26.54
11	34.76	32.21	30.99
12	31.13	28.00	26.96
13	33.15	31.05	29.71
14	32.10	28.20	27.18
15	39.24	32.39	31.10

The energy supplied to the system from the ESS (estimated as SOC change between the start and end of the route), which is in fact replacing part of the fuel consumed, is not included in Table XII.

To compare these values with the total energy consumed, Table XIII shows the energy consumed from the ESS in kJ in the first two columns, and the energy consumed from diesel fuel in the third and forth columns and in the same units (both cases without and with AI route recognition).

TABLE XIII
ENERGY CONSUMPTION FROM THE ESS AND FROM THE DIESEL FUEL IN THE DIFFERENT ROUTES

ROUTE	HYBRID HYDRAULIC POWERTRAIN WITHOUT AI ZONE RECOGNITION (ESS KJ)	HYBRID HYDRAULIC POWERTRAIN WITH AI ZONE RECOGNITION (ESS KJ)	HYBRID HYDRAULIC POWERTRAIN WITHOUT AI ZONE RECOGNITION (FUEL KJ)	HYBRID HYDRAULIC POWERTRAIN WITH AI ZONE RECOGNITION (FUEL KJ)
1	7229	9585	1.314.636	1.260.534
2	7091	8281	1.275.018	1.225.176
3	2605	8789	1.336.362	1.295.040
4	7266	10870	1.114.416	1.067.513
5	3086	10854	1.155.738	1.101.210
6	7249	10848	1.211.970	1.162.980
7	7257	10250	1.099.080	1.071.518
8	3098	10842	1.132.734	1.087.152
9	7157	10830	1.166.388	1.123.362
10	2389	10872	1.176.612	1.130.604
11	3490	10872	1.372.146	1.320.174
12	7254	7123	1.192.800	1.148.496
13	7318	7316	1.322.730	1.265.646
14	7264	7263	1.201.320	1.157.868
15	6652	3845	1.379.814	1.324.860

To reduce the powertrain consumption of two sources to one single value, additional studies should be performed (such as well to wheel). This is considered to be out of the scope of the present project, and the ESS energy consumption values of Table XIII are clearly two orders of magnitude lower than the values of diesel fuel energy consumption. Therefore, these energies have been neglected.

To get an easier reading of Table XII, all their values have been reduced to the equivalent fraction of the ICE consumption, as shown in Table XIV. In addition, the global average value for the 15 routes has been estimated and presented in Table XIV.

TABLE XIV

EQUIVALENT FUEL CONSUMPTION FRACTION OF THE DIFFERENT ARCHITECTURES

ROUTE	CONVENTIONAL POWERTRAIN (DIESEL)	HYBRID HYDRAULIC POWERTRAIN WITHOUT ZONE RECOGNITION (DIESEL)	HYBRID HYDRAULIC POWERTRAIN WITH ZONE RECOGNITION(DIESEL)
1	1	0.89	0.86
2	1	0.91	0.87
3	1	0.95	0.92
4	1	0.89	0.85
5	1	0.92	0.88
6	1	0.91	0.87
7	1	0.83	0.81
8	1	0.84	0.81
9	1	0.89	0.86
10	1	0.90	0.86
11	1	0.93	0.89
12	1	0.90	0.87
13	1	0.94	0.90
14	1	0.88	0.85
15	1	0.83	0.79
Average	1	0.89	0.86

As mentioned previously, simulation has been executed in quasistatic mode, which means that the transients have not been modelled and some of the losses, such as intermediate positions on the directional valve, unfinished displacements of the variable displacement pumps, or pressure drops in the lines have been ignored because of representing a lower order of magnitude. Therefore, the results of the simulations should not be understood as a final value of the powertrain improvements but as an asymptotic value, i.e., the better the powertrain components' control strategy is, the closer the consumption results will be to these values.

It can be appreciated that the Hybrid Hydraulic powertrains, both with and without zone recognition, show relevant fuel efficiency improvements if compared with conventional powertrains.

When comparing the ICE and the Hybrid Hydraulic without neural adaptation, the average efficiency improvement is about 10% to 11%. When comparing the Hybrid Hydraulic with neural adaptation, the average efficiency improvement is about 13% to 14%. That means that most of the improvement is due to hardware modification. However, the implementation of the neural recognition system remains interesting because its implementation in an industrialized system has a very low cost (just software development and maintenance) and the impact is still meaningful in terms of fuel consumption.

With regard to its potential industrialization, the implementation of hybrid hydraulics is a very interesting option. On the one hand, there is a very deep experience in the implementation of these components in commercial vehicles and mobile machines. On the other hand, the fact of being series production components means that they will have low cost and high reliability, compared to components that are currently produced in smaller series such as ultracapacitors or batteries (when batteries are not related to big series automotive applications).

Finally, the hybrid electric powertrain remains an interesting area to be studied, and the development of this study is the goal of the chapter 8 of this thesis.

8.

Topological Analysis for Hybrid Electric Powertrain

In this chapter three different hybrid electric powertrain architectures are proposed and modeled. The proposed powertrain models are executed using data obtained from real routes. Finally the results of these simulations are contrasted with the results of chapter 7, based on the hybrid hydraulic powertrain; the results are summarized in a table and conclusions are presented.

CONTENTS:

8.1. Introduction

The most frequent technical alternative for hybridizing a truck is the electric, as commented in the section “1.4 State of the Art. Commercial proposals for hybrid RCV”. Nevertheless, no previous literature comparing hydraulic and electric powertrain performances for a given drive cycle has been found.

Compared with hydraulic hybridization, electric hybridization offers higher energy density but lower power density. On the other hand, the physical principles on which the electric powertrain components are based are more efficient than those on which the hydraulic powertrain is based. This gives the electric powertrain a better long-term perspective.

The main goal of this chapter is to perform a comparative study of different electric-based powertrain architectures in a refuse-collection vehicle (RCV) for a real drive cycle, and compare its performance with a hydraulic-based powertrain.

As the goal of the study is to contrast the efficiency of these hardware topologies and not to optimize the corresponding control strategies for each powertrain configuration, the implemented control strategy is quite simple and is the same for all the powertrains evaluated.

8.2. Powertrain Models

All the powertrain architectures proposed in this work consist of four elements: an energy storage system (ESS), an energy generation system (EGS), an energy consumption system (ECS), and the DC bus. Each element interacting with the DC bus has its own power converter to get the maximum possible control of the energy flow.

Different works that enhance these topologies and reduce the number of inverters needed are available in the literature [36], but these kinds of studies have been considered out of the scope of this thesis.

The first powertrain model (PWT1) object of this study is composed of a fuel cell as the EGS, an ultracapacitor (UC) as the ESS, and two inverter-motor systems as the ECS. The reason in having two inverter-motor systems is that one will be used to propel the vehicle and the other will be used to power the RCV body ancillaries (compactor and refuse container lifter). As the power demand for propulsion and ancillaries have different magnitude orders, the inverter-motor groups have been sized to match their high efficiency points with the working power demanded by the applications (propulsion and ancillaries).

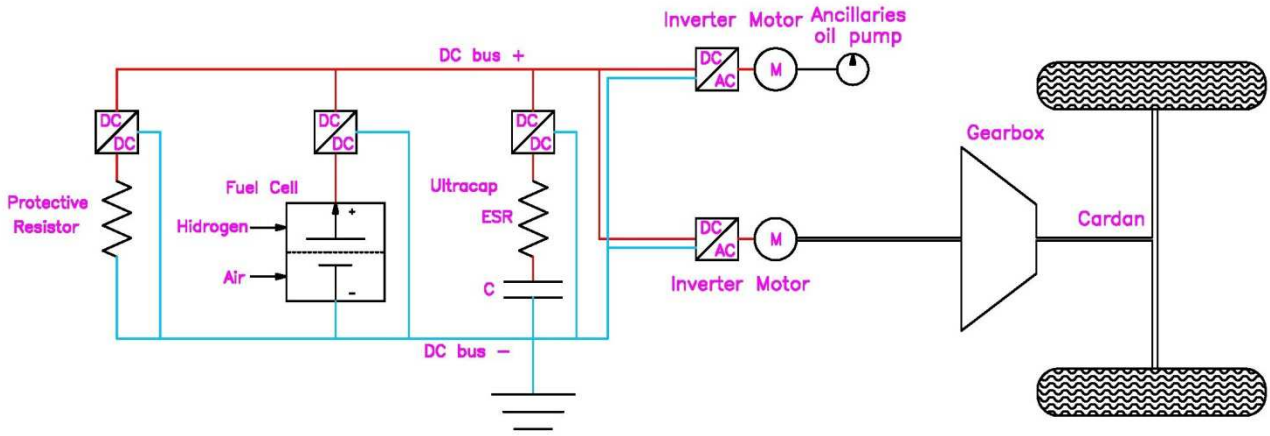

Fig. 67. Details of the powertrain 1 configuration PWT1

The second proposed powertrain (PWT2) is in fact an evolution of PWT1. As the average power value demanded by the powertrain is different in the 'transport mode' than in the 'collecting mode', two independent fuel cells sized to match with the power demands have been chosen.

The constraints include having the sum of the maximum power of the two fuel cells equal to the maximum power of the fuel cell of PWT1 and one of the fuel cells sized to work at its maximum efficiency at the average power value of the 'collecting mode'.

Considering the realistic approach of this work, the proposed architecture is the same as in the case of PWT1 but with cells that can be controlled independently (as in [59]) in two sets. One can be set

to standby mode (consuming power to keep themselves prepared to deliver power), while the other can be set to a certain power generation value.

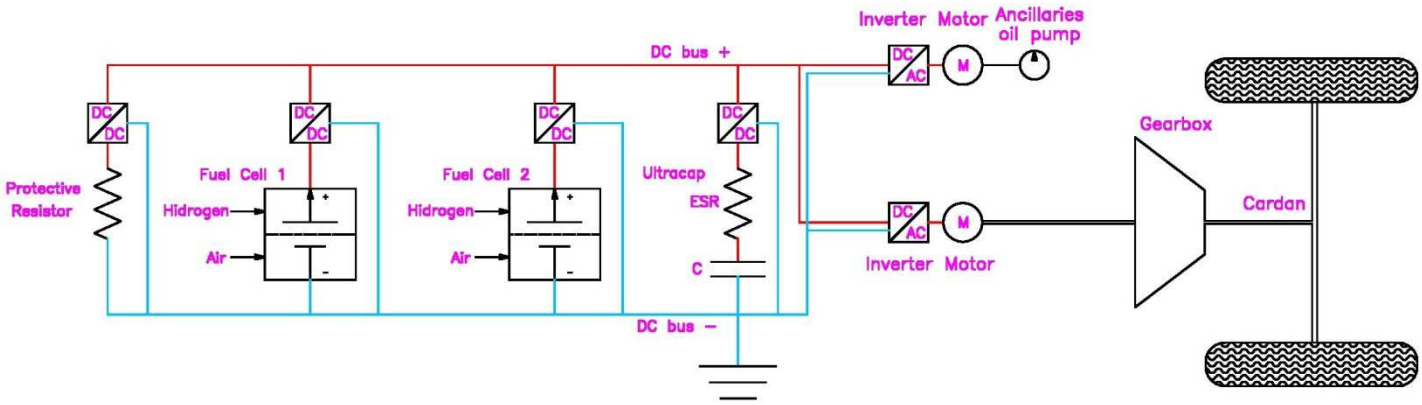

Fig. 68. Details of the powertrain 2 configuration PWT2

The third proposed powertrain PWT3 is also an evolution of the PWT2. The EGS is the same as that of the second powertrain, but the ESS has been modified with an added battery.

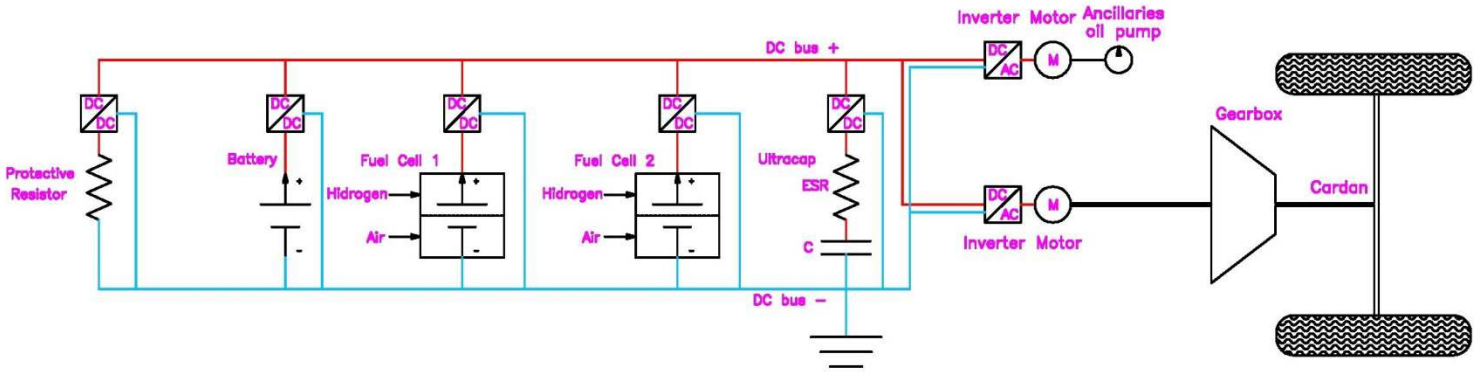

Fig. 69. Details of the powertrain 3 configuration PWT3

Several authors have proposed the use of a combination of batteries, fuel cells, and ultracapacitors for vehicular powertrains [38]-[42]. From a conceptual point of view, this is very interesting because the physical principles of each element (ultracapacitors, battery, and fuel cells) have different power dynamics. Additionally, the correct energy management system (EMS) can obtain the highest performance working with most adequate elements for each energy flow.

8.2.1. Fuel Cell Models

It is assumed that the fuel cells can be modularly assembled based on individual cells that can be stacked getting fuel cell packs [59].

The efficiency maps of the fuel cell stack are based on the efficiency of the individual fuel cell efficiency maps (taken from [35]). In this work, the fuel cell power axes (ordinates in Fig. 70) in these maps have been changed and maintain the same specific consumption (g/kWh) and efficiency. This is representative of a modular fuel cell system [59] built with individual cells.

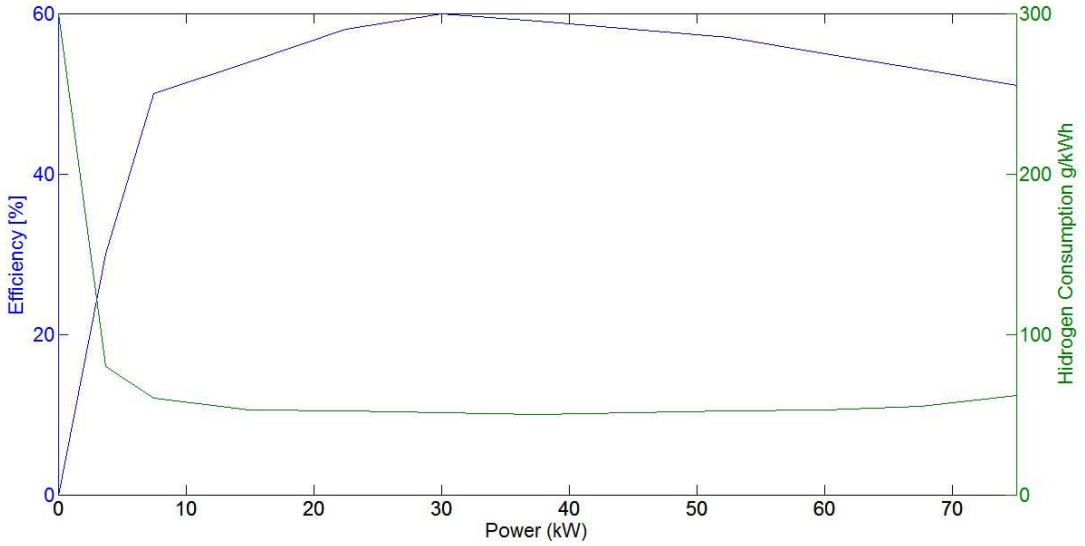

Fig. 70. Efficiency and consumption map for a 75 kW fuel cell

While the fuel cells are generating power, their hydrogen consumption for a certain power is taken from the right abscises axis of Fig. 70 (for a 75 kW fuel cell). While they are not generating power, it is assumed that they are at standby mode, which means the fuel cell ancillaries are consuming parasitic power to keep the fuel cell ready to deliver power despite the fact that no power is demanded from the fuel cell by external load.

The power that can be demanded from the fuel cell is limited to the maximum slope for transients, which guarantees long lifecycle of the fuel cell. In this work, this slope is defined as 100% power transitory in 100 s, which is quite a conservative value.

8.2.2. Battery Models

The batteries are based on commercial information of individual cell models [60]. These individual cells are characterized as:

TABLE XV
INDIVIDUAL BATTERY CELLS

Composition	Lithium Iron Magnesium Phosphate ($LiFeMgPO_4$)
Voltage	3.2 VDC
Useful energy	0.008 kWh
Max continuous charging	6.25 A
Max continuous discharging	25 A
Weight	0.04 kg
Volume	0.0218 l

The battery pack model is characterized by two architecture parameters (rows and columns), which define how many cells are mounted in series and in parallel.

The battery pack model (energy, charge power, and discharge power) is defined from the row number (Nr), column number (Na), and individual cell parameters as follows:

$$\mathrm{E_{BAT}(kWh)} = \mathrm{Nr} \cdot \mathrm{Na} \cdot 0.008\ (\mathrm{kWh}) \tag{64}$$

$$\mathrm{P_{CH}(kW)} = \mathrm{Nr} \cdot \mathrm{Na} \cdot \frac{6.25 \cdot 3.2}{10^3}\ (\mathrm{kW}) \tag{65}$$

$$\mathrm{P_{DSCH}\ (kW)} = \mathrm{Nr} \cdot \mathrm{Na} \cdot \frac{25 \cdot 3.2}{10^3}\ (\mathrm{kW}) \tag{66}$$

The power that can be demanded from the battery is limited to a maximum slope for transients, which will guarantee the long lifecycle of the battery. In this work, this slope will be defined as 100% of the maximum power transitory (in both charging and discharging) in 4 seconds, which is quite a conservative value.

8.2.3. Ultracapacitor Model

As in the battery models, the ultracapacitor pack model is based on individual cell characteristics, with values taken from commercial UC [61].

TABLE XVI
INDIVIDUAL ULTRACAPACITOR CELLS

Nominal voltage	48.6 VDC
Usable power	45000 W
Dimensions	416.2 x 210.8 x 178 mm
ESR, DC	0.0063 Ω
C	165 F
Weight	13.64 kg
Volume	15.75 l (0.179 x 0.418 x 0.211 m)

The characteristics of the ultracapacitor pack can be estimated based on Na and Nr, and the equations are equivalent to (64, 65, 66) as in the battery pack.

The ultracapacitor pack equations for estimations are based on [35], where the maximum available power can be estimated from the available energy as follows:

$$E_{SC}(t) = \frac{1}{2} C V_{SC}^2(t) \tag{67}$$

$$P_{DSCH}(t) = \frac{k_{SC} \cdot V_{SC}^2(t)}{ESR} \tag{68}$$

$$P_{DSCH}(t) = \left(\frac{k_{SC} \cdot 2}{ESR \cdot C}\right) \cdot E_{SC}(t) \tag{69}$$

As the term $\frac{k_{SC} \cdot 2}{ESR \cdot C}$ is a constant of the ultracapacitors, the available discharge power (P_{DSCH}) at a certain instant (t) is proportional to the energy stored at the same time:

$$\frac{P_{DSCH}(t)}{P_{MAX}} = \frac{E_{SC}(t)}{E_{MAX\_SC}} \tag{70}$$

The available charge power is equal to the maximum power minus the discharge power:

$$P_{CH}(t) = P_{MAX} - P_{DSCH}(t) \tag{71}$$

The power transients of the ultracapacitors have not been limited at all.

8.2.4. Electric Motor Generator Model

The electric motor (which works also as a generator) model is developed from commercial standard motors (the manufacturer wants to remain confidential), and is based on its maximum torque and its efficiency at each working point.

In Fig. 71, two different types of lines can be observed. The wide red line identifies the limit at which the motor can operate under steady-state conditions. The narrower lines identify the iso-efficiency contours. They are also coloured from blue (low efficiency areas) to red (high efficiency areas).

Fig. 71. Efficiency and maximum torque of the motor

To integrate this map into the simulation software, a function has been generated which estimates the power demanded from the current motor Torque, the RPM, and its efficiency (Eff), which is extracted from Fig. 71.

$$\mathrm{Eff} = \mathrm{f}(\mathrm{Torque}, \mathrm{RPM}) \tag{72}$$

$$\mathrm{P(kW)} = \mathrm{Eff} \cdot \mathrm{Torque} \cdot \mathrm{RPM} \cdot \frac{2\pi}{60 \cdot 1000} \tag{73}$$

The efficiency map for the generator has a similar profile. However, its efficiency values are slightly lower (the map has not been included in this work because of it does not add significant value). The efficiency map is supposed to correspond to the motor working from 300 VDC to 350 VDC.

8.2.5. Inverter Models

The inverter models used are based on commercial solutions. In these commercial equipment [62], [63], the inverter efficiency varies from 89% to 98%, depending basically on voltage. In this work, a 6% power loss in the inverters is taken into account each time power flows through it (so 94% efficiency), which is a conservative value if compared to [62], working from 300 VDC to 350 VDC.

8.3. Control Strategies

The Control Strategy proposal is similar to the presented in 7.3.

8.3.1. Driving Mode Identification

Detailed information about the drive cycles in an RCV can be found in [47]. Using an artificial intelligence-based algorithm, it is possible to identify the driving mode in real time, that is, if the RCV is working in either 'Collecting mode' or 'Transport mode'. In the present work, this information is assumed to be available.

8.3.2. Proposed Fuel Cell Control Strategy

As the main goal of this thesis is to compare the three different hardware architectures, the control strategy selected for each one of the proposed powertrains is the same. In this way, the impact of the control strategy is minimized, and the differences found in the simulation results will be considered the result of the hardware differences.

The power generated by the fuel cells, based on [30], is a function of the state of energy of the ESS (SOE_{ESS}). The SOE_{ESS} indicates the relative amount of energy in the ESS. Detailed information on how the SOE_{ESS} of each powertrain is estimated can be found at the end of this section (81)-(83).

$$\mathrm{P_{FUELCELL}(kW)} = \mathrm{f(SOE_{ESS})} \tag{74}$$

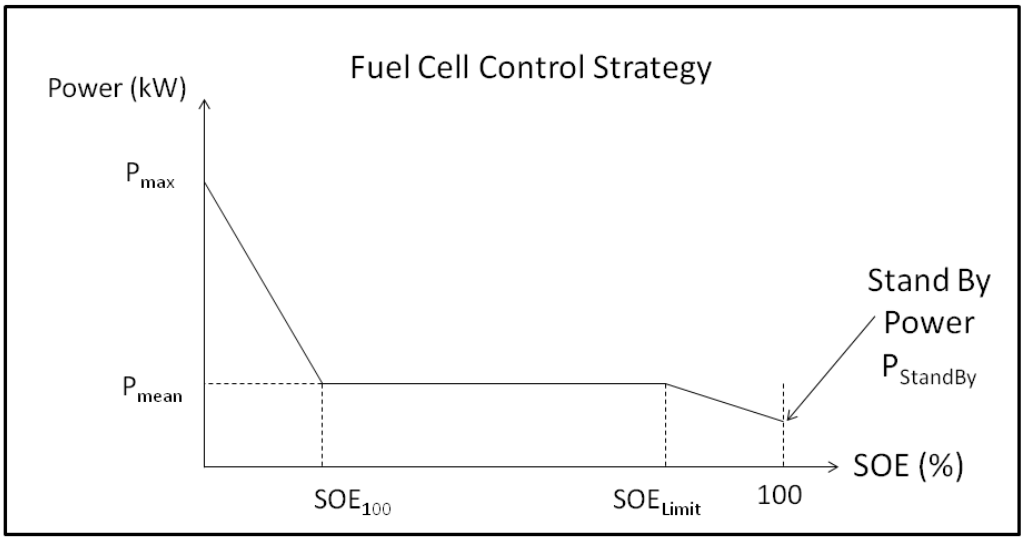

Fig. 72. Control strategy of the fuel cell

In Fig. 72, the abscissa corresponds to the SOE_{ESS}, while the ordinate is the demanded power from the fuel cell.

The fuel cell has two operating modes: enabled mode and standby mode. When the SOE_{ESS} reaches 100%, it is set to standby mode, and it will be set again to enabled mode only if the SOE_{ESS} falls below SOE_{100}.

When the fuel cell is set to standby mode, the consumption of the fuel cell is the standby power, but it does not deliver energy to the powertrain. This power is necessary to keep the fuel cell ancillaries (humidifier, compressors, membrane stack, etc.) in the operative conditions and to avoid the start and stop processes of the fuel cell.

When the fuel cell is set to the enabled mode, it follows the following rules:

If the SOE_{ESS} is between two values (SOE_{100} and SOE_{Limit}), the power demanded from the fuel cell is the average power of the driving mode (P_{mean}).

If the SOE_{ESS} is below SOE_{100}, the power demanded from the fuel cell will proportionally increase to the distance from SOE_{100} and will reach the maximum nominal power (P_{max}) of the fuel cell when the SOE is zero.

If the SOE_{ESS} is over the SOE_{Limit}, the power demanded from the fuel cell is proportionally decreased to the distance from the SOE_{Limit} and reaches the standby power of the fuel cell (P_{stand_by}) when the SOE_{ESS} is 100. When the SOE_{ESS} is 100, the standby power is used to estimate the hydrogen consumption, but no power is delivered by the fuel cell.

The following equations summarize the control algorithm used in the control of the fuel cell:

$$\text{if Fuel Cell} = \text{ENABLED}$$

$$\text{if } \mathrm{SOE_{ESS}} \leq \mathrm{SOE_{100}}$$

$$\mathrm{P(kW)} = \mathrm{P_{mean}} + (\mathrm{P_{max}} - \mathrm{P_{mean}})\left(\frac{\mathrm{SOE_{100}} - \mathrm{SOE}}{\mathrm{SOE_{100}}}\right) \quad (75)$$

$$\text{if } \mathrm{SOE_{100}} < SO\mathrm{E_{ESS}} \leq \mathrm{SOE_{Limit}}$$

$$\mathrm{P(kW)} = \mathrm{P_{mean}} \quad (76)$$

$$\text{if } \mathrm{SOE_{Limit}} < SO\mathrm{E_{ESS}} < 100$$

$$\mathrm{P(kW)} = \mathrm{P_{mean}} - \left(\mathrm{P_{mean}} - \mathrm{P_{StandBy}}\right)\left(\frac{\mathrm{SOE} - \mathrm{SOE_{Limit}}}{100 - \mathrm{SOE_{Limit}}}\right) \quad (77)$$

$$\text{if SOE} = 100$$

$$\mathrm{P(kW)} = \mathrm{P_{StandBy}} \quad \text{and} \quad \text{Fuel Cell = DISABLED} \quad (78)$$

$$\text{if Fuel Cell} = \text{DISABLED}$$

$$\text{if } \mathrm{SOE_{ESS}} \leq \mathrm{SOE_{100}}$$

$$\mathrm{P(kW)} = 0 \text{ and Fuel Cell} = \text{ENABLED} \quad (79)$$

$$\text{if } \mathrm{SOE_{ESS}} > SO\mathrm{E_{100}}$$

$$\mathrm{P(kW)} = 0 \text{ and Fuel Cell} = \text{DISABLED} \quad (80)$$

In the PWT1 and PWT2, the ESS is an ultracapacitor pack, and the $\mathrm{SOE_{ESS}}$ is the state of energy of the ultracapacitors ($\mathrm{SOE_{UC}}$), which is defined as in [43] and uses the notation introduced in (67) and (70):

$$\mathrm{SOE_{ESS}(t) = SOE_{UC}(t) = \frac{E_{SC}(t)}{E_{MAX\_SC}}} \tag{81}$$

where $E_{SC}(t)$ is the energy stored in the ultracapacitor at an instant t, and E_{MAX_SC} is the maximum energy that can be stored in the ultracapacitor.

In the PWT3, the ESS is a combination of ultracapacitors and batteries. To have available power on both subsystems, the $\mathrm{SOE_{ESS}}$ is the minimum of the $\mathrm{SOE_{UC}}$ (81) and an energy based weighted average of the energy of both systems $\mathrm{SOE_{UC+BAT}}$ (83).

The fuel cell control cannot be implemented by just using $\mathrm{SOE_{UC+BAT}}$ because in the weighted average, the battery is heavier than the UC and it could happen that with no energy available on the UC, the fuel cell would not deliver power because of high $\mathrm{SOE_{UC+BAT}}$ values. Under these conditions all the transients would be 100% supported by the battery.

$$\mathrm{SOE_{ESS} = MIN(SOE_{UC+BAT};\ SOE_{UC})} \tag{82}$$

$$\mathrm{SOE_{UC+BAT} = \frac{SOE_{BAT}(t)\cdot E_{MAX\_BAT} + SOE_{UC}(t)\cdot E_{MAX\_SC}}{E_{MAX\_BAT} + E_{MAX\_SC}}} \tag{83}$$

where E_{MAX_BAT} is the maximum energy that can be stored in the battery, and the $SOE_{BAT}(t)$ is the expression equivalent to (81), but using the battery parameters $E_{BAT}(t)$ and E_{MAX_BAT}, instead of the ultracapacitor parameters.

SOE_{Limit} and SOE_{100} are control parameters of the fuel cell. Their values are fixed in this work to 30% and 70%, respectively, for the three powertrains. The P_{max} and P_{mean} values will be defined in section 8.4.

8.3.3. Proposed Battery Control Strategy

The maximum charge and discharge powers of the battery are limited by its transient slopes, as defined in section '8.2.2 Battery models'.

The battery control strategy is characterized by two control parameters 'Battery Low Control Point' and 'Battery High Control Point'.

When the $\mathrm{SOE_{ESS}}$, as defined in (82), is below the 'Battery Low Control Point', the energy demanded by the ESS is consumed from the battery. If the battery cannot deliver this power because of

the mentioned limitations, then, it is assisted by the ultracapacitor pack. The battery is never charged for these SOE values of the ESS, and the excess power is always stored in the ultracapacitors.

When the $\mathrm{SOE_{ESS}}$ is over the 'Battery High Control Point', the energy supplied to the ESS is stored into the battery. If the battery cannot receive this power because of the above-mentioned limitations, then it is assisted by the ultracapacitors.

When the $\mathrm{SOE_{ESS}}$is between the 'High' and 'Low Control Points', the battery is not used, and all the power flows are managed from the ultracapacitor pack. In this work, the values for the 'Low' and 'High Control Points' are set to 35% and 50%, respectively.

$$\text{if SOE} < BATTERY\_LOW\_CONTROL\_POINT$$

$$\text{if P} > 0 \qquad if\ \left(\mathrm{P} < \mathrm{P_{MAX_{BAT}}}\right)$$

$$\mathrm{P_{BAT}(kW)} = \mathrm{P};\ \mathrm{P_{SC}(kW)} = 0 \tag{84}$$

$$\text{else}$$

$$\mathrm{P_{BAT}(kW)} = \mathrm{P_{MAX\_BAT}};\ \mathrm{P_{SC}(kW)} = \mathrm{P} - \mathrm{P_{MAX\_BAT}} \tag{85}$$

$$\text{if P} < 0 \qquad \mathrm{P_{SC}(kW)} = \mathrm{P};\ \mathrm{P_{BAT}(kW)} = 0 \tag{86}$$

$$\text{if SOE} > BATTERY\_HIGH\_CONTROL\_POINT$$

$$\text{if P} > 0$$

$$\mathrm{P_{SC}(kW)} = \mathrm{P};\ \mathrm{P_{BAT}(kW)} = 0 \tag{87}$$

$$\text{if P} < 0$$

$$if\ \left(\mathrm{P} < \mathrm{P_{MAX_{BAT}}}\right)$$

$$\mathrm{P_{BAT}(kW)} = \mathrm{P};\ \mathrm{P_{SC}(kW)} = 0 \tag{88}$$

$$\text{else}$$

$$\mathrm{P_{BAT}(kW)} = \mathrm{P_{MAX\_BAT}};\ \mathrm{P_{SC}(kW)} = \mathrm{P} - \mathrm{P_{MAX\_BAT}} \tag{89}$$

$$\text{if BATTERY\_LOW\_CONTROL\_POINT} < SOE < BATTERY\_HIGH\_CONTROL\_POINT$$

$$\mathrm{P_{SC}(kW)} = \mathrm{P};\ \mathrm{P_{BAT}(kW)} = 0 \tag{90}$$

where P is the power consumed from the ESS (if P>0, the ESS is delivering power; if P<0, the SOE is storing power), P_{BAT} is the power consumed from the battery, P_{MAXBAT} is the maximum power the battery can charge/discharge, and P_{SC} is the power consumed from the ultracapacitors.

8.4. Component Sizing

As this work is the basis before detail engineering is performed to assemble a real vehicle, all the components have to be sized with respect to realistic values, and all components have to be integrated in an RCV without losing an excessive payload or load volume of the RCV.

As in this application the peak power demanded by the ECS is much higher than its average values, the concept of EGS downsizing is considered. The target is to find a suitable ESS that can supply the energy that the EGS cannot provide in all the transients of the considered drive cycles.

The method for sizing the different elements is based on the concept that an RCV repeats similar drive cycles daily [28]. According to this principle, the first four routes (Tables XII - XIV) will be used to size the elements, while drive cycles 5 to 15 will be used to validate the component sizing.

This method could also be extrapolated to other types of vehicles, such as buses and delivery trucks, which repeat usually the same drive cycles. In fact, most of the private vehicles perform most of their kilometres in repetitive cycles [44].

The sizing process begins at the motor. The proposed motor is designed to work between 300 VDC and 350 VDC. All the elements will be defined to work at this voltage range.

Based on the experience in RCV drive cycle analysis, the following values have been found to be representative:

The average power consumption in the ‘refuse collecting’ mode is between 17 kW and 25 kW. The average power consumption while the vehicle is running during the ‘refuse transport’ mode is between 90 kW and 120 kW. The average power of the whole route is between 40 kW and 70 kW.

Based on these considerations, the fuel cell of the PWT1 has been sized. Considering the fuel cell map sizing concept defined in section ‘8.2.1. Fuel cells models’, a 150 kW fuel cell has been selected (with a standby power of 4kW), with a maximum efficiency power generation between 40 kW and 70 kW, which is the average value of the whole drive cycle.

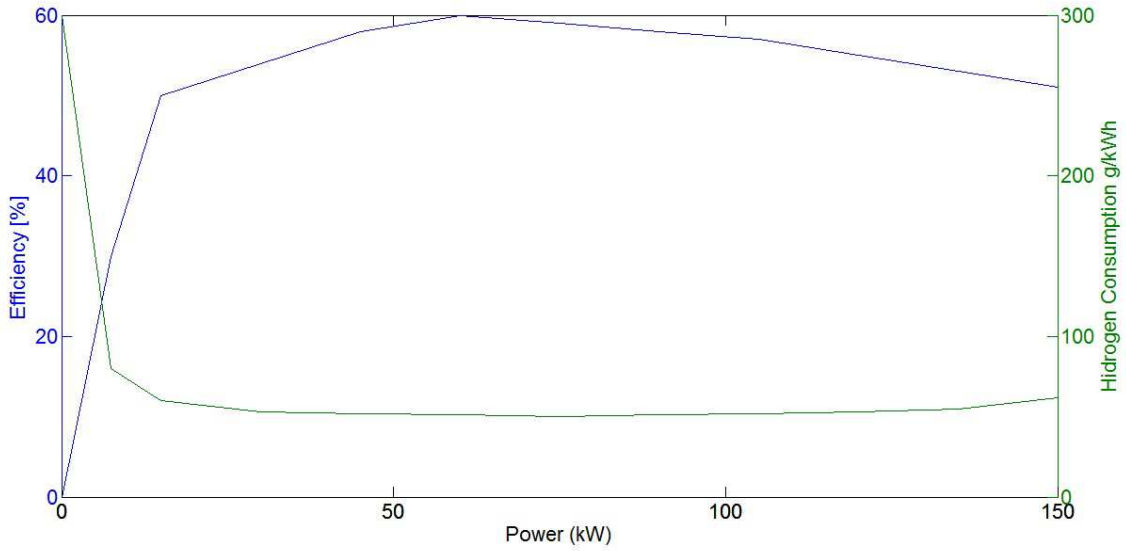

Fig. 73. Efficiency map for a 150 kW fuel cell

Based on the same concept, the first FC of PWT2 and PWT3 has been sized. A 50 kW fuel cell has been selected, with a maximum efficiency power generation between 17 kW and 25 kW, which is the average value of the collecting mode.

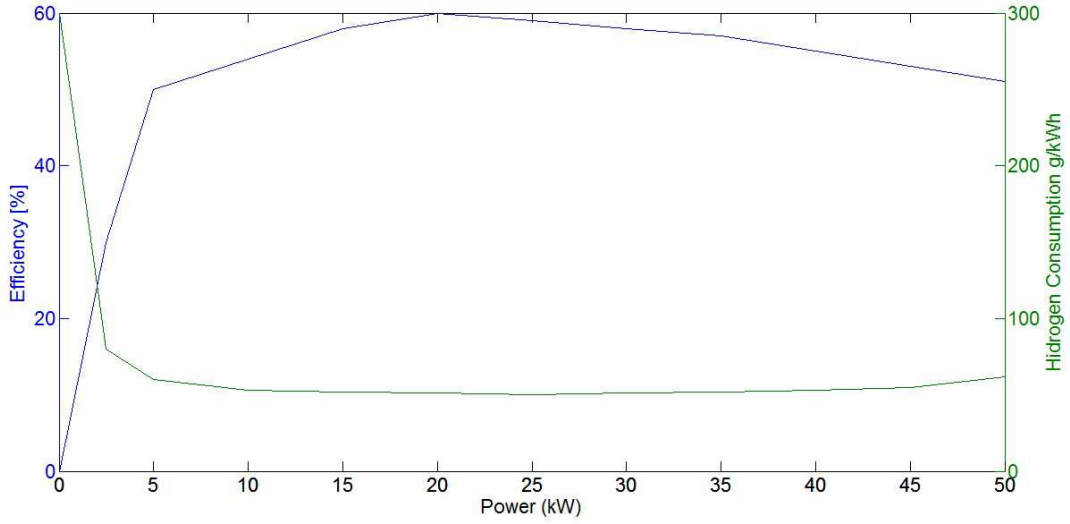

Fig. 74. Efficiency map for a 50 kW fuel cell

To have the same available power as in PWT1 (as mentioned in section 8.2), the second fuel cell of PWT2 is a 100 kW fuel cell. This is not considered as two different fuel cells but a single fuel cell whose cell rows can be enabled or set to standby, separating the 150 kW fuel cell in two independently controlled sectors of 50 kW and 100 kW [59].

For the ESS sizing, the first four routes will be used in a trial-and-error method. The ultracapacitor pack of PWT1 is dimensioned to 7 rows because the ideal motor voltage is between 300 VDC to 350 VDC, and each UC has a nominal voltage of 48.6 VDC. Routes 1 to 4 are sequentially simulated, and the number of ultracapacitor columns is increased one by one to reach a minimum value

at which the SOE is always higher than zero in the four routes (negative SOE at any point means the powertrain could not deliver enough power). The resulting number of columns is 8.

Using the same criterion for PWT2, the minimum required number of columns is 11.

The battery pack of PWT3 is dimensioned to 100 rows, and the ultracapacitor pack of the powertrain is dimensioned to 7 rows, both due to the motor voltage.

At this point, PWT3 battery and ultracapacitor sizing becomes an optimization problem with two degrees of freedom (number of columns for ultracapacitors and batteries), and one target is to be able to work through the whole driving cycle always delivering the necessary power and minimizing ESS volume and weight. To estimate the basic possibilities, the required number of battery columns as a function of the number of ultracapacitor columns has been estimated, as shown in Table XVII.

TABLE XVII
BATTERY AND ULTRACAPACITOR COMBINATIONS FOR PWT3

Battery and UC combination	1	2	3	4
UC columns	1	2	3	4
Battery columns	22	15	10	9
Weight (kg)	183.4	250.9	326.4	417.8
Volume (l)	158.6	253.8	353.4	461.7

The chosen option is the number 1 in Table XVII (1 UC x 22 batteries) because of its lower volume and weight. As suggested by other authors [37], the current cost of ultracapacitors is currently much higher than the cost of batteries at equivalent mass or volume, which would give the first combination a higher potential degree of industrialization. However, avoiding this type of arguments is preferred because the costing question is usually circumstantial rather than structural, and a potential mass production of UCs could change this situation.

A summary of the ESS of the different powertrains is presented in Table XVIII. The resulting architectures for the ESS of PWT1 and PWT2 are shown in the second and third columns of Table XVIII, respectively. The resulting architecture of the ESS of PWT3 (based on the first combination of Table XVII) can be found on the fourth (PWT3 (UC)) and fifth columns (PWT3 (BAT)) of the same table. It can be seen that the impact of the ESS of PWT3 in the needed volume and payload reduction will be lower on PWT3 than in any other architectures.

TABLE XVIII
SUMMARY OF THE DIFFERENT ESS

	PWT1(UC)	PWT2(UC)	PWT3(UC)	PWT3(BAT)
Discharge Power(kW)	2520	3465	630	120
Charge Power (kW)	2520	3465	630	30
Stored Energy (kWh)	3.02	4.15	0.75	12
Total Volume (l)	884	1215	158	
Total Mass (kg)	763	1050	183	

8.5. Calculation Engine

The calculation engine for this chapter has been developed in Matlab.

With the data logging kit mentioned in chapter 3, a significant number of real drive cycles have been logged, and using the techniques proposed in [28], the useful power has been estimated. As a result, two vectors (RPM and Power) containing samples at 0.1Hz during the whole collecting work (from about 7 to 8 hours) have been generated daily in 15 days.

In the calculation engine, the engine RPM value is extracted from the logged data, and the power demand is estimated by post-processing the logged data.

At each sample time (at 0.1Hz), the algorithm estimates the instantaneous power consumption of the motors (propulsion or ancillaries) based on the logged data.

The instantaneous power generated by the fuel cell pack is based on the $\mathrm{SOE}_{\mathrm{ESS}}$ of the previous instant.

If the addition of the two previous values is negative, the power consumption is supplied by the ESS. If it is positive, the power excess is stored on the ESS.

Using this method, a total of 15 routes are simulated, and the instantaneous SOE of the system is evaluated during all simulations. If at any moment the $\mathrm{SOE}_{\mathrm{ESS}}$ is lower than zero, it is understood as the powertrain not being able to supply the demanded power. As a result, the hardware combination is not viable. This method is useful in estimating if the proposed powertrain can provide exactly the same performance as that of the original powertrain in which the routes were registered.

In the flow chart shown in Fig. 75, the input data are in square boxes, while the output data are in balloons. The SOC and fuel cell status, which are outputs for a certain instant ‘t’, are used as inputs for the next instant ‘t+1’. The consumed hydrogen will be useful in estimating the fuel consumption of the powertrain and the route combination.

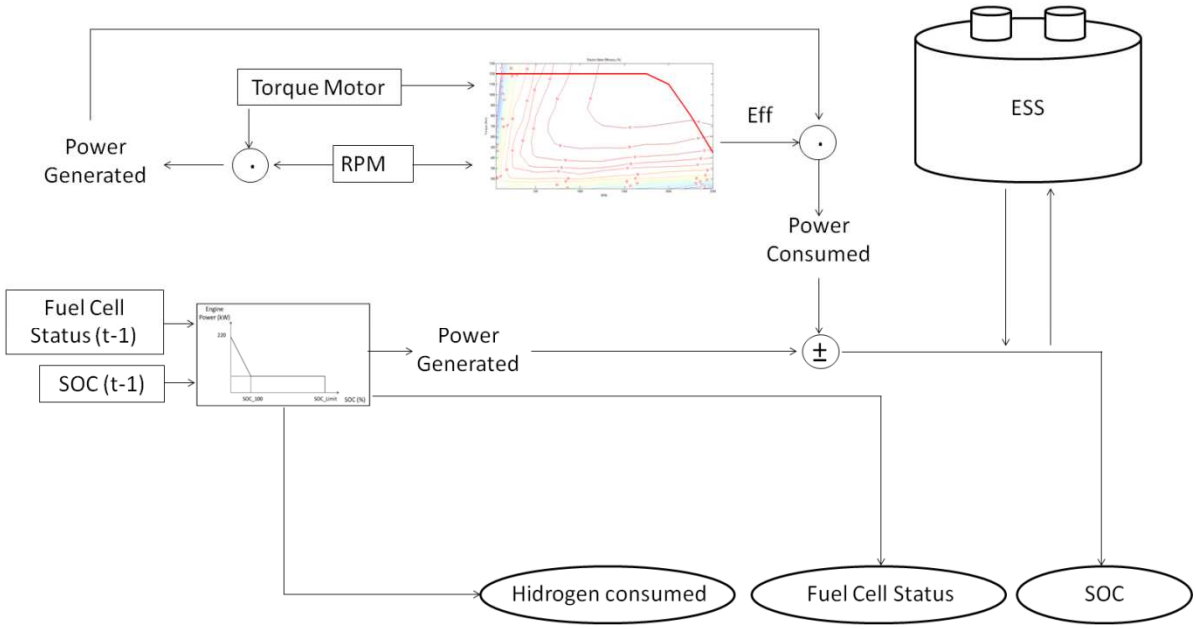

Fig. 75. Information flow in the calculation engine

8.6. Simulations Results and Conclusions

The performed simulations reflect only the power demanded by the powertrain and the body ancillaries, so no power consumption happens when the vehicle is stopped because of traffic. To compare the ICE in equity with the other powertrains, the idling periods have been excluded in the simulation so it would really reflect a diesel start/stop ICE.

The resulting fuel consumption values are used to compare a Start/Stop diesel engine, two hybrid hydraulic powertrains proposed in chapter 7 of this work, and the three powertrains proposed in this chapter 8.

In Table XIX, the first three columns reflect the equivalent mass of diesel consumed by the pure ICE (P_ICE), the hybrid hydraulic without mode identification (HH_NZI), and the hybrid hydraulic with mode identification (HH_WZI). Columns 5, 6, and 7 show the equivalent mass of hydrogen consumed by the fuel cells in its PWT1, 2, and 3 configurations. As the mode identification demonstrated to improve vehicle efficiency in chapter 7 of this thesis, all the hybrid electric controls are based on this concept.

TABLE XIX
SUMMARY OF FUEL CONSUMPTIONS (KG) FOR EACH POWERTRAIN AND ROUTE

ROUTE	PURE ICE (KG OF DIESEL)	HYBRID HYDRAULIC WITHOUT ZONE IDENTIFICATION (KJ DIESEL)	HYBRID HYDRAULIC WITH ZONE IDENTIFICATION (KJ DIESEL)	PWT1 (KG H2)	PWT2 (KG H2)	PWT3 (KG H2)
1	34.51	30.86	29.59	9.40	8.07	8.17
2	33.05	29.93	28.76	9.46	8.05	8.09
3	33.08	31.37	30.40	9.37	8.46	8.27
4	29.49	26.16	25.06	8.63	7.32	7.52
5	29.53	27.13	25.85	8.58	7.38	7.43
6	31.25	28.45	27.30	9.21	7.99	7.94
7	30.98	25.80	25.15	9.21	7.58	7.77
8	31.67	26.59	25.52	9.44	7.95	7.92
9	30.76	27.38	26.37	9.03	7.71	7.80
10	30.81	27.62	26.54	9.01	7.72	7.73
11	34.76	32.21	30.99	10.38	9.35	9.43
12	31.13	28.00	26.96	9.58	8.56	8.51
13	33.15	31.05	29.71	10.20	8.99	9.02
14	32.1	28.20	27.18	10.26	8.97	8.91
15	39.24	32.39	31.10	11.83	10.79	10.74

As the values of Table XIX are expressed in two different magnitudes (kg of diesel and kg of hydrogen), it is quite difficult to compare them. To establish a direct comparison, the values in table XIX

have been reduced to the same physical magnitude (kJ) based on the lower heating values (LHV) found in [46]. The results are presented in Table XX.

TABLE XX
SUMMARY OF FUEL CONSUMPTIONS (KJ) FOR EACH POWERTRAIN AND ROUTE

ROUTE	P_ICE (KG DIESEL)	HH_NZI (KJ DIESEL)	HH_WZI (KJ DIESEL)	PWT1 (KJ H2)	PWT2 (KJ H2)	PWT3 (KJ H2)
1	1,470,126	1,314,636	1,260,534	1,136,885	976,357	988,091
2	1,407,930	1,275,018	1,225,176	1,144,023	973,333	978,534
3	1,409,208	1,336,362	1,295,040	1,133,377	1,023,173	1,000,672
4	1,256,274	1,114,416	1,067,513	1,043,859	884,903	909,339
5	1,257,978	1,155,738	1,101,210	1,038,173	892,524	898,452
6	1,331,250	1,211,970	1,162,980	1,113,901	966,195	960,510
7	1,319,748	1,099,080	1,071,518	1,114,264	916,960	939,340
8	1,349,142	1,132,734	1,087,152	1,142,208	961,961	957,848
9	1,310,376	1,166,388	1,123,362	1,092,368	933,049	943,211
10	1,312,506	1,176,612	1,130,604	1,090,433	933,291	935,227
11	1,480,776	1,372,146	1,320,174	1,255,679	1,131,079	1,140,757
12	1,326,138	1,192,800	1,148,496	1,158,902	1,035,512	1,029,463
13	1,412,190	1,322,730	1,265,646	1,237,533	1,087,529	1,091,158
14	1,367,460	1,201,320	1,157,868	1,241,162	1,085,110	1,077,852
15	1,671,624	1,379,814	1,324,860	1,431,087	1,305,277	1,299,229

There is part of the consumed energy in the route that is not included in the fuel consumption presented in Table XX, as the ESS_{SOE} is at 100% at the beginning of the route and it is not necessarily 100% at the end of the route. This consumed energy has to be considered also. This energy is in fact replacing fuel (diesel or hydrogen). In Table XXI, these values are shown for a more realistic comparison of the different powertrains.

TABLE XXI
SUMMARY OF THE ESS SOC CONSUMPTION

ROUTE	HH_NZI (kJ BLADDER)	HH_WZI (kJ BLADDER)	PWT1 (kJ UC)	PWT2 (kJ UC)	PWT3 (kJ UC)	PWT3 (kJ UC)
1	523	530	1287	9787	140	0
2	513	668	2591	6287	1817	14403
3	5159	5154	2083	9620	1831	3192
4	494	494	2	9349	0	0
5	4674	4673	18	3	6	0
6	508	511	24	10	8	0
7	5319	503	622	185	925	0
8	4663	4661	30	15	10	0
9	494	602	42	10149	13	0
10	5324	5371	0	2202	0	0
11	4268	4270	0	8586	1776	2298
12	505	636	163	10350	29	0
13	442	443	2685	2706	771	0
14	496	497	3	0	1330	929
15	1107	3914	1433	4602	4	0

The integration of the information in Table XXI into the information in Table XX is not evident because when comparing different energy sources, they have to be reduced to the same units and format. The only way to do this with accuracy would be to use data from a well to wheel study, in which the energetic pool (nuclear, gas combined cycles, coal, wind, etc.) of the electric energy used to charge the ESS at the base, to produce hydrogen and to extract oil and refine diesel, has to be considered.

As this is considered to be out of the scope of the present project and the values of Table XXI are clearly three to five orders of magnitude lower than the values of Table XX, these energies have been considered negligible.

To get an easier comparison, Table XXII is presented, where the diesel consumption in kJ of pure ICE (P_ICE) has been considered to be the reference value (1). And the rest of the columns indicate the fuel consumption referred to this base value (from 0 to 1). The last row of this table indicates the average values of each powertrain result over the whole set of routes.

TABLE XXII
SUMMARY OF THE FUEL CONSUMPTIONS FOR EACH POWERTRAIN AND ROUTE

ROUTE	P_ICE (%)	HH_NZI (%)	HH_WZI (%)	PWT1 (%)	PWT2 (%)	PWT3 (%)
1	1.000	0.894	0.857	0.773	0.664	0.672
2	1.000	0.906	0.870	0.813	0.691	0.695
3	1.000	0.948	0.919	0.804	0.726	0.710
4	1.000	0.887	0.850	0.831	0.704	0.724
5	1.000	0.919	0.875	0.825	0.709	0.714
6	1.000	0.910	0.874	0.837	0.726	0.722
7	1.000	0.833	0.812	0.844	0.695	0.712
8	1.000	0.840	0.806	0.847	0.713	0.710
9	1.000	0.890	0.857	0.834	0.712	0.720
10	1.000	0.896	0.861	0.831	0.711	0.713
11	1.000	0.927	0.892	0.848	0.764	0.770
12	1.000	0.899	0.866	0.874	0.781	0.776
13	1.000	0.937	0.896	0.876	0.770	0.773
14	1.000	0.879	0.847	0.908	0.794	0.788
15	1.000	0.825	0.793	0.856	0.781	0.777
AVERAGE	1.000	0.893	0.858	0.840	0.729	0.732

Several conclusions can be drawn from the results shown in Table XXII.

Comparing columns 2 (P_ICE) and 3 (HH_NZI), it can be concluded that the fact of keeping the ICE working at high efficiency points and recuperating the braking energy by hydraulic devices can decrease energy consumption by about 11%.

Comparing columns 3 (HH_NZI) and 4 (HH_WZI), it can be seen that the adaptive control strategy with zone identification adds a substantial value (about 3.5%) of savings because the number of ICE start/stops and the ESS load/unload cycles are reduced.

Analyzing the values in columns 6 (PWT2) and 7 (PWT3), it can be seen that from energy point of view, both PWT2 and PWT3 are the best candidates, especially PWT2 that shows the lowest consumption of all. Nevertheless, from industrialization point of view, PWT2 represents an option that would be difficult to implement in a real vehicle nowadays because of size and weight constraints (Table XVII) and the excessive cost in the current ultracapacitor prices [37].

Comparing the values in columns 5 (PWT1), 6 (PWT2), and 7 (PWT3), it can be appreciated that a combination of ultracapacitors and batteries and a suitable control strategy, which can take advantage of the properties of each one, can provide an efficient solution with a significant reduction in the required hardware and can also get very good efficiency results that are very close to the optimal powertrain (PWT2), despite the fact of not being optimal.

Comparing the best hybrid hydraulic architecture (HH_WZI) to the best hybrid electric architecture (PWT2), it can be concluded that the electric architecture has greater potential for savings.

Nevertheless, we consider that this straight comparison is unfair in some point because a lot of important information is missing. The industry of mobile hydraulics is a very mature one and is already installed in mass production systems, which offers a lot of advantages. Due to a higher production volume, this industry offers lower prices, better availability, and higher reliability.

Skilled technicians are also easier to find, and after-sales services are widely available. Hydraulic powertrains do not need to prepare facilities, such as battery chargers, which usually require modifying the electrical installations of the facilities.

On the other hand, by its physical nature, electric systems will always be more efficient. Therefore, electric powertrains are considered the best long-term solution.

From our point of view, we can conclude that hydraulic powertrain can be considered a very good option in the short and medium term, and the electric powertrain will be the best option in the long term.

9.

General Conclusions and Future Work

The main contributions of this research work, as well as the conclusions and future work, are presented in this chapter.

CONTENTS:

9.1. General Conclusions

The main conclusions of this thesis are commented in the following lines. Detailed conclusions related to each work package can be found below after the bold headings.

Main Conclusions:

In this research work high accuracy energetic models of RCV have been developed and empirically contrasted by the use of low cost devices. The experimental test result shows that these models can offer estimations with errors lower than 5%. These models are highly interesting in simulating powertrains and their performances.

RCV drive cycles have been analyzed in depth to understand how the powertrain works in regular service. Based on the fact that the drive cycles follow a well-defined pattern and are repetitive, two predictive algorithms have been developed. The first one is an algorithm which can identify the next power demands of the vehicle. This algorithm is based on artificial neural networks and showed a success rate (S_r) of over 95%. The second one is an algorithm which can estimate the energy left to finish the current trip (E_L), this algorithm can be implemented in auto-learning algorithms.

Two alternative powertrain architectures (hybrid hydraulic and hybrid electric) have been proposed and evaluated. Both alternatives have been dimensioned considering they have to be feasible from an industrial point of view, with the corresponding weight and volume restrictions. The hybrid hydraulic powertrain showed a fuel consumption reduction of 14%. The hybrid electric powertrain showed a fuel consumption reduction of over 26%.

It has also to be considered that hydraulic and electric architectures cannot be compared directly because they belong to different industries and have different constraints. Hydraulic parts for heavy duty powertrains have, in fact, been state of the art in the industry for decades, are already mass-produced, show high reliability and are available at competitive costs. Skilled technicians familiar with these technologies are also easy to find.

Electric architectures have been state of the art in the industry in recent years (the first Toyota Prius was commercialized worldwide in 2000 [68]), and so far are unusual in heavy duty vehicles. Electric parts for heavy duty powertrains are usually unavailable, and when available they tend to be taken from non-automotive sectors [69], or produced by small companies [70]. Both options are more expensive than standard off-the-shelf automotive components. Skilled technicians are also more difficult to find.

The author considers this as a scenario which defines the hybrid hydraulic alternative as currently very interesting, and the hybrid-electric alternative as the most interesting option once the industry has reached a more mature stage.

Conclusions related to RCV energy models:

A new methodology to define and adjust energy consumption models of RCVs has been defined. This method is based on the classic approach for both the vehicle and body mathematical models, with specific tests to adjust all the vehicle parameters related to aerodynamics, rolling resistance, inertias, road profile and body pressure and flow.

This adjustment is done using low-cost hardware, information available on the vehicle J1939 CAN bus, cartographical information and information supplied by parts manufacturers. Different algorithms to correct deviations in the measured vehicle speed and distance, oil flow, and road profile have been proposed and validated.

Specific tests to show the precision of the data post-processing system have been performed and the results shown. A final test has been performed in which the fuel consumption of an RCV has been calculated and compared to the fuel consumption measured at the fuel station, getting estimations with errors lower than 5%.

There are still a few parameters which are not taken into account by the proposed model. For example, the fuel LHV dispersion (in CNG from 43650 to 46500 kJ/kg according to [46]). In Spain the national gas company (ENAGAS) analyzes the supplied CNG composition and its properties daily, the analysis results being publicly available on Internet [48]. This information could be used to generate a correction parameter. The gas analysis found in the testing period included in section VI of this work shows minor variations in the gas properties; in the period August 20th to December 7th the minimum and maximum values of LHV have been 10.869 and 10.727 kWh/Nm^3, respectively.

Also the engine maps used to calculate the fuel consumption are taken from steady conditions instead of transient, the rolling resistance is simplified to the tire, the rest negligible, and wind speeds up to 10 km/h are accepted and not considered for the calculation.

The result of the test shows that even neglecting these parameters, high accuracy energetic consumption models (errors lower than 5%) can be built and adjusted by the use of this approach. This methodology opens the possibility of developing high quality vehicle energy studies at low cost, it being also possible to study the interaction between the body consumption and powertrain energetic generation.

This method can be used to study alternative vehicle components, architectures and management strategies which could lead to a reduction of fuel consumption in vehicles.

Conclusions related to cycle identification and energy demand estimation:

Some vehicles (such as RCV, buses or delivery trucks) follow the same route daily, performing drive cycles which are not entirely the same but still very similar in many aspects.

This route repetition can be understood as an information source which can provide real time knowledge about the future power and energy demands for drive cycles being executed on repeated routes. Several authors have also demonstrated that most of the kilometers or distances travelled by a standard driver pertain to a small number of routes [21] which would open the application of these concepts to other machines.

In this work, two different algorithms have been developed and tested and which will help improve the energy management algorithms for hybrid vehicles.

The first algorithm is an artificial intelligence system which has been used to identify the power demand mode of the vehicle (transport or collection), showing an average accuracy higher than 94% tested in real-world circumstances. Based on this information, the powertrain management strategy can be adapted for the power demand mode, reducing transients in the internal combustion engine or keeping it working for longer periods at its high-efficiency points.

The second algorithm is an analytic algorithm which can estimate the energy necessary for the vehicle to finish its daily work. Based on this information, the power train management strategy can deplete the energy storage system of a hybrid vehicle before the end of its trip, thus optimizing the substitution of fossil fuel by electricity.

Several automotive manufacturers have already started working on this subject [25]-[26].

Conclusions related to Hybrid Hydraulic Powertrains Applied to RCVs:

A hybrid hydraulic powertrain for an RCV has been proposed, modeled and simulated on real drive cycles. The powertrain is based on an architecture similar to the proposals found in other scientific articles. The powertrain component models are based on commercial parts.

These hybrid hydraulic powertrains have been controlled by adaptive strategies depending on drive cycle recognition and also in fixed strategies.

When comparing the ICE and the Hybrid Hydraulic without drive cycle recognition, the average fuel consumption reduction is about 10% to 11%. When comparing the Hybrid-Hydraulic with drive cycle recognition, the average fuel consumption reduction is about 13% to 14%. Despite the fact that most of the improvement is due to hardware modification, the implementation of the neural recognition system remains interesting. Its implementation in an industrialized production has a very low cost and the impact is still meaningful in terms of fuel consumption.

Regarding its potential industrialization, the implementation of hybrid hydraulics is a very interesting option. On the one hand, there is considerable experience in the implementation of these components in commercial vehicles and mobile machines. On the other hand, the fact of being series production components means that they will have low cost and high reliability.

Conclusions related to Hybrid Electric Powertrains Applied to RCVs:

Three hybrid electric powertrains for an RCV have been proposed, modeled and simulated on real drive cycles. Two architecture models are built with ultracapacitors and fuel cells, and the third architecture is built with ultracapacitors, fuel cells and batteries. The powertrain component models are based on commercial parts and information found in scientific publications. All these models have been controlled by drive cycle adaptive means.

The first two architecture proposals show a comparison of two different control strategies. The first one uses a unique control strategy for the whole fuel cell, the second one uses a control strategy sectorized by fuel cell stacks. The second control strategy shows 11% lower fuel consumption.

Comparing the performance values of these powertrains, it can be appreciated that a combination of ultracapacitors and batteries with a suitable control strategy, which can take advantage of the properties of each one, can provide an efficient solution with a significant reduction in the required hardware. Despite the fact that the combination of ultracapacitors, fuel cells and batteries is not the best from the energetic point of view, it has by far the best weight and volume compromise. And its fuel consumption values still remain close to the most efficient solution (ultracapacitors and fuel cells).

9.2. Future Work

During the development of this research work, although the defined aims and objectives have been covered, some points have been detected that could be further investigated to increase progress in the respective fields.

Future work related to RCV energy models:

Regarding the RCV energetic models proposed in the first work package of this thesis. The angle of the road parameter 'α' with after-treatment had a very good average performance, but circumstantially a bad performance. That makes the registered value useful for global consumption studies, which was the goal of the authors, but not if the aim is to use this parameter for local drive cycle studies.

The correction algorithm used the values taken from the inclinometer, vehicle speed data, relative axis position data, and correction algorithms to consider the offset of the sensor installation.

The data acquisition system can generate wrong data for the 'α' parameter when the vehicle climbs a curb, when passing over an elevated pedestrian walkway and occasionally in aggressive maneuvers. The use of GPS, as commented before, also has limitations. The authors consider that the combined use of inclinometers and GPS could take the best of each and obtain an improved measurement of 'α' which could offer a very good performance under any circumstances.

Future work related to cycle identification and energy demand estimation:

Two parameter prediction algorithms have been proposed in this part of the research work.

The first one is a neural network (AI) based algorithm which can predict the power consumption mode of an RCV on a real drive cycle. Despite the fact that the algorithm has been shown to work with high accuracy, and it is valid for implementation on a real vehicle, it still needs a human to do the drive cycle recognition which will be used in the network training phase. This remains a difficulty for the application of these techniques in real vehicles. The development of methods to automate the training phase would ease the introduction of these algorithms in real vehicles.

The second algorithm is a deterministic algorithm which combines the use of statistical data with infinitesimal calculus to estimate the energy left to finish the present trip (E_L) in real time. Additionally, in this algorithm the data collection and treatment to estimate the Gaussian function parameters have been done by a human. The development of a method to automate this phase would facilitate the introduction of this algorithm in real vehicles.

Future work related to Hybrid Hydraulic Powertrains Applied to RCVs:

A hybrid hydraulic architecture has been modeled and simulated to estimate its performance. The main weakness of the proposed architecture is that the proposed ESS (hydraulic accumulators) work based on an elastic foam accumulator filled with nitrogen, which supplies the flow according to an

adiabatic law (as standard in these devices). This is a problem when feeding the RCV ancillaries, which are designed to work (also as standard in these devices) with a fixed flow or fixed pressure pump. As the accumulators are incompatible with the RCV ancillaries it has been decided to feed the ancillaries directly from the engine. As the engine in this mode is working far from its high efficiency points, the efficiency of the powertrain is severely penalized.

The development of any device which could couple an adiabatic accumulator with a fixed flow device while keeping high efficiency values would significantly increase the efficiency of the whole powertrain.

Future work related to Hybrid Electric Powertrains Applied to RCVs:

In this work an optimal hybrid electric powertrain has been implemented. This powertrain is based on the use of fuel cell batteries and ultracapacitors. One of the weakest points of this architecture, as commented before, is that the components selected are highly efficient, but are components which are produced so far in small series. Being produced in small series makes the parts expensive, less reliable and adds an additional difficulty when spare parts are sought.

An interesting alternative could be to look for different EGS, such as ICE. Despite the fact of being less efficient, ICE represents a very mature technology which can offer competitive costing and high reliability. Also the ultracapacitors could be partially replaced by batteries.

The combination of ICE and batteries are in fact state of the art in cars [68], [71], but not commercially available so far (December 2014) in European medium or heavy duty applications.

10. Thesis Dissemination

Publications directly related with the thesis contributions

Journals:

Soriano, F., Alvarez-Florez, J., and Moreno-Eguilaz, M., “Experimentally Compared Fuel Consumption Modelling of Refuse Collecting Vehicles for Energy Optimization Purposes,” SAE Int. J. Commer. Veh. 7(1):324-336, 2014, doi:10.4271/2014-01-9023.

Soriano, F.; Moreno Eguilaz, M.; Alvarez-Florez, J., "Drive Cycle Identification and Energy Demand Estimation for Refuse-Collecting Vehicles," Vehicular Technology, IEEE Transactions on , vol.PP, no.99, pp.1,1 doi: 10.1109/TVT.2014.2382591.

Soriano, F.; Moreno Eguilaz, M.; Alvarez-Florez, J.; Riera, J " Topological Analysis of Powertrains for Refuse-Collecting Vehicles based on Real Routes.Part I: Hybrid Hydraulic Powertrain”. Submitted to Vehicular Technology, IEEE Transactions on.

Soriano, F.; Moreno Eguilaz, M.; Alvarez-Florez, J.; Riera, J, " Topological Analysis of Powertrains for Refuse-Collecting Vehicles Based on Real Routes. Part II: Hybrid Electric Powertrain”. Submitted to Vehicular Technology, IEEE Transactions on.

Projects impacted by this thesis:

Project Title: Hybrid Integrated Urban Commercial Vehicle.

Founding entity: Technology Strategy Board (United Kingdom)

Partners: Dennis Eagle Ltd, Ros Roca Group (Lead Participant, Participant)

MTL Group Limited, (Participant)

Magnomatics Limited (Participant)

MIRA Ltd, United Kingdom (Participant)

Duration: sep 10 - jun 14

Project tasks impacted by this thesis: Development of datalogging systems, Matlab models and algorithms to identify drive modes.

11. References

1. British Petroleum. “BP Statistical Review of world energy 2014.” http://www.bp.com/en/global/corporate/about-bp/energy-economics/statistical-review-of-world-energy.html

2. Baseley, S., Ehret, C., Greif, E., and Kliffken, M., "Hydraulic Hybrid Systems for Commercial Vehicles," SAE Technical Paper 2007-01-4150, 2007, doi:10.4271/2007-01-4150.

3. Martin Larsson, “Road Slope Estimation”, Master Thesis in Automatic control, Tekniska högskolan in Linköping ,2010.

4. Rene Hulin, "Boite de vitesses", Traité Génie Mécanique. Les techniques de l'ingenieur. B-5-660.

5. Tony Sandberg. “Heavy Truck Modelling for Fuel Consumption Simulations and Measurements”. Thesis 924, Linköping Studies in Science and Technoloy, Linköping University. 2001.

6. Matthew Barth, Theodore Younglove, Georges Scora. “Development of a heavy duty Diesel modal emissions and fuel consumption”.California Path Research Project, University of California, 2005. ISSN 1055-1425.

7. Sahlholm, P. & Henrik, K., 2010. “Road grade estimation for look-ahead vehicle control using multiple measurement runs”. Control Engineering Practice, 18(2010)1328-1341, doi 10.1016/j.conengprac.2009.09.007

8. Mangan, S.; Wang, J.; Wu, Q.H.; , "Measurement of the road gradient using an inclinometer mounted on a moving vehicle," Computer Aided Control System Design, 2002. Proceedings. 2002 IEEE International Symposium on , vol., no., pp. 80- 85, 2002. 0-7803-7388-X, doi 10.1109/CACSD.2002.1036933.

9. Alexander Ravey, Nicolas Watrin, Benjamin Blunier, David Bouquain, Abdellatif Miraoui. “Energy Sources Sizing Methodology for Hybrid Fuel Cell Vehicles Based on Statistical Description of Driving Cycles”. IEEE transaction on Vehicular Technology, Volume 60, Issue 9. November 2011, doi: 10.1109/TVT.2011.2158567.

10. Nicholas Dembski, Giorgio Rizzoni, Ahmed Soliman. “Development of Refuse Driving and Duty Cycles”. SAE Technical Paper Series 2005-01-1165, doi:10.4271/2005-01-1165.

11. Tobias Knoke, Joachim Böcker. “Optimal power train design for a hybrid refuse collector truck”. Vehicle Power and Propulsion, 2007. VPPC 2007 IEEE. 978-0-7803-9760-6, doi 10.1109/VPPC.2007.4544237.

12. vePower Technologies & CEVEQ. “Hybrid Refuse Truck Feasability Study”. Transport development centre of Canada. September 2005.

13. Taghavipour, A.; Alasty, A.; Saadat, M.F., "Nonlinear Power Balance Control of a SPA hydraulic hybrid truck," Advanced Intelligent Mechatronics, 2009. AIM 2009. IEEE/ASME International Conference on , vol., no., pp.805,810, 14-17 July 2009 doi: 10.1109/AIM.2009.5229911 URL: http://ieeexplore.ieee.org/stamp/stamp.jsp?tp=&arnumber=5229911&isnumber=5229709

14. Serrao, L.; Rizzoni, G., "Optimal control of power split for a hybrid electric refuse vehicle," American Control Conference, 2008 , vol., no., pp.4498,4503, 11-13 June 2008 doi: 10.1109/ACC.2008.4587204 URL: http://ieeexplore.ieee.org/stamp/stamp.jsp?tp=&arnumber=4587204&isnumber=4586444

15. Clark, N., Rapp, B., Gautam, M., Wang, W. et al., "A Long Term Field Emissions Study of Natural Gas Fueled Refuse Haulers in New York City," SAE Technical Paper 982456, 1998, doi:10.4271/982456.

16. Ivanco, A., Johri, R., and Filipi, Z., "Assessing the Regeneration Potential for a Refuse Truck Over a Real-World Duty Cycle," SAE Int. J. Commer. Veh. 5(1):364-370, 2012, doi:10.4271/2012-01-1030.

17. Menyang Zhang, Yan Yang, Chunting Chris Mi. “Analytical Approach for the Power Management of Blended-Mode Plug-In Hybrid Electric Vehicles”. IEEE transactions of vehicular technology, vol 61 no 4 may 2012. 0018-9545, doi 10.1109/TVT.2012.2187318.

18. S. Kermani, S. Delprat, T.M. Guerra, R. Trigui, B. Jeanneret. “Predictive energy management for hybrid vehicle”. Control Engineering Practice. Vol 20 Issue 4. Elsevier. DOI: 10.1016/j.conengprac.2011.12.001

19. Frank A. Bender, Martin Kaszynski, Oliver Sawodny. “Drive Cycle Prediction and Energy Management Optimization for Hybrid Hydraulic Vehicles”. IEEE Transactions on vehicular technology 2013. DOI: 10.1109/TVT.2013.2259645

20. Johannesson, L., Asbogard, M., Egardt, B. “Assessing the potential of predictive control for hybrid vehicle powertrains using stochastic dynamic programming “Intelligent Transportation Systems, 2005. Proceedings. 2005 IEEE 13-15 Sept. 2005. DOI: 10.1109/ITSC.2005.1520076

21. Joe Froehlich, John Krumm “Route Prediction from Trip Observations” SAE World Congress & Exhibition. Paper 2008-01-0201 DOI: 10.4271/2008-01-0201

22. Jungme Park, Zhihang Chen, Kiliaris, L., Kuang, M.L., Masrur, M.A., Phillips, A.M., Murphey, Y.L.” Intelligent Vehicle Power Control Based on Machine Learning of Optimal Control Parameters and Prediction of Road Type and Traffic Congestion”. Vehicular Technology, IEEE Transactions on, On page(s): 4741-4756 Volume: 58, Issue:91, Nov. 2009

23. Langari, R., Jong-Seob Won “Intelligent energy management agent for a parallel hybrid vehicle-part I: system architecture and design of the driving situation identification process” Vehicular Technology, IEEE Transactions on (Volume:54 , Issue: 3) DOI: 10.1109/TVT.2005.844685

24. Jong-Seob Won, Langari, R. “Intelligent energy management agent for a parallel hybrid vehicle-part II: torque distribution, charge sustenance strategies, and performance results” Vehicular Technology, IEEE Transactions on (Volume:54 , Issue: 3) DOI: 10.1109/TVT.2005.844683

25. Andrew A. Frank. Frank Transportation Technology, Llc, “Fuel consumption control for charge depletion hybrid electric vehicles”, US6116363 A, September 12, 2000.

26. Joanne T. Woestman, Prabhakar B. Patil, Ross M. Stunz, Thomas E. Pilutti. Ford Global Technologies, Inc. “Strategy to use an on-board navigation system for electric and hybrid electric vehicle energy management”, US6487477 B1, November 26, 2002.

27. Ivanič, Ž., "Data Collection and Development of New York City Refuse Truck Duty Cycle," SAE Technical Paper 2007-01-4118, 2007, doi:10.4271/2007-01-4118.

28. Soriano, F., Alvarez-Florez, J., and Moreno-Eguilaz, M., “Experimentally Compared Fuel Consumption Modelling of Refuse Collecting Vehicles for Energy Optimization Purposes,” SAE Int. J. Commer. Veh. 7(1):324-336, 2014, doi:10.4271/2014-01-9023.

29. Z. Filipi, Y. J. Kim. “Hydraulic Hybrid Propulsion for Heavy Vehicles: Combining the Simulation and Engine-In-the-Loop Techniques to Maximize the Fuel Economy and Emission Benefits”. Oil Gas Sci. Technol. – Rev. IFP . Volume 65, Number 1, January-February 2010 . IFP International Conference – Advances in Hybrid Powertrains. http://dx.doi.org/10.2516/ogst/2009024

30. Kim, Y. and Filipi, Z., "Simulation Study of a Series Hydraulic Hybrid Propulsion System for a Light Truck," SAE Technical Paper 2007-01-4151, 2007, doi:10.4271/2007-01-4151.

31. Bin Wu, Chan-Chiao Lin, Zoran Filipi, Huei Peng and Dennis Assanis. “Optimization of Power Management Strategies for a Hydraulic Hybrid Medium Truck” Proceedings of the 2002 Advanced Vehicle Control Conference, Hiroshima, Japan, September 2002.

32. Wohlgemuth, S., Wachtmeister, G., and Kloft, P., "Development of a Hydraulic Hybrid System for Urban Traffic," SAE Technical Paper 2013-01-1479, 2013, doi:10.4271/2013-01-1479.

33. Surampudi, B., Nedungadi, A., Ostrowski, G., Montemayor, A. et al., "Design and Control Considerations for a Series Heavy Duty Hybrid Hydraulic Vehicle," SAE Technical Paper 2009-01-2717, 2009, doi:10.4271/2009-01-2717.

34. Bin Wu , Chan-chiao Lin , Zoran Filipi , Huei Peng. “Optimal power management for a hydraulic hybrid delivery truck (2004) “.Vehicle System Dynamics: International Journal of Vehicle Mechanics and Mobility, Volume 42, Issue 1-2, 2004, doi: 10.1080/00423110412331291562.

35. Diego Feroldi, Maria Serra, Jordi Riera“Energy Management Strategies based on efficiency map for Fuel Cell Hybrid Vehicles”Journal of Power Sources. Volume 190, Issue 2, 15 May 2009, Pages 387–401. DOI: 10.1016/j.jpowsour.2009.01.040

36. Bauman, J.; Kazerani, M., “An improved powertrain topology for fuel cell-battery-ultracapacitor vehicles,” Industrial Electronics, 2008. ISIE 2008. IEEE International Symposium on , vol., no., pp.1483,1488, June 30 2008-July 2 2008 doi: 10.1109/ISIE.2008.4677252

37. Khaligh, A.; Zhihao Li, “Battery, Ultracapacitor, Fuel Cell, and Hybrid Energy Storage Systems for Electric, Hybrid Electric, Fuel Cell, and Plug-In Hybrid Electric Vehicles: State of the Art,” Vehicular Technology, IEEE Transactions on , vol.59, no.6, pp.2806,2814, July 2010 doi: 10.1109/TVT.2010.2047877

38. Pablo García, Luis M. Fernández, Juan P. Torreglosa, Francisco Jurado, “Operation mode control of a hybrid power system based on fuel cell/battery/ultracapacitor for an electric tramway”. Computers & Electrical Engineering.Volume 39, Issue 7, October 2013, Pages 1993–2004. DOI: 10.1016/j.compeleceng.2013.04.022

39. Esteves Araujo, R.; de Castro, R.; Pinto, C.; Melo, P.; Freitas, D., “Combined Sizing and Energy Management in EVs With Batteries and Supercapacitors,” Vehicular Technology, IEEE Transactions on , vol.63, no.7, pp.3062,3076, Sept. 2014 doi: 10.1109/TVT.2014.2318275
URL: http://ieeexplore.ieee.org/stamp/stamp.jsp?tp=&arnumber=6800120&isnumber=6895341

40. Thounthong, P.; Chunkag, V.; Sethakul, P.; Davat, B.; Hinaje, M., “Comparative Study of Fuel-Cell Vehicle Hybridization with Battery or Supercapacitor Storage Device,” Vehicular Technology, IEEE Transactions on , vol.58, no.8, pp.3892,3904, Oct. 2009 doi: 10.1109/TVT.2009.2028571 URL: http://ieeexplore.ieee.org/stamp/stamp.jsp?tp=&arnumber=5184856&isnumber=5277109

41. Camara, M.B.; Gualous, H.; Gustin, F.; Berthon, A., “Design and New Control of DC/DC Converters to Share Energy Between Supercapacitors and Batteries in Hybrid Vehicles,” Vehicular Technology, IEEE Transactions on , vol.57, no.5, pp.2721,2735, Sept. 2008 doi: 10.1109/TVT.2008.915491 URL: http://ieeexplore.ieee.org/stamp/stamp.jsp?tp=&arnumber=4425796&isnumber=4626110

42. Qi Lia, Weirong Chena, YankunLia, Shukui Liub, Jin Huanga ‘Energy management strategy for fuel cell/battery/ultracapacitor hybrid vehicle based on fuzzy logic’ International Journal of Electrical Power & Energy Systems.Volume 43, Issue 1, December 2012, Pages 514–525. DOI: 10.1016/j.ijepes.2012.06.026

43. Feroldi, D.; Serra, M.; Riera, J., “Design and Analysis of Fuel-Cell Hybrid Systems Oriented to Automotive Applications,” Vehicular Technology, IEEE Transactions on , vol.58, no.9, pp.4720,4729, Nov. 2009 doi: 10.1109/TVT.2009.2027241

44. Joe Froehlich, John Krumm “Route Prediction from Trip Observations” SAE World Congress & Exhibition.Paper 2008-01-0201 DOI: 10.4271/2008-01-0201

45. http://www.slideshare.net/anepma_es/ponencia-innovaciones-tecnolgicas-vehculo-recolector-elctricohibrido-alfonso-garca-fcc

46. Jean Claude Guibet. “Les carburants et la combustion”. Les techiniques de l’ingenieur. BM2-520

47. Soriano, F.; Moreno Eguilaz, M.; Alvarez-Florez, J., "Drive Cycle Identification and Energy Demand Estimation for Refuse-Collecting Vehicles," Vehicular Technology, IEEE Transactions on , vol.PP, no.99, pp.1,1 doi: 10.1109/TVT.2014.2382591.

48. ENAGAS daily CNG gas composition and properties: http://www.enagas.es/cs/Satellite?cid=1324380952260&language=es&pagename=ENAGAS%2FPage%2FENAG_CalidadGasMunicipio.

49. Key World Energy Statistics. “Key World Energy Statistics“ http://www.iea.org/publications/freepublications/publication/KeyWorld2013_FINAL_WEB.pdf

50. Mangan, S., Jihong Wang, “Development of a Novel Sensorless Longitudinal Road Gradient Estimation Method Based on Vehicle CAN Bus Data,” Mechatronics, IEEE/ASME Transactions on, vol.12, no.3, pp.375-386, June 2007.

51. King Tin Leung, James F. Whidborne, David Purdy, Phil Barber, “Road vehicle state estimation using low-cost GPS/INS”, Mechanical Systems and Signal Processing, Volume 25, Issue 6, August 2011, Pages 1988-2004, doi: 10.1016/j.ymssp.2010.08.003

52. Bosch Rexroth, “Hydrostatic regenerative braking System HRB”, RE 94850/10.2012.

53. Parker Runwise, “Advanced Series Hybrid Drive”, HY34-1000, 03/2013.

54. Proclain, “Front wheel assistance”, 2012.

55. Zhengce Cao; Sen Wu; Mingze Li; Changqing Du, "Series and Parallel Hybrid System Performance Comparison Based on the City bus Cycle," Power and Energy Engineering Conference, 2009. APPEEC 2009. Asia-Pacific , vol., no., pp.1,5, 27-31 March 2009. doi: 10.1109/APPEEC.2009.4918739.

56. Luke Wadsley “Optimal system solutions enabled by Digital Pumps”, International Exposition for Power Transmission, IFPE, Las Vegas, 2011

57. Artemis Intelligent Power Ltd. Personal communication.

58. Hydac. “Sizing Accumulators”. Innovative Fluid Power. PN#02068195/04.13/ACU1102-1326, 2013.

59. Palma, L.; Enjeti, P.N., “A Modular Fuel Cell, Modular DC–DC Converter Concept for High Performance and Enhanced Reliability,” Power Electronics, IEEE Transactions on , vol.24, no.6, pp.1437,1443, June 2009 doi: 10.1109/TPEL.2009.2012498

60. Valence 26650 Power Cell IFR 26650PC

61. [19] Maxwell Technologies BMO D0165

62. http://www.brusa.eu/fileadmin/Diverses/Download/Datenblaetter/BRUSA_DB_EN_BDC546.pdf

63. http://www.flexiva.eu/en/alternative-energy-systems/products/bidirectional-converter-modules.html

64. Institut Cartogràfic de Catalunya. http://www.icc.cat/cat/Home-ICC/Geoinformacio-digital/Sobre-la-geoinformacio-ICC/Especificacions-tecniques

65. Felipe Jiménez, “Improvements in road geometry measurement using inertial measurement systems in datalog vehicles”, Measurement 44 (2011) 102-112, Issue 1, January 2011. doi:10.1016/j.measurement.2010.09.029

66. Fathy, H. K., Kang, D., Stein, J. L., ”Online vehicle mass estimation using recursive least squares and supervisory data extraction,” presented at American Control Conference, Seattle, USA, June 11—13, doi: 10.1109/ACC.2008.4586760

67. Matsuura, M., Korematsu, K., and Tanaka, J., "Fuel Consumption Improvement of Vehicles by Idling Stop," SAE Technical Paper 2004-01-1896, 2004, doi:10.4271/2004-01-1896

68. http://en.wikipedia.org/wiki/Toyota_Prius

69. https://www.swe.siemens.com/spain/web/es/industry/drive_tech/motores/Documents/ws-elfa-en.pdf

70. http://www.magnomatics.com/pages/about-us/the-company.htm

71. http://en.wikipedia.org/wiki/Honda_Civic_Hybrid

UNIVERSITAT POLITÈCNICA
DE CATALUNYA
BARCELONATECH